Oxidative stress-related molecules in ticks and potential utilization of their characteristics for tick control strategies

マダニ制御に向けたマダニの酸化ストレス関連分子の特性利用

The United Graduate School of Veterinary Science

Yamaguchi University

Emmanuel Pacia Hernandez

March 2020

TABLE OF CONTENTS

LIST OF TABLES AND FIGURES

.

ABBREVIATIONS

AAALAC:	Association for Assessment and Accreditation of Laboratory Animal Care
ACD:	accidental cell death
ANOVA:	analysis of variance
ATP:	adenosine triphosphate
bp:	base pairs
BCIP/NBT	5-Bromo-4-chloro-3-indolylphosphate/Nitroblue Tetrazolium
CDNB:	1-chloro-2,4-dinitrobenzene
DCNB:	1,2-dichloro-4-nitrobenzene
dsRNA:	double stranded RNA
EGFP:	enhanced green fluorescent protein
EST:	expressed sequence tags
Fer:	ferritin
Fer1:	intracellular ferritin
Fer2:	secretory ferritin
GFP:	green fluorescent protein
GSH:	glutathione
GST:	glutathione S-transferase
HlFer1:	*Haemaphysalis longicornis* ferritin 1
HlGST:	GST of *H. longicornis*
HRP:	horseradish peroxidase
IFAT:	immunofluorescent antibody test
IPTG:	isopropyl β-D-1-thiogalactiopyranoside

IRE: iron responsive element

IRP: iron regulatory protein

ISE6: *Ixodes scapularis* embryo derived tick cell line

LB: Luria-Bertani

Luc2: firefly luciferase

MDA: malondialdehyde

MRP: multidrug resistance-related protein

NNPP: neural network for promoter prediction

ORF: open reading frame

PBS: phosphate-buffered saline

PCR: polymerase chain reaction

PGK: phosphoglycerate kinase

PVDF: polyvinylidene difluoride

pI: isoelectric point

PPX: exopholyphosphate

rBaGST: recombinant GST of *R.*(*B.*) *annulatus*

RCD: regulated cell death

rHlPRX2: recombinant 2-cys-peroxiredoxin of *H. longicornis*

RNAi: RNA interference

ROS: reactive oxygen species

SDS-PAGE: sodium dodecyl sulphate polyacrylamide gel electrophoresis

SFTSV: severe fever with thrombocytopenia virus

TAE: Tris-acetate-EDTA

TBARS: thiobarbituric acid reactive substances

TCE2: *T. cinnabarinus* esterase

TFIID: transcription factor II D

TSS: transcription starting site

GENERAL INTRODUCTION

Ticks and oxidative stress

Parts of this introduction has been published as:

Hernandez EP, Talactac MR, Fujisaki K, Tanaka T. (2019). The case for oxidative stress molecule involvement in the tick-pathogen interactions -an omics approach. *Dev Comp Immunol,* **100**, 103409.

Ticks are considered to be the second-most important vector, after mosquitoes, in the transmission of human diseases. However, in domestic and wild animals, they are the most important vectors of disease-causing pathogens. The diverse pathogens that ticks carry include viruses, bacteria, protozoa, and nematodes [1–5].

Ticks being obligate blood-feeding arthropods need blood at almost all their stages of life. Due to their feeding behavior, ticks are exposed to elevated amounts of reactive oxygen species (ROS). The presence of ferrous iron from iron-containing proteins in the host sera could trigger the production of ROS through the Fenton reaction [6–9]. The blood-meal also contains heme, a pro-oxidant protein from hemoglobin digestion, that could catalyze the production of ROS [10]. ROS are also generated from neutrophils and macrophages from the mammalian host through the lesion brought about by blood feeding [11,12]. Aside from blood feeding, a multitude of cellular processes and enzyme activity could result in ROS production and eventually increased oxidative stress levels (Table 1) [13]. In ticks, this includes embryonic development and larval maturation after egg hatching [14]. ROS could severely harm the cellular components. ROS could further generate hydroxyl radicals, superoxide anions (O_2^-), and hydrogen peroxide (H_2O_2). However, ROS could also be a signal in the promotion of apoptosis and the H_2O_2 could be a messenger in cellular proliferation, particularly transcription regulation [15–

18]. Therefore, the balance between positive and negative aspects of ROS must be carefully maintained in ticks. If this balance is disturbed and the ROS level becomes too high, it causes harm to proteins, lipids, or DNA and eventually leads to cellular death and cellular necrosis. This is known as oxidative stress [8,19–21]. Oxidative stress not only results in individual cell death, but also affects tick blood feeding and reproduction [20,22,23]. To achieve redox homeostasis, the ticks have a complex anti-oxidant system composed of enzymes including glutathione-S-transferases (GST) and ferritins (Fer) [11,15,20,24–28].

Table 1. ROS generation in the ticks

Function	Reference
Metabolic activity for survival and growth	
1. Cellular processes and enzyme activity (including hatching and molting)	[29]
2. Embryonic development and larval maturation	[14]
Blood-feeding	
1. Fenton reaction due to the ferrous iron in the blood-meal	[26]
2. ROS from the neutrophils and macrophages in the host blood	[11]
3. ROS generation by the normal microflora during blood-meal	[15]
Pathogen infection	
1. Microbial killing by ROS	[30]
2. Apoptosis signaling by ROS	[31]

Glutathione s-transferases are ubiquitous enzymes found in diverse organisms, from microbes to arthropods to mammals. They are known to be involved in the Phase-II metabolism, wherein they catalyze the conjugation of xenobiotics to a reduced glutathione (GSH) for further elimination [32,33]. This detoxification activity placed GST among the most studied molecules with regard to acaricide metabolism in ticks [34–37]. Besides xenobiotic compounds, GST also metabolizes oxidative stress products and possesses peroxidase activity [33]. A recent study also showed an inducble GST in ticks with heme-binding ability that may reduce the heme's pro-oxidant activity [38]. Ticks are exposed to high amounts of ROS during blood feeding and the expression of *GST* genes are upregulated as a protection of the tick cells from oxidative stress [39–41].

Ferritin is an iron-binding molecule that is present in almost all organisms [8]. In hard ticks, two types of Fer have been identified, the intracellular type and the secretory type [7,26]. Oxidative stress in ticks is usually brought by ROS generated in the Fenton reaction due to the ferrous iron in the tick's diet. The tick utilizes Fer by sequestering ferrous iron and converting it to the less toxic ferric iron in its core [8]. The secretory Fer is transcriptionally regulated during blood feeding, but the intracellular *Fer* gene is constitutively expressed [26,42]. The intracellular Fer is post-transcriptionally regulated

through the interaction of iron-responsive elements in the *Fer* mRNA and iron-regulatory proteins [7,24].

In this study, I explored the role of oxidative stress molecules in ticks particularly the GSTs and Fer and their properties. The oxidative stress related molecules are few of the leading candidates in the continuous search for target molecules for tick and tick-borne pathogen control. Their properties, including their temporal and spatial expression during blood-feeding, also led to their exploration in improvement of existing tick and tick-borne pathogen control methods as well as developing new ones.

This dissertation describes studies on GSTs and Fer of ticks and tick cells with the following specific objectives:

1. To identify and characterize the GSTs of *H. longicornis* during blood-feeding;
2. To evaluate the role of the GSTs in acaricide metabolism in *H. longicornis* ticks;
3. To characterize the expression of the oxidative stress molecules GST and Fer during the embryogenesis of *H. longicornis;*
4. To investigate on the inducibility of the expression of the intracellular Fer in a tick-derived cell line (ISE6 cells);
5. To develop an expression system-derived from tick cell line that is dependent on iron concentration.

CHAPTER 1

Identification and characterization of GSTs of the hard tick *Haemaphysalis longicornis* during blood-feeding

This work has been published as:

Hernandez EP, Kusakisako K, Talactac MR, Galay RL, Hatta T, Matsuo T, Fujisaki K, Tsuji N, Tanaka T. (2018). Characterization and expression analysis of a newly identified glutathione S-transferase of the hard tick *Haemaphysalis longicornis* during blood-feeding. *Parasit Vectors*, **11**, 91.

1.1 Introduction

Ticks are obligate hematophagous parasites prevalent worldwide. They serve as several disease vectors in humans and other animals [43]. *Haemaphysalis longicornis* is a tick with a distribution in Australia, New Zealand and eastern Asia [44]. Ticks are known for their ability to ingest large volumes of blood from their hosts [45]. Blood contains potentially toxic molecules, such as iron, which can promote the production of hydroxyl radicals and reactive oxygen species (ROS) that can lead to oxidative stress [8]. Therefore, ticks must have protective mechanisms against oxidative stress. Previous studies have shown the role of ferritins, catalases and peroxiredoxins as coping mechanism during periods of oxidative stress [14].

Glutathione S-transferases (GSTs) are enzymes known to conjugate xenobiotic compounds, such as drugs and pesticides, with glutathione (GSH) for their metabolism. Aside from this, they are also involved in the catalysis of fatty acid reduction and the metabolism of phospholipids and DNA hydroperoxidases, which are all products of oxidative stress [33]. Several studies of GSTs either involved measuring their enzymatic activity [46] or analyzing their gene expression profile [41]; however, these methods have limitations. According to Hayes et al. [47], studies of GST activity do not take into consideration GST's ability to bind to molecules other than its substrate that would inhibit

its activity. On the other hand, several studies have shown the presence of post transcriptional factors that could present differences between gene and protein expressions of GSTs [48,49]. Thus, studies involving immunohistochemistry are necessary to establish the relationship between GST localization and its function to fully understand the tick detoxification pathway involving GSTs.

A GST of *H. longicornis* has been previously identified and partially characterized [44]. Additionally, GSTs of other tick species such as *Rhipicephalus* (*Boophilus*) *microplus*, *R. appendiculatus*, *Dermacentor variabilis*, *R.* (*B.*) *annulatus* and *R. sanguineus*, have been identified and characterized [35,37,40,44,50,51]. Here, I have identified a novel GST from *H. longicornis* and characterized its role through its activity, gene transcription, protein expression, and protein localization during the course of blood-feeding to evaluate its potential in designing a new method of tick control.

1.2 Materials and Methods

1.2.1 Ticks and animals

The parthenogenetic Okayama strain of *H. longicornis* was used in all experiments throughout this study. Ticks were maintained by feeding on the ears of Japanese white rabbits (KBT Oriental, Saga, Japan) for several generations at the

Laboratory of Infectious Diseases, Joint Faculty of Veterinary Medicine, Kagoshima University, Kagoshima, Japan [52]. Rabbits were also used in all tick infestation experiments. Twelve 4-week-old female ddY mice (Kyudo, Kumamoto, Japan) were used for GST antiserum preparation. Experimental animals were kept at 25 °C and 40% relative humidity, with a constant supply of water and commercial feeds. The ticks, on the other hand was maintained in glass tubes sealed with cotton plug and maintained at 15 °C and 80–85% relative humidity in an incubator until use. The care and use of experimental animals in this study were approved by the Animal Care and Use Committee of Kagoshima University (approval numbers VM15055 and VM15056 for the rabbits and mice, respectively) in accordance with the standards of the Association for Assessment and Accreditation of Laboratory Animal Care (AAALAC) International.

1.2.2 Identification and characterization of GST cDNA clones

The expressed sequence tags (EST) database of *H. longicornis* was analyzed and searched for genes encoding GSTs. Plasmids containing inserts for the two *GST*s were extracted using the Qiagen Plasmid Mini Kit (Qiagen, Hilden, Germany) and underwent sequencing using an automated sequencer (ABI PRISM 3100 Genetic Analyzer; Applied Biosystems, Foster City, CA, USA) to determine the full-length sequence. The deduced

amino acid translation of GST genes was determined using GENETYX software (Genetyx, Tokyo, Japan). A homologous search of the full-length *GST* sequences was performed using BLAST programs, through which conserved domains were also identified. The presence of a signal peptide was checked using the SignalP 3.0 prediction server (http://www.cbs.dtu.dk/services/SignalP/), and the predicted molecular weight and isoelectric points (pIs) were determined using the ExPASy server (http://web.expasy/org/peptide_mass/). Analysis for *N*-glycosylation was performed using the NetNGLyc 1.0 server (http://www.cbs.dtu.dk/services/NetNGlyc/). A phylogenetic tree was constructed based on the amino acid sequences of GSTs from selected species by the neighbor-joining method using the Phylogeny.fr server (http://www.phylogeny.fr/). Multiple sequence alignments between GSTs among tick species were also done using the BOXSHADE software (http://www.ch.embnet.org/software/BOX_form.html). Molecular models of GSTs were also constructed using PHYRE2 software (http://www.sbg.bio.ic.ac.uk/phyre2/) and analyzed using PyMOL software (www.pymol.org).

1.2.3 Preparation of recombinant GSTs

The open reading frames (ORF) of the two *GST* genes were amplified using gene-specific primers: HlGST *Bam*HI forward, HlGST *Eco*RI reverse, HlGST2 *Bam*HI forward, and HlGST2 *Eco*RI reverse (Table 1.1). PCR was conducted using a KOD-Plus-Neo PCR Kit (Toyobo, Osaka, Japan) following the manufacturer's protocol. The PCR profile was as follows: 94 °C for 2 min, 45 cycles of the denaturation step at 98 °C for 10 s, and an annealing/extension step at 68 °C for 45 s. PCR products were purified using a GENECLEAN II Kit (MP Biomedicals, Solon, OH, USA), and then subcloned into the pRSET A vector (Invitrogen, Carlsbad, CA, USA). The resulting plasmids were checked for accurate insertion through the analysis by restriction enzymes *Bam*HI and *Eco*RI, and the target sequences were read using the automated sequencer. The plasmids were purified using the Qiagen Plasmid Mini Kit (Qiagen). The purified plasmids were expressed in *Escherichia coli* BL21 cells, grown in Luria-Bertani (LB) broth medium with ampicillin. The synthesis of recombinant GSTs tagged with histidine was induced with isopropyl β-D-1-thiogalactiopyranoside (IPTG) at a final concentration of 1 mM. Cells were collected by centrifugation, and protein was extracted through ultrasonication. Purification was carried out using a HisTrap column (GE Healthcare, Uppsala, Sweden) and then dialyzed against phosphate buffered saline (PBS). The purity was checked using

sodium dodecyl sulphate polyacrylamide gel electrophoresis (SDS-PAGE) analysis and Western blotting using the anti-Histidine antibody (GE Healthcare). The protein concentration was determined through SDS-PAGE using bovine serum albumin as the standard. Micro BCA Protein Assay Kit (Thermo Scientific, Rockford, IL, USA) was also used to check the protein concentration.

1.2.4. Enzyme activity assay

The enzymatic activity of recombinant GSTs was measured according to the methods of Habig [53] using 1-chloro-2,4-dinitrobenzene (CDNB) (Sigma-Aldrich, St. Louis, MO, USA) as a substrate. Two hundred microliters of the reaction mixture consisting of a final concentration of 1 mM CDNB dissolved in methanol, 5 mM glutathione, and 120 μM recombinant GSTs in 100 mM Tris-HCl (pH 7.5) or without recombinant GST for the blank was tested in a 96-well plate. Methanol concentration was maintained at 5%. Equine liver GST and the *H. longicornis* peroxiredoxin enzyme were used as the positive and negative control, respectively. The absorbance (A_{340nm}) was measured each minute in an SH-9000 microplate reader (Corona Electric, Ibaraki, Japan) at 25 °C for 5 min. The extinction coefficient of 9.6 $mM^{-1}cm^{-1}$, corrected for the 96-well microplate light path, was used. Each assay was done in triplicate, and the results were

expressed as the mean of three separate experiments. The effect of pH on the recombinant GSTs was measured, using the previously described procedure and changing the buffer to either 100 mM citrate buffer (pH 5.0 and 5.5) or Tris-HCl buffer (pH 6.8, 7.5, 8.0 and 9.5).

The same procedure was utilized for enzymatic activity; however, different concentrations of CDNB (0.125, 0.25, 0.5, 1 and 2 mM) in methanol and a constant 5 mM GSH or different concentrations of GSH (0.5, 1, 2 and 5 mM) with a constant 1 mM CDNB in 100 mM Tris-HCl buffer (pH 7.5) were used. Each assay was done in triplicate, and the results are expressed as the mean of three separate experiments. Kinetic constants K_m and V_{max} were calculated from a double-reciprocal plot of 1/v *versus* a 1/[S] or Lineweaver-Burk plot in which V_{max} = 1/y-intercept of the regression line and $K_m = V_{max}$ × slope of the regression line.

1.2.5. Preparation of mouse anti-GST sera

To prepare mouse anti-GST sera, 6 mice for each GST were used and each mouse was injected intraperitoneally with 0.5 ml of 200 μg/ml of recombinant GST completely mixed with an equal volume of Freund's Complete Adjuvant (Sigma-Aldrich) to give each mouse 100 μg recombinant protein. Immunization was repeated 14 and 28 days after

the first immunization; however, recombinant GST was mixed with incomplete adjuvant (Sigma-Aldrich). All sera were collected 14 days after the last immunization. Antisera were tested using Western blotting, using both recombinant GSTs and tick protein.

1.2.6. RNA interference

RNA interference using double-stranded RNA (dsRNA) was performed to check for cross-reactivity between the GST antisera. The PCR primers used for the synthesis of dsRNA are listed in Table 1.1. The *HlGST* and *HlGST*2 fragments were amplified by PCR from plasmid clones using oligonucleotides, including HlGST T7 forward with HlGST RNAi reverse and HlGST T7 reverse with HlGST RNAi forward primers, as well as HlGST2 T7 forward with HlGST2 RNAi reverse and HlGST2 T7 reverse with HlGST2 RNAi forward primers, to attach the T7 promoter recognition sites on both forward and reverse ends. Enhanced green fluorescent protein (*EGFP*) was amplified from *pEGFP* through PCR using oligonucleotides containing EGFP T7 forward and EGFP T7 reverse primers as well. PCR products were purified using a GENECLEAN II Kit (MP Biomedicals). The T7 RiboMAX Express RNAi System (Promega, Madison, WI, USA) was used to synthesize dsRNA by *in vitro* transcription. The successful construction of dsRNA was confirmed by running 1 µl of the dsRNA products in 1.5% agarose gel in a

TAE buffer. 0.5 µl of 2 µg/µl of *HlGST*, *HlGST2*, and *HlGST1/2* (*HlGST* and *HlGST2* mixed at 2 µg/µl concentration each) dsRNA dissolved in high-purity water were injected to the hemocoel of unfed adult female ticks through the fourth coxae to give each tick 1 µg of dsRNA. A total of 10 ticks per group were injected with dsRNA. The control group was injected with *EGFP* dsRNA. After injection, the ticks were held for 24 h in a 25 °C incubator to check for mortality resulting from injury during injection. The ticks were then to feed on rabbits for four days, and then the partially fed ticks were collected. Total RNA was extracted from five whole 4-day-fed ticks, and their cDNA was synthesized. cDNA was subjected to RT-PCR with a Hot Start Pol system (Jena Bioscience, Jena, Germany) using *GST*-specific primers, HlGST RT forward and HlGST RT reverse primers, and HlGST2 RT forward and HlGST2 RT reverse primers, following the manufacturer's instructions. The PCR cycle profile was as follows: 94 °C for 8 min, 30 cycles of a denaturation step at 94 °C for 30 s, an annealing step at 68 °C for 60 s, and an extension step at 72 °C for 60 s. The PCR products were run in 1.5% TAE agarose gels and stained with ethidium bromide. *Actin* was used as a loading control. The absence of bands corresponding to *HlGST* and *HlGST2* in their corresponding GST knockdown group demonstrates that silencing was successful (Fig 1.1). Proteins were extracted and prepared from the remaining ticks of different knockdown groups for Western blotting

using the prepared anti-GST sera. Mouse tubulin antiserum was used as a control for Western blotting. The absence of signals corresponding to HlGST in the *HlGST* knockdown group and HlGST2 in the *HlGST2* knockdown group demonstrates that the antibodies produced are specific and do not cross react; therefore, they could be used in succeeding experiments (Fig 1.1).

1.2.7. Total RNA extraction and real-time PCR analysis

Total RNA was extracted from different developmental stages (egg, larva, nymph and adult) and organs of adult female ticks, including the midgut, salivary glands, ovaries, fat body, and hemocytes during blood-feeding. Whole tick samples were homogenized using an automill (Tokken, Chiba, Japan) and were added to TRI® Reagent (Sigma-Aldrich). On the other hand, organs such as salivary glands, midguts, fat bodies, and ovaries were dissected and washed in PBS, placed directly in tubes with the TRI reagent, and homogenized. Hemocytes were collected through the legs of ticks as previously described [54]. RNA extraction was performed following the manufacturer's protocol. Subsequently, single-strand cDNA was prepared by reverse transcription using the ReverTra Ace® cDNA Synthesis Kit (Toyobo), following the manufacturer's protocol. Transcription analysis of *HlGST* and *HlGST2* genes was performed through

real-time PCR using THUNDERBIRD™ SYBR® qPCR Mix (Toyobo) with an Applied Biosystems 7300 Real-Time PCR System using gene-specific primers, HlGST real-time forward and HlGST real-time reverse, and HlGST2 real-time forward and HlGST2 real-time reverse primers (Table 1.1). Standard curves were made from fourfold serial dilutions of the cDNA of adult ticks fed for 3 days. The PCR cycle profile was as follows: 95 °C for 10 min, 40 cycles of a denaturation step at 95 °C for 15 s, and an annealing/extension step at 60 °C for 60 s. The data was analyzed with Applied Biosystems 7300 system SDS software. In the first step of real-time PCR, *actin*, *tubulin*, *P0*, and *L23* genes were evaluated for standardization. *P0* genes were selected as an internal control for the whole ticks, while *L23* genes were chosen for the tick organs.

1.2.8. Protein extraction and Western blotting analysis

Protein was extracted at different developmental stages and from different organs of adult female ticks during blood-feeding. For different developmental stages, whole tick samples were homogenized using an automill (Tokken), and then suspended in PBS treated with Complete Mini Proteinase Inhibitor Cocktail Tablets (Roche, Mannheim, Germany). Eggs and organs were homogenized using a mortar, and they were also suspended in PBS treated with a proteinase inhibitor. After sonication and recovery

of the supernatant, tick proteins were separated with a 12% SDS-polyacrylamide gel electrophoresis (SDS-PAGE) and transferred to a polyvinylidene difluoride (PVDF) membrane (Millipore, Billerica, MA, USA). The membrane was blocked overnight with 3% skim milk in PBS with 0.05% Tween 20, and then incubated with a primary antibody using mouse anti-GST sera (1:1000 dilution) for 1 h. β-tubulin was used as a control [55]. After incubation with horseradish peroxidase-conjugated goat anti-mouse IgG (1:50,000 dilution; DakoCytomation, Glostrup, Denmark) for 1 h, the signal was detected using Clarity™ Western ECL Substrate (Bio-Rad Laboratories, Hercules, CA, USA) or Amersham™ ECL™ Prime Western Blotting Detection Reagent (GE Healthcare, Buckinghamshire, UK). It was analyzed using FluorChem FC2 software (Alpha Innotech, San Leandro, CA, USA).

1.2.9. Indirect immunofluorescent antibody test

An indirect immunofluorescent antibody test (IFAT) was performed to demonstrate the endogenous localization of GSTs, as described previously [23]. The salivary glands, midguts, ovaries, and fat bodies of ticks at different stages of blood-feeding were immediately dissected under a stereo microscope. Dissected organs were fixed overnight in 4% paraformaldehyde in PBS with 0.1% glutaraldehyde and then

washed with different concentrations of sucrose in PBS. The organs were embedded in Tissue-Tek OCT Compound (Sakura Finetek Japan, Tokyo, Japan) and then frozen using liquid nitrogen. Sections 10 μm thick were cut using a cryostat (Leica CM3050; Leica Microsystems, Wetzlar, Germany) and placed on MAS-coated glass slides (Matsunami Glass, Osaka, Japan). After blocking for 1 h with 5% skim milk in PBS at room temperature, sections were incubated with a 1:100 dilution of anti-GST sera overnight at 4 °C. Normal mouse serum at the same dilution was used as a negative control. Sections were washed with PBS and then incubated with Alexa Fluor 488-conjugated goat anti-mouse IgG (1: 1,000; Invitrogen) for 1 h at room temperature. After washing with PBS, sections were mounted in Vectashield with DAPI (Vector Laboratories, Burlingame, CA, USA). Images were taken using a confocal fluorescence microscope mounted with an LSM 700 (Carl Zeiss, Jena, Germany).

1.2.10. Statistical analysis

Student's *t*-test was used to analyze data from the real-time PCR of ticks and organs. A significant difference is defined as $P < 0.05$. All experiments were done at least twice for validation.

1.3 Results

1.3.1 Identification and characterization of GST cDNAs

Two cDNAs encoding glutathione S-transferase were identified and cloned. The open reading frame of the first *GST* gene contains 672 base pairs (bp) from the predicted start codon to the predicted end codon, encodes 223 amino acid polypeptides (Fig. 1.2), and has a calculated molecular weight of ~25.7 kDa and a pI of 7.67. No glycosylation site or signal peptide was predicted. An N-terminal domain containing the glutathione binding site and a C-terminal domain containing the 105 amino acids substrate binding site were present (Fig 1.3). Since BLAST and multiple sequence alignment analysis showed that it has 99% homology with the previously identified *H. longicornis* GST (HlGST) (GenBank: AAQ74441), it is considered the same as HlGST (Fig 1.4). It also showed high homology to the GSTs of *D. variabilis* (91%), *R. sanguineus* (87%), and *I. scapularis* (GenBank: XP_002401749.1) (85%) (Fig. 1.4).

On the other hand, the open reading frame of the second GST has 693 bp from the predicted start codon to the predicted end codon, encodes 230 amino acid polypeptides (Fig 1.2), and has a calculated molecular weight of ~26.3 kDa and a pI of 6.83. No glycosylation site or signal peptide was predicted. It also has an N-terminal domain containing the glutathione binding site and a C-terminal domain containing the 65 amino

acids substrate binding site (Fig 1.3). I found the second GST novel and submitted to GenBank where it was assigned the accession number LC270263.1. I refer to the novel GST as HlGST2. HlGST2 has 64% homology with the putative GST of *I. scapularis* (GenBank: XP_002434207.1) (Fig. 1.4).

A phylogenetic tree was also constructed using amino acid sequences of GSTs from different species to further analyze the identity of the GSTs (Fig. 1.5). HlGST was found to be closely related to the mu-class GSTs of *D. variabilis* and *I. scapularis* (GenBank: XP_002401749.1), while HlGST2 is closely related to *I. scapularis* GST (GenBank: XP_002434207.1). These results demonstrate that the newly identified HlGST2 also belongs to the mu-class of GST, due to its more than 40% similarity to the mammalian mu-class of GST [33] and the presence of the mu-loop (Fig. 1.3) [56].

1.3.2 Expression of recombinant GSTs

The expression of recombinant GSTs was performed using *E. coli* BL21 cells with pRSET A as the vector. The expression was induced by IPTG at a final concentration of 1 mM at 37 °C. After expression, purification by affinity chromatography was carried out. The eluted protein was checked by 12% SDS-PAGE and seen as single bands, which indicated purity. The purified recombinant HlGST molecular weight was approximately

28 kDa, while recombinant HlGST2 has an approximate molecular weight of 29 kDa. Recombinant GSTs contain fragments of the his-tag protein, which could account for the difference in the calculated molecular weights of 25.7 kDa and 26.3 kDa for HlGST and HlGST2, respectively (Fig. 1.6a). Western blotting using an anti-histidine antibody showed positive signals, indicating the presence of histidine-tagged GSTs (Fig. 1.6b). These results demonstrate the successful expression of histidine-tagged recombinant GST using the *E. coli* expression system.

1.3.3 GST specific enzymatic activity

The specific activity of recombinant HlGST and HlGST2 was determined through its ability to conjugate CDNB. CDNB has been used as a substrate in previous studies, and it has shown that mu-class GSTs react better with CDNB as compared with other substrates, such as 1,2-dichloro-4-nitrobenzene (DCNB) [51]. The enzymatic activity of recombinant GSTs toward CDNB is 9.75 ± 3.04 units/mg protein for recombinant HlGST and 11.63 ± 4.08 units/mg protein for recombinant HlGST2 (Table 1.2). Recombinant HlGST2 appears to have higher enzymatic activity than HlGST. To further characterize the GSTs, the optimum pH of the activity of recombinant GSTs was determined by checking its activity in buffer with different pHs. The pH at which the

activity of both GSTs is the highest, or the optimum pH, is 7.5–8.0 (Fig. 1.7). These results demonstrate that the expressed recombinant GSTs could conjugate GSH with the substrate CDNB and possess almost the same rate of conjugation activity in a similar range of pH.

1.3.4 Enzyme kinetics of GSTs

To further establish the characteristics of these GSTs, lethal doses of acaricides. I determined the enzyme kinetics constants of these GSTs, using the Michaelis-Menten equation and the Lineweaver-Burk plot. When the concentration of GSH is kept constant, HlGST has a V_{max} of 11.70 ± 1.92 units/mg protein and a K_m of 0.82 ± 0.14 mM, whIdetermined the enzyme kinetics constants of these GSTs, using the Michaelis-Menten equation and the Lineweaver-Burk plot. When the concentration of GSH is kept constant, HlGST has a V_{max} of 11.70 ± 1.92 units/mg protein and a K_m of 0.82 ± 0.14 mM, whereas HlGST2 has a V_{max} of 14.72 ± 0.56 units/mg protein and a K_m of 0.61 ± 0.20 mM. Meanwhile, when the concentration of CDNB is kept constant, HlGST has a V_{max} of 10.40 ± 1.77 units/mg protein and a K_m of 0.64 ± 0.32 mM, whereas HlGST2 has a V_{max} of 11.01 ± 0.21 units/mg protein and a K_m of 0.53 ± 0.19 mM (Table 1.3). These results demonstrate that recombinant GSTs have a high affinity toward GSH and the known GST

substrate, CDNB. They also indicate a high ability of the recombinant GSTs to conjugate with CDNB and GSH.

1.3.5 Transcription profiles of GSTs

The transcription profiles of *HlGST* and *HlGST2* genes from different developmental stages and organs of ticks during blood-feeding were checked using real-time PCR (Fig. 1.8). It was observed that both *HlGST* and *HlGST2* genes were constitutively expressed at all developmental stages, with increasing expression observed toward engorgement in the nymph and adult stages for *HlGST* genes and in all stages for *HlGST2* genes. Relatively strong expressions of both *HlGST* and *HlGST2* genes were observed in the eggs. The gene transcription during the larval stages shows that *HlGST* appears to be maintained at a high transcription level. Both *HlGST* and *HlGST2* genes were also expressed in all organs. In different organs of female ticks, such as the salivary glands, ovaries, fat bodies, and hemocytes, gene expression increases as blood-feeding progresses, continuously increasing until engorgement. In the midgut, increasing transcription during the course of blood-feeding was also observed, except in the engorged stage, wherein there is a decreased expression of both HlGST and HlGST2 genes. These results demonstrate that blood-feeding can trigger an upregulation of the

transcription of GST genes. This fact could indicate the genes' possible role in coping with oxidative stress caused by blood-feeding.

1.3.6 Protein expression profiles of GSTs

The protein expression of endogenous GSTs in different developmental stages and organs was determined through Western blotting analysis using specific anti-GST sera (Fig. 1.9). The GST protein expression during the larval stage has a tendency to decrease during the course of blood-feeding to engorgement, while in the nymph and adult stages, protein expression tends to increase during feeding and then decrease at the end of blood-feeding. In the midgut and hemocytes, GST expression increased during the partially fed state of blood-feeding; however, in other organs examined, such as the salivary glands, fat body, and ovaries, the expression of both HlGST and HlGST2 proteins decreased as blood-feeding progressed to engorgement. These results demonstrate that GST protein expression in ticks is upregulated during periods of increased oxidative stress, specifically on organs exposed to such oxidative stress, such as the midgut. This further confirms the anti-oxidant function of GSTs during blood-feeding.

1.3.7 Localization of HlGST and HlGST2 in different organs using IFAT

The localizations of endogenous HlGST and HlGST2 in partially fed adult salivary glands, midguts, fat bodies, ovaries, and hemocytes were demonstrated using IFAT (Fig. 1.10). Both HlGST and HlGST2 are found in the cytoplasm of cells. GSTs in the salivary glands are observed in the ducts and its epithelial cells of the non-degenerated acinus. A positive reaction was observed in the apical part of the epithelium of the midgut cells. In the fat body, a positive reaction was observed in the tracheal complex. In the ovaries, a positive reaction for GST was observed mainly in the pedicels and ovarian wall. Positive fluorescence in the cytoplasm of hemocytes was also observed. However, strong HlGST2 fluorescence was observed on the periphery of the hemocytes, while for HlGST, it was observed at scattered locations throughout.

IFAT was used to further characterize the role of GSTs in major organs such as salivary glands, midguts, and ovaries from female ticks at different blood-feeding stages (Fig. 1.11). In the salivary glands, GSTs are spread throughout the acinus; however, during blood-feeding, GSTs shift to being more expressed in the ducts during the partially fed and engorged stages. In the unfed midgut, fluorescence is also scattered throughout the digestive cells, then shifts toward the apical part of the epithelium in partially fed ticks and toward the basal membrane in the engorged stage. Fluorescence is limited in the

ovarian wall and the pedicels of the ovary, but not in the oocytes, throughout the duration of blood-feeding. These results demonstrate that GST proteins tend to vary depending on the blood-feeding stage and eventually the levels of oxidative stress.

1.4 Discussion

Multiple isoenzymes of GSTs have been observed in all eukaryotes. *In silico* analysis of the *Ixodes scapularis* gene database showed 35 genes of *GST*s, of which 14 belong to the mu-class GST [57]. In *Dermacentor variabilis* and *Rhipicephalus* (*Boophilus*) *annulatus*, multiple GSTs have also been found [40,58]. The presence of multiple forms of GSTs could prove to be important for species to counter most, if not all, foreign or endogenous compounds that could affect them [51]. One GST has already been identified and partially characterized in *H. longicornis* [44]. Here, a novel GST from *H. longicornis*, HlGST2, was identified and characterized with the previously identified HlGST.

The smaller predicted substrate binding site of HlGST2 located at the C-terminal domain could account for the faster activity rate of HlGST2 because of the possibly fewer enzyme-substrate interactions that could slow the rate of product release from the enzymes [59].

The effect of pH on enzymatic activity has been an important factor in determining the protein structure and function [51]. The optimal pH for activity toward CDNB of 7.5–8.0 is in the same range as that of *R.* (*B.*) *annulatus* GST. The optimum pH could vary depending on the compound used to test the GST activity, which could range from 6.5–9.5. If I consider only CDNB, the values also represent the modal tendency of several species at pH 7.5–8.0. Loss or decrease of enzymatic activity at lower or higher pH could be the result of the ionizing activity of both CDNB and GSH that occurs at pH 6–7 [51,60]. This result could indicate stability and the capability of GSTs to function in conditions closer to intracellular conditions.

The V_{max} values for both recombinant GSTs are below those of the recombinant GST of *R.* (*B.*) *annulatus* (rBaGST), which are 75.2 units/mg protein for CDNB and 48.8 units/mg protein for GSH, it is important to consider that the presence of galactosidase in rBaGST or the histidine tag in *H. longicornis* recombinant GSTs could result in an altered level of activity of recombinant GSTs. The relatively low K_m values (< 1) of both GSTs for both GSH and CDNB may indicate a high rate of conjugation that could be attributed to the enzymes [56]. These K_m values are close to the K_m values for rBaGST, which are 0.57 mM and 0.79 mM for functions of CDNB and GSH, respectively [35]. The K_m values of GSH are also close to the values frequently cited in various literature (61%), which fall

in a range of 0.19–0.79 mM [60]. Thus, it is reasonable to think that this newly identified HlGST2 of the hard tick, *H. longicornis*, could provide the tick with a coping mechanism for metabolizing xenobiotic and endogenous products. In addition, these enzyme kinetic parameters could be a basis for comparison for future inhibition studies, in which changes in these values could determine the type of inhibition if an inhibitor is added.

Upregulation of *GST* genes during blood-feeding suggest the importance of GSTs to oxidative stress management. It has also been assumed that reactive oxygen is a transduction signal that mediates the gene transcription of *GSTs* [61]. Thus, during blood-feeding, when the intracellular digestion of blood is high, high levels of reactive oxygen species are produced, which could induce the transcription of *GST* genes [40]. Upregulation brought about by blood-feeding was also observed in other blood-feeding arthropods, such as the *Aedes aegypti* [46], and in other ticks, such as *I. ricinus* and *R.* (*B.*) *microplus* [37,62]. A high gene transcription profile is observed in eggs since they undergo rapid metabolism due to embryonic development, which could result in the production of an endogenous toxic substance in the eggs; thus, detoxification enzymes are important [14]. Interestingly, the downregulation of *GST* genes during blood-feeding was only observed in the engorged midgut. This could indicate that during this state, the amount of oxidative stress in midgut cells is reduced. The decreased expression could be

a result of the nature of blood-feeding in ticks. At the start of blood-feeding, gut epithelia undergo a slow feeding phase, in which the tick prepares its midgut cells for blood intake. Here, some undifferentiated cells begin to differentiate and proliferate. This is also the period in which there is a rapid digestion of ingested cells. In effect, during this stage, ticks are more prone to oxidative stress brought about by rapid metabolism due to cell differentiation and proliferation, and the lysis of ingested cells that leads to the liberation of compounds may also trigger oxidative stress, such as heme aggregates. Afterward, ticks undergo a fast feeding period and eventually drop off the host. During this stage, the midgut would then act as a blood reservoir and the rate of intracellular digestion also becomes low [1]. Low intracellular digestion also results in low ROS emergence and low iron metabolism. The downregulation of mu-class *GST*s was also observed in engorged midgut cells of *I. ricinus.* [40]. Since GST proteins are said to be transcriptionally regulated [61], protein expression in the midgut also appeared to decrease during the engorged stage.

Western blotting analysis revealed decreasing expression in several organs, such as salivary glands, fat bodies, and ovaries, as compared with their increasing gene transcription profile. The decreased oxidative stress during the engorged stage, even with increased transcription in these organs, resulted in an expression level of GST proteins

below the Western blotting's capability to detect. The movement of heme, a potentially oxidant molecule, through its carrier protein throughout blood-feeding and, most especially, during the post attachment stage [6,63], could trigger the upregulation of gene transcription in these organs.

In the salivary glands, the decrease in GST protein expression could also be due to GSTs being secreted through the saliva during the fully engorged stage, as previously observed in other tick species, such as *H. longicornis*, *I. scapularis*, and *Amblyomma americanum* [64–66]. IFAT results also demonstrated this possible release, as manifested by the apparent shift of GSTs from the acinus toward the salivary ducts during blood-feeding. The release of GST from its cytosolic localization has also been reported in mammalian organs such as plasma from the platelets, bile from the liver, and seminiferous tubule fluid from the testes. The release is said to be an energy-requiring active process rather than a secretory process [67–69]. The release could be a possible extracellular detoxification capability of GSTs. The degeneration process in the salivary glands during the end of blood-feeding could also be a factor in the decrease of protein expression, as it may cause the release of the GST protein. However, these are just proposed theories, and further studies are warranted to validate these claims. IFAT results also indicated an apparent movement of GSTs from whole cells in the unfed to the apical area of the

epithelium in the partially fed to the basal cells in the engorged stage. This apparent movement of GSTs during blood-feeding could indicate the specific location in the midgut where there is exposure to exogenous substances in the blood meal. GST expression could then be an indicator of the amount and location of oxidative stress in the midgut. Among the organs, the midgut showed the highest gene and protein expression; its level of expression could determine the overall trend of GST protein in whole ticks as observed in nymphs and adults.

IFAT results of the fat bodies showed positive fluorescence on the tracheal complex of ticks. This could indicate the role of GST in the detoxification of xenobiotic compounds that may enter ticks through their spiracles. The spiracles and tracheal systems of insects were also observed to be points of entry for insecticides. The presence of GSTs on the organs responsible for the exchange of gases was also observed in the gills of several marine species as well as human lungs [60,70–72]. In hemocytes, differences in localization were observed. While it is scattered in HlGST, surface localization was observed in HlGST2. Surface localization in mu-class GSTs was also observed in goat sperm [73]. This could be a key feature that needs further study as to how GSTs could play a role in the defense mechanism of the tick's hemocytes and its role in tick immunity.

IFAT of the ovaries showed positive fluorescence in the ovarian wall and into the pedicels. This could be an indication of the mechanism protecting the ovaries of ticks from environmental chemicals that may be acquired through the genital aperture, which is connected to the ovary *via* the oviduct [60,74]. Also, signals in the pedicels of the ovary could reflect its role in the development of oocytes. The presence of numerous mitochondria in the pedicels [75] indicates that they have very high activity, thus consuming lots of oxygen for ATP production. Therefore, pedicels are very metabolically active cells that generate ROS, which in turn could result in the expression of GSTs.

The possibility of the HlGST and HlGST2 antisera to cross react with other GSTs of *H. longicornis* in Western blotting and IFAT remains uncertain since anti-GST sera are known to cross react with other GST proteins with high homology [44,76]. Nevertheless, the similarity in the trend in expression and localization indicate how at least HlGST and HlGST2, if not all mu-class GSTs of *H. longicornis*, responds to the oxidative stress.

The expression and localization of GSTs in different organs may indicate how ticks use GSTs as protective mechanism to cope with oxidative stress that may vary according to the specific needs of each organ for the enzyme, either as a carrier protein or as being metabolically active [47].

To further investigate the importance of GST and its effects on tick survival during blood-feeding and on reproductive parameters such as engorgement weight, egg weight, and hatching rate, a gene knockdown experiment was performed; however, results of the gene knockdown experiment (Table 1.4) showed no significant differences in the above-mentioned parameters between the *GST*-knockdown group and the *EGFP*-knockdown group. In *R. microplus*, no significant differences were observed in terms of tick mortality and oviposition when *GST* is knocked down [77]. The probable reason is that GSTs could provide functional compensation between members of each family [78], although further studies must be conducted to prove this hypothesis. Vaccination experiments using the HlGST as the antigen, on the other hand, showed a decrease in the engorgement rate of ticks [76]. This could further establish the role of the GSTs during blood-feeding and reproduction, although the exact mechanism should be a subject of future studies.

In summary, a new GST in the hard tick *H. longicornis* was identified, and recombinant GSTs were synthesized. Both GSTs of *H. longicornis* were characterized *in silico*, using various available software applications; *in vitro*, through studying the enzymatic activity and kinetics; and *in vivo*, through its gene and protein expression in whole ticks and different organs during blood-feeding and organ localization. The results

have shown a positive correlation between the degree and localization of the GSTs with the degree and localization of oxidative stress occurring within the tick during blood-feeding. This close relationship could indicate that GSTs play a possible role in coping with oxidative stress brought about by blood-feeding

Tables and Figures in CHAPTER 1

Table 1.1 Gene-specific primers used in this study. Underlined letters indicate the enzymes recognition sites. RNA polymerase promoter sequence is indicated in italic

Primer	Sequence (5' → 3')
HlGST real-time forward	CTTCTTGGATCTTGGCGGGT
HlGST real-time reverse	CGATGTCCCAGTAGCCGAG
HlGST *Bam*HI forward	CGGGATCCATGGCTCCTATTCTCGGCT
HlGST *Eco*RI reverse	CGGAATTCTCAGCAGTCGTCAGCGGGCG
HlGST RT forward	ACGTGAAGCTCACCCAGAGCAT
HlGST RT reverse	AAGCTAGCCATGTCGCCGTTGA
HlGST RNAi forward	GCCTGGCTCAAGGAGAAACACA
HlGST RNAi reverse	ACAAAGGCCTTCAGGTTGGGGA
HlGST T7 forward	*TAATACGACTCACTATAGG*GCCTGGCTCAAGGAGAAACACA
HlGST T7 reverse	*TAATACGACTCACTATAGG*ACAAAGGCCTTCAGGTTGGGGA
HlGST2 real-time forward	CCCTTCCGGGAATGAAGGAG
HlGST2 real-time reverse	GATCGCTCAGCAGTCGTCAG
HlGST2 *Bam*HI forward	CGGGATCCATGGCCCCTGTGCTGGGATA
HlGST2 *Eco*RI reverse	CGGAATTCTCAGCAGTCGTCAGCGGGCG
HlGST2 RT forward	ACGTCAAGCTGACGCAGAGCAT
HlGST2 RT reverse	ATGGGCCAAGCCTTGAAGCGAT
HlGST2 RNAi forward	AGGATAAAAGGTACGGCTTCGGCA
HlGST2 RNAi reverse	TTTCACGATCTGGAGAGCCTCGTA
HlGST2 T7 forward	*TAATACGACTCACTATAGG*AGGATAAAAGGTACGGCTTCGGCA
HlGST2 T7 reverse	*TAATACGACTCACTATAGG*TTTCACGATCTGGAGAGCCTCGTA
P0 real-time forward	CTCCATTGTCAACGGTCTCA
P0 real-time reverse	TCAGCCTCCTTGAAGGTGAT
L23 real-time forward	CACACTCGTGTTCATCGTCC
L23 real-time reverse	ATGAGTGTGTTCACGTTGGC
Actin real-time forward	ATCCTGCGTCTCGACTTGG
Actin real-time reverse	GCCGTGGTGGTGAAAGAGTAG
Actin RT forward	CCAACAGGGAGAAGATGACG
Actin RT reverse	ACAGGTCCTTACGGATGTCC
Tubulin real-time forward	TTCAGGGGCCGTATGAGTAT
Tubulin real-time reverse	TGTTGCAGACATCTTGAGGC
EGFP T7 forward	*TAATACGACTCACTATAGG*GACGTAAACGGCCACAAGTT
EGFP T7 reverse	*TAATACGACTCACTATAGG*TGCTCAGGTAGTGGTTGTCG

Table 1.2 Specific activity of each recombinant GST with the substrate CDNB. Values are presented as mean ± SD. The concentration of CDNB and GSH used are 1 mM and 5 mM, respectively. Each experiment was performed at least three times and each assay was run in triplicate

Enzyme	**Enzyme activity (units/mg protein)**
Equine liver GST[a]	11.01 ± 2.60
rHlPRX2[b]	Nd
rHlGST[c]	9.24 ± 3.05
rHlGST2[d]	9.46 ± 1.97

[a]Equine liver GST was used as a positive control

[b]Recombinant *H. longicornis* peroxiredoxin2 was used as the negative control

[c]Recombinant HlGST

[d]Recombinant HlGST2

Abbreviation: nd, none detected

Table 1.3 Recombinant GST kinetic constants. Values are presented as mean ± SD. Each experiment was performed at least three times and each assay was run in triplicate

Enzyme	CDNB kinetic constant[a]	GSH kinetic constant[b]
rHlGST[c]		
V_{max} (units/mg protein)	11.70 ± 1.92	10.40 ± 1.77
K_m (mM)	0.82 ± 0.14	0.64 ± 0.32
rHlGST2[d]		
V_{max} (units/mg protein)	14.72 ± 0.56	11.01 ± 0.21
K_m (mM)	0.61 ± 0.20	0.53 ± 0.19

[a]CDNB, the common substrate, is used in increasing concentration from 0.125–2 mM to determine the kinetic constants

[b]GSH is used in increasing concentration for 0.5–5 mM to determine the kinetic constants

[c]Recombinant HlGST

[d]Recombinant HlGST2

Table 1.4 Effect of *HlGST* and/or *HlGST2* knockdown on ticks' engorgement and reproductive parameters

Groups	Engorgement rate of ticks (%)	Engorged body weight of ticks (mg)	Percentage of ticks that laid eggs (%)	Egg weight (mg)	Hatching rate (%)
dsEGFP	83.33 (25/30)	92.3±30.5	84.00 (21/25)	43.4±21.0	85.71 (18/21)
dsHLGST	86.67 (26/30)	116.2±29.2	100.00 (26/26)	51.6±20.4	84.62 (22/26)
dsHlGST2	83.33 (25/30)	129.6±31.6	92.00 (23/25)	60.0±18.9	91.30 (21/23)
dsHLGST1/2	93.33 (28/30)	130.46±36.1	92.86 (26/28)	59.8±21.0	61.54 (16/26)

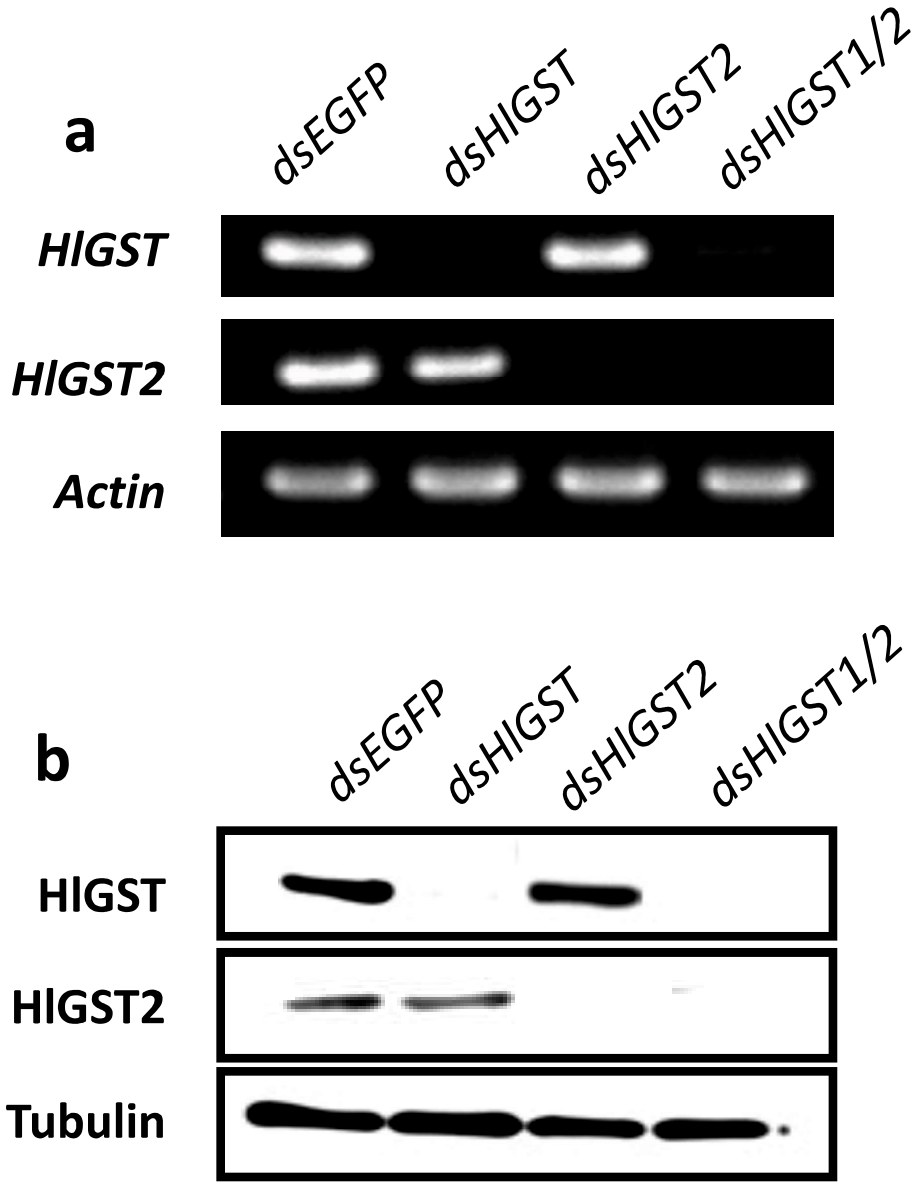

Fig. 1.1 RT-PCR(**a**) and Western blotting (**b**) of knockdown ticks. Ticks were silenced by injecting 1 μg of double-stranded RNA (dsRNA) per tick. **a** Total RNA was extracted from whole 4-day fed *GST* and *EGFP* knockdown ticks. cDNA was synthesized and subjected to RT-PCR. PCR products were run on 1.5% TAE agarose gel and stained with ethidium bromide. *Actin* was used as loading control. **b** Protein lysates were extracted from whole 4-day-fed *HlGST, HlGST*2*, HlGST1/2,* and *EGFP* knockdown ticks. Protein lysates were run on 12% SDS-PAGE gel before being transferred to polyvinylidene difluoride (PVDF) membranes and subjected to Western blotting. Mouse tubulin antiserum was used as control.

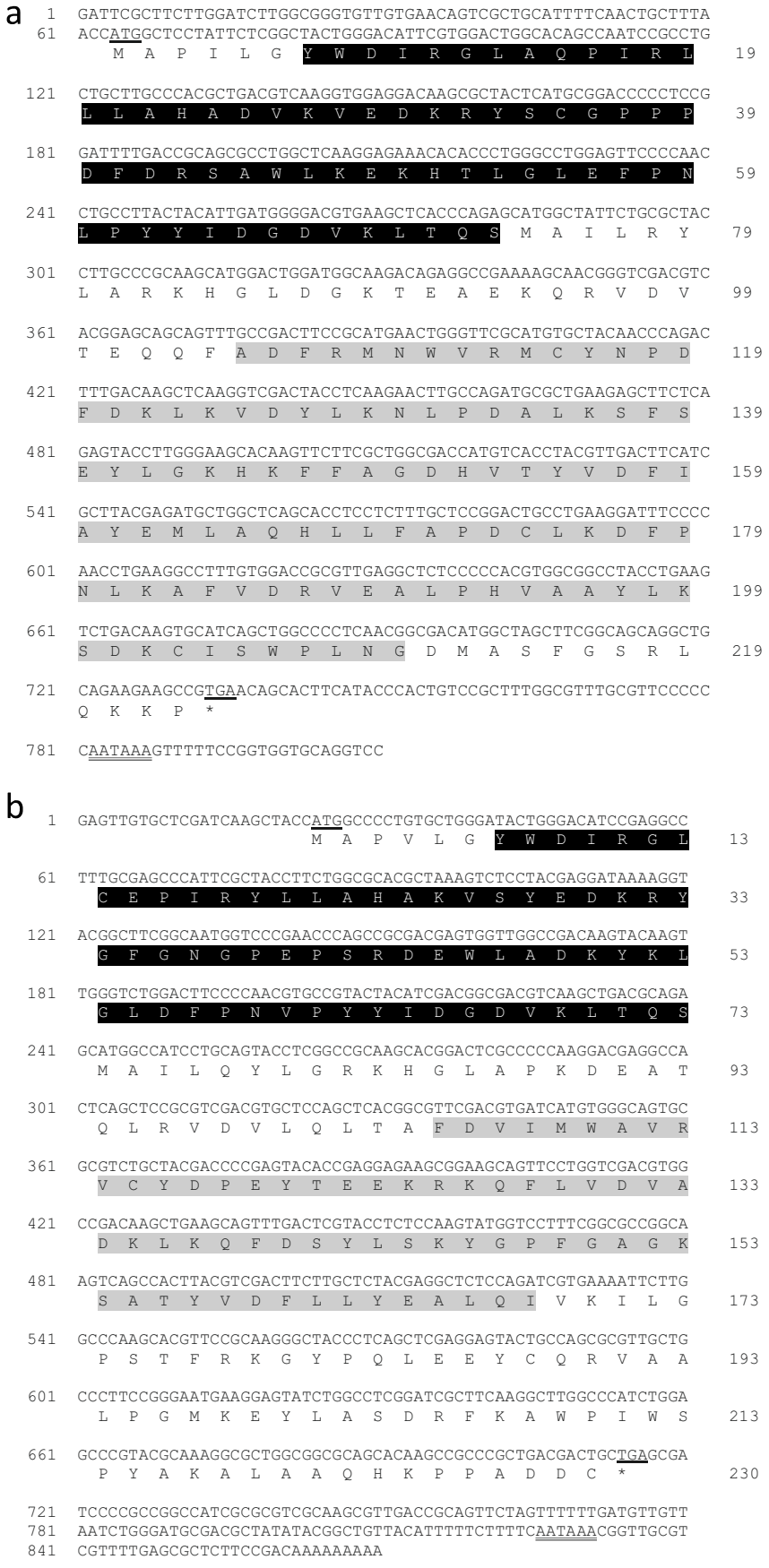
a
1 GATTCGCTTCTTGGATCTTGGCGGGTGTTGTGAACAGTCGCTGCATTTTCAACTGCTTTA
61 ACCATGGCTCCTATTCTCGGCTACTGGGACATTCGTGGACTGGCACAGCCAATCCGCCTG
M A P I L G Y W D I R G L A Q P I R L 19
121 CTGCTTGCCCACGCTGACGTCAAGGTGGAGGACAAGCGCTACTCATGCGGACCCCCTCCG
L L A H A D V K V E D K R Y S C G P P P 39
181 GATTTTGACCGCAGCGCCTGGCTCAAGGAGAAACACACCCTGGGCCTGGAGTTCCCCAAC
D F D R S A W L K E K H T L G L E F P N 59
241 CTGCCTTACTACATTGATGGGGACGTGAAGCTCACCCAGAGCATGGCTATTCTGCGCTAC
L P Y Y I D G D V K L T Q S M A I L R Y 79
301 CTTGCCCGCAAGCATGGACTGGATGGCAAGACAGAGGCCGAAAAGCAACGGGTCGACGTC
L A R K H G L D G K T E A E K Q R V D V 99
361 ACGGAGCAGCAGTTTGCCGACTTCCGCATGAACTGGGTTCGCATGTGCTACAACCCAGAC
T E Q Q F A D F R M N W V R M C Y N P D 119
421 TTTGACAAGCTCAAGGTCGACTACCTCAAGAACTTGCCAGATGCGCTGAAGAGCTTCTCA
F D K L K V D Y L K N L P D A L K S F S 139
481 GAGTACCTTGGGAAGCACAAGTTCTTCGCTGGCGACCATGTCACCTACGTTGACTTCATC
E Y L G K H K F F A G D H V T Y V D F I 159
541 GCTTACGAGATGCTGGCTCAGCACCTCCTCTTTGCTCCGGACTGCCTGAAGGATTTCCCC
A Y E M L A Q H L L F A P D C L K D F P 179
601 AACCTGAAGGCCTTTGTGGACCGCGTTGAGGCTCTCCCCCACGTGGCGGCCTACCTGAAG
N L K A F V D R V E A L P H V A A Y L K 199
661 TCTGACAAGTGCATCAGCTGGCCCCTCAACGGCGACATGGCTAGCTTCGGCAGCAGGCTG
S D K C I S W P L N G D M A S F G S R L 219
721 CAGAAGAAGCCGTGAACAGCACTTCATACCCACTGTCCGCTTTGGCGTTTGCGTTCCCCC
Q K K P *
781 CAATAAAGTTTTTCCGGTGGTGCAGGTCC
b
1 GAGTTGTGCTCGATCAAGCTACCATGGCCCCTGTGCTGGGATACTGGGACATCCGAGGCC
M A P V L G Y W D I R G L 13
61 TTTGCGAGCCCATTCGCTACCTTCTGGCGCACGCTAAAGTCTCCTACGAGGATAAAAGGT
C E P I R Y L L A H A K V S Y E D K R Y 33
121 ACGGCTTCGGCAATGGTCCCGAACCCAGCCGCGACGAGTGGTTGGCCGACAAGTACAAGT
G F G N G P E P S R D E W L A D K Y K L 53
181 TGGGTCTGGACTTCCCCAACGTGCCGTACTACATCGACGGCGACGTCAAGCTGACGCAGA
G L D F P N V P Y Y I D G D V K L T Q S 73
241 GCATGGCCATCCTGCAGTACCTCGGCCGCAAGCACGGACTCGCCCCCAAGGACGAGGCCA
M A I L Q Y L G R K H G L A P K D E A T 93
301 CTCAGCTCCGCGTCGACGTGCTCCAGCTCACGGCGTTCGACGTGATCATGTGGGCAGTGC
Q L R V D V L Q L T A F D V I M W A V R 113
361 GCGTCTGCTACGACCCCGAGTACACCGAGGAGAAGCGGAAGCAGTTCCTGGTCGACGTGG
V C Y D P E Y T E E K R K Q F L V D V A 133
421 CCGACAAGCTGAAGCAGTTTGACTCGTACCTCTCCAAGTATGGTCCTTTCGGCGCCGGCA
D K L K Q F D S Y L S K Y G P F G A G K 153
481 AGTCAGCCACTTACGTCGACTTCTTGCTCTACGAGGCTCTCCAGATCGTGAAAATTCTTG
S A T Y V D F L L Y E A L Q I V K I L G 173
541 GCCCAAGCACGTTCCGCAAGGGCTACCCTCAGCTCGAGGAGTACTGCCAGCGCGTTGCTG
P S T F R K G Y P Q L E E Y C Q R V A A 193
601 CCCTTCCGGGAATGAAGGAGTATCTGGCCTCGGATCGCTTCAAGGCTTGGCCCATCTGGA
L P G M K E Y L A S D R F K A W P I W S 213
661 GCCCGTACGCAAAGGCGCTGGCGGCGCAGCACAAGCCGCCCGCTGACGACTGCTGAGCGA
P Y A K A L A A Q H K P P A D D C * 230
721 TCCCCGCCGGCCATCGCGCGTCGCAAGCGTTGACCGCAGTTCTAGTTTTTTGATGTTGTT
781 AATCTGGGATGCGACGCTATATACGGCTGTTACATTTTTCTTTTCAATAAACGGTTGCGT
841 CGTTTTGAGCGCTCTTCCGACAAAAAAAAA

Fig. 1.2 Nucleotide and deduced amino acid sequences of HlGST (**a**) and HlGST2 (**b**) of *Haemaphysalis longicornis.* Start and stop codons are underlined. Predicted glutathione and substrate binding sites are shaded in black and gray, respectively. The putative polyadenylation signal, AATAAA, is double underlined.

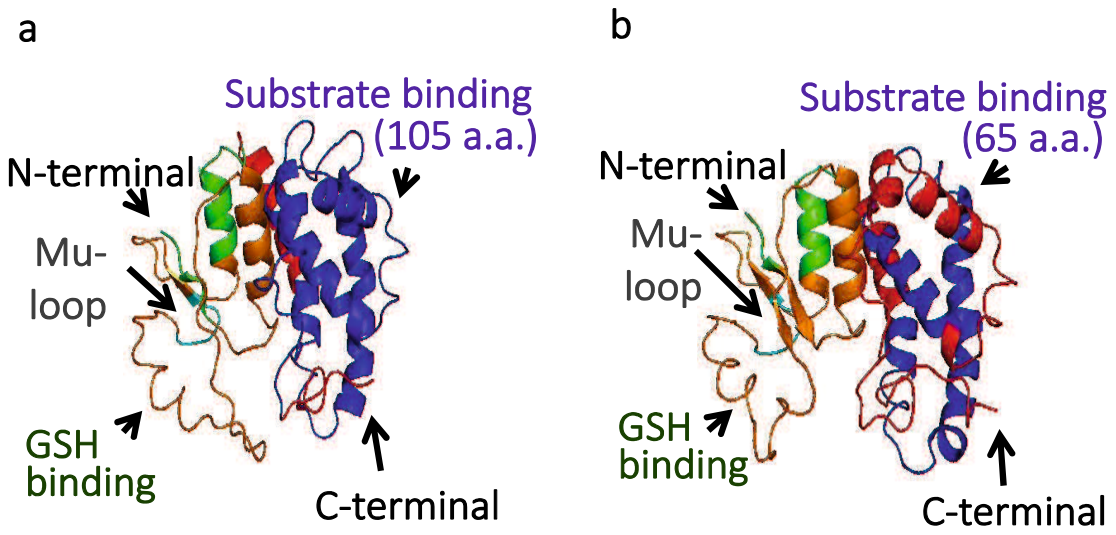

Fig. 1.3 The modeled tertiary structures of HlGST (**A**) and HlGST2 (**B**). The model is based on template c1b8xA [79] constructed using PHYRE2 software [80]. Green indicates the N-terminal domain containing the GSH binding site (orange), while red indicates the C-terminal domain containing the substrate binding site (blue). The mu-loop is indicated by bluish green.

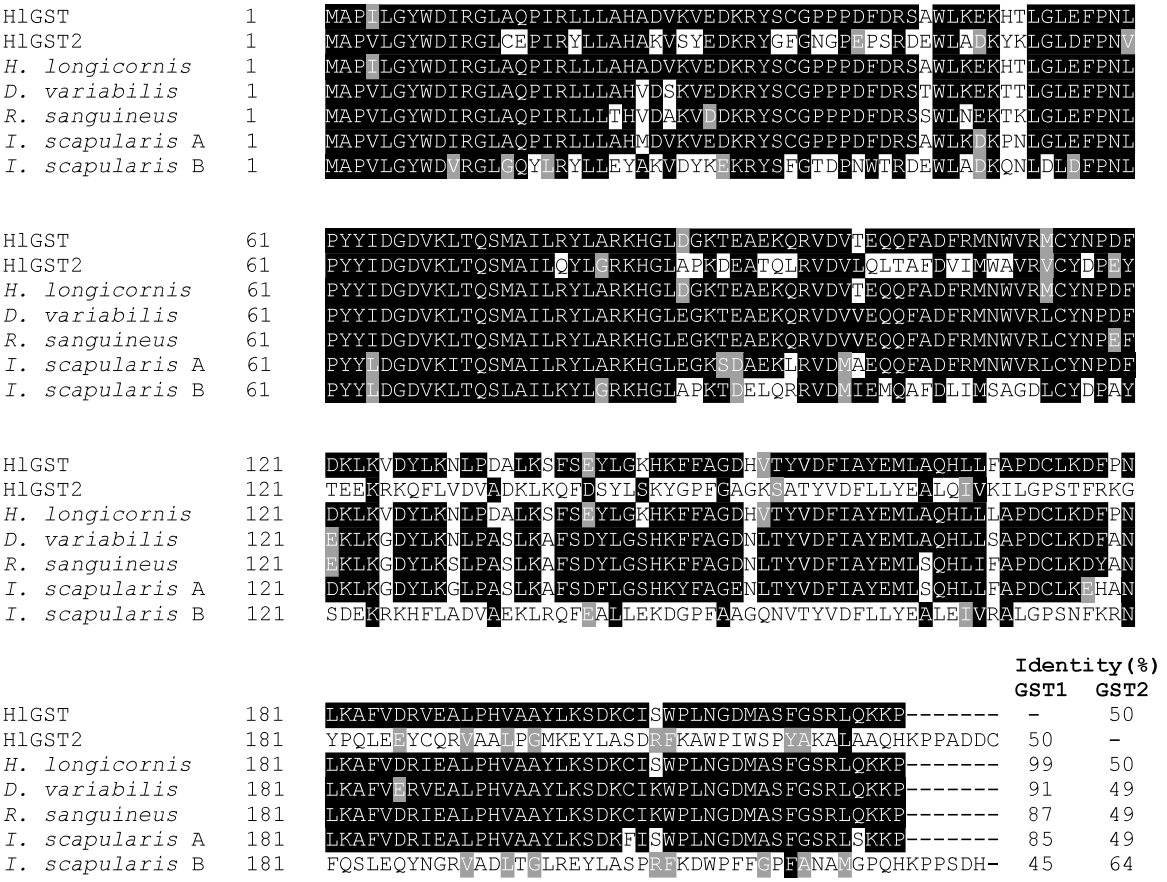

Fig. 1.4 Multiple sequence alignment of the deduced amino acid sequences of HlGST and HlGST2 with other tick GSTs. Identical residues are shaded black, while similar residues are shaded gray. The percent identities with HlGST and HlGST2 are placed at the end of the sequences. The GenBank accession number GST sequences are as follows: *Haemaphysalis longicornis* (AAQ74441.1), *Dermacentor variabilis* (ACF35504.1), *Rhipicephalus sanguineus* (AGK29895.1), *Ixodes scapularis* A (XP_002401749.1), and *Ixodes scapularis* B (XP_002434207.1)

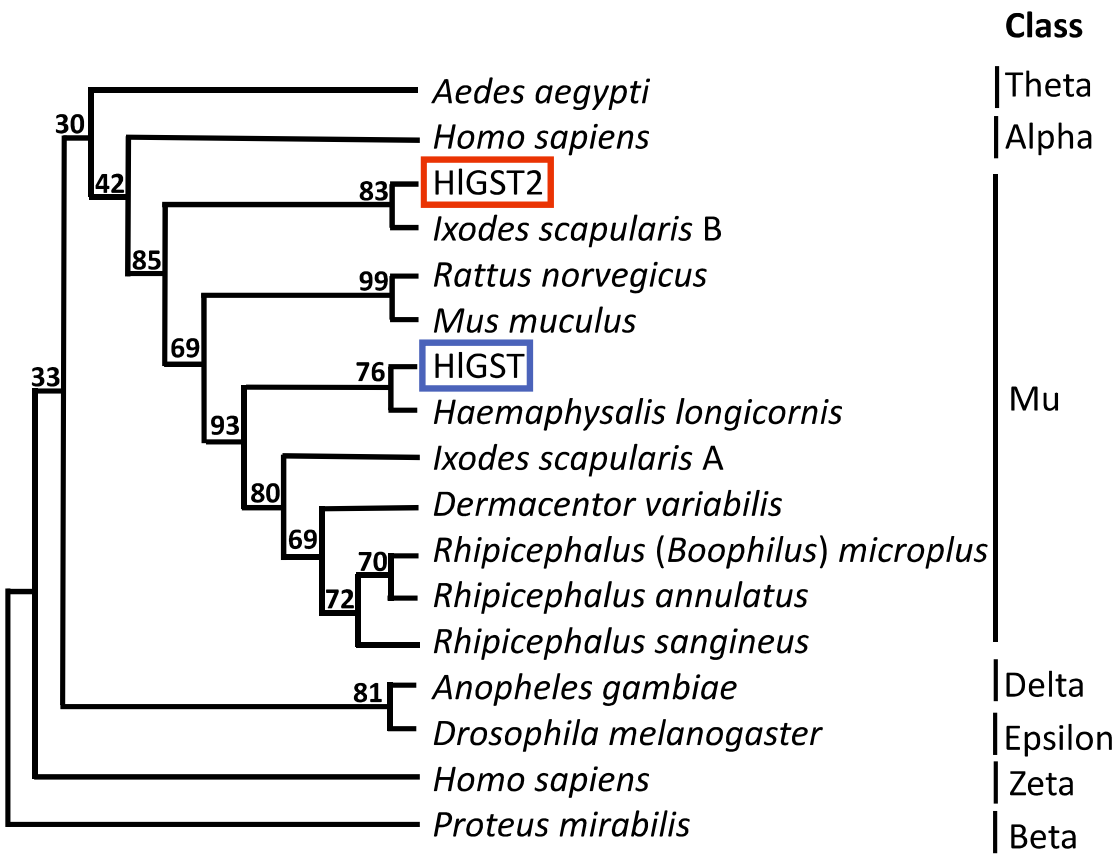

Fig. 1.5 Phylogenetic tree of GSTs from different species of ticks, selected vertebrates, and invertebrates. A dendogram was created by the neighbor-joining method based on the deduced amino acid sequence of GSTs. Bootstrap values are placed at the nodes. GenBank accession numbers are as follows: *Aedes aegypti* (Theta), Q16X19; *Homo sapiens* (Alpha), P08263; *Ixodes scapularis* A, XP_002401749.1; *Ixodes scapularis* B, XP_002434207.1; *Rattus norvegicus*, NP_803175.1; *Mus muculus,* NP_032209.1; *Haemaphysalis longicornis*, AAQ7444.1; *Dermacentor variabilis*, ACF35504.1; *Rhipicephalus* (*Boophilus*) *annulatus,* ABR24785.1; *Rhipicephalus sanguineus*, AGK29895.1; *Anopheles gambiae* (Delta), Q8MUS1; *Drosophila melanogaster*, (Epsilon) Q7KK90; *Homo sapiens*, (Zeta) O43708; and *Proteus mirabilis*, (Beta) P15214

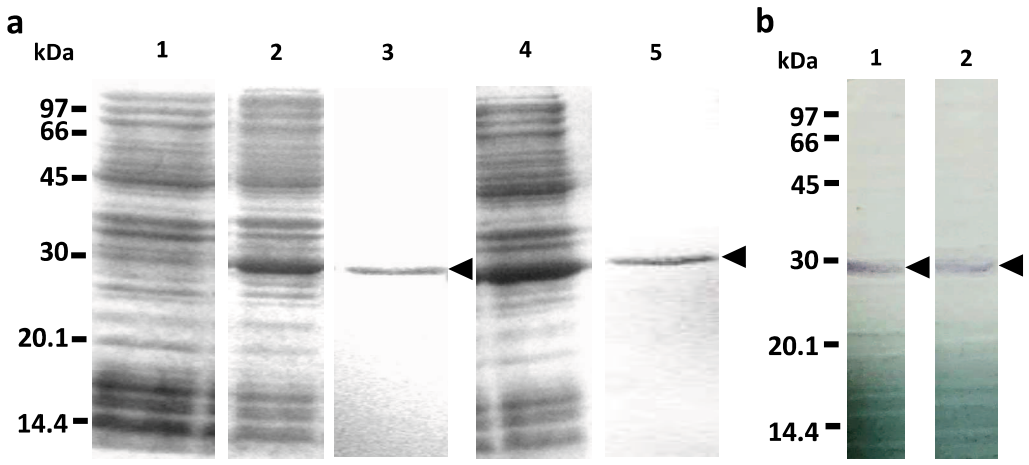

Fig. 1.6 SDS-PAGE (**a**) and Western blotting (**b**) of recombinant GSTs. **a** The column farthest left includes markers of molecular weights. Lane 1: bacterial lysate of empty vector; Lane 2: bacterial lysate of HlGST after induction by 1 mM IPTG; Lane 3: bacterial lysate of HlGST after purification by HisTrap affinity chromatography; Lane 4: bacterial lysate of HlGST2 after induction by 1 mM IPTG; Lane 5: bacterial lysate of HlGST2 after purification by HisTrap affinity chromatography. The lysates were run on a 12% SDS-PAGE gel. Gels were stained using Coomassie Blue staining solution. **b** The column farthest left indicates molecular weight markers. Lane 1: recombinant HlGST; Lane 2: recombinant HlGST2. Bands were visualized using 5-Bromo-4-chloro-3-indolylphosphate/Nitroblue Tetrazolium (BCIP/NBT) Calbiochem® (Merck KGaA, Darmstadt, Germany). Arrowheads indicate the bands for recombinant HlGST and HlGST2 proteins

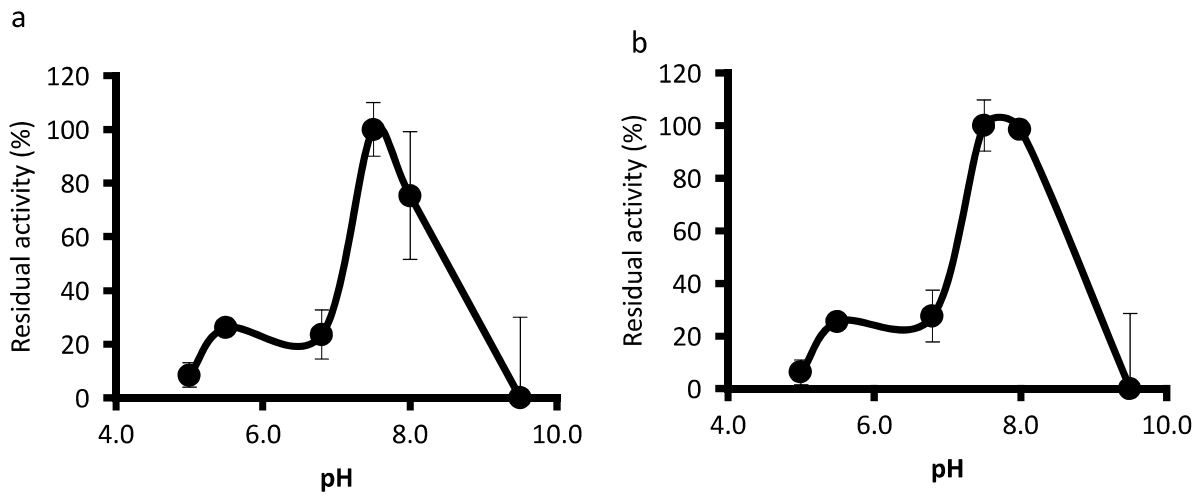

Fig. 1.7 Effect of pH on the enzymatic activity of recombinant HlGST (**a**) and HlGST2 (**b**). Buffers were 0.1 M citrate for pH 5.0–5.5 and Tris-HCl for pH 6.5–8.5. Error bars represent the standard deviation of three replicates, and the remaining activities were recorded as percentages relative to the highest activity

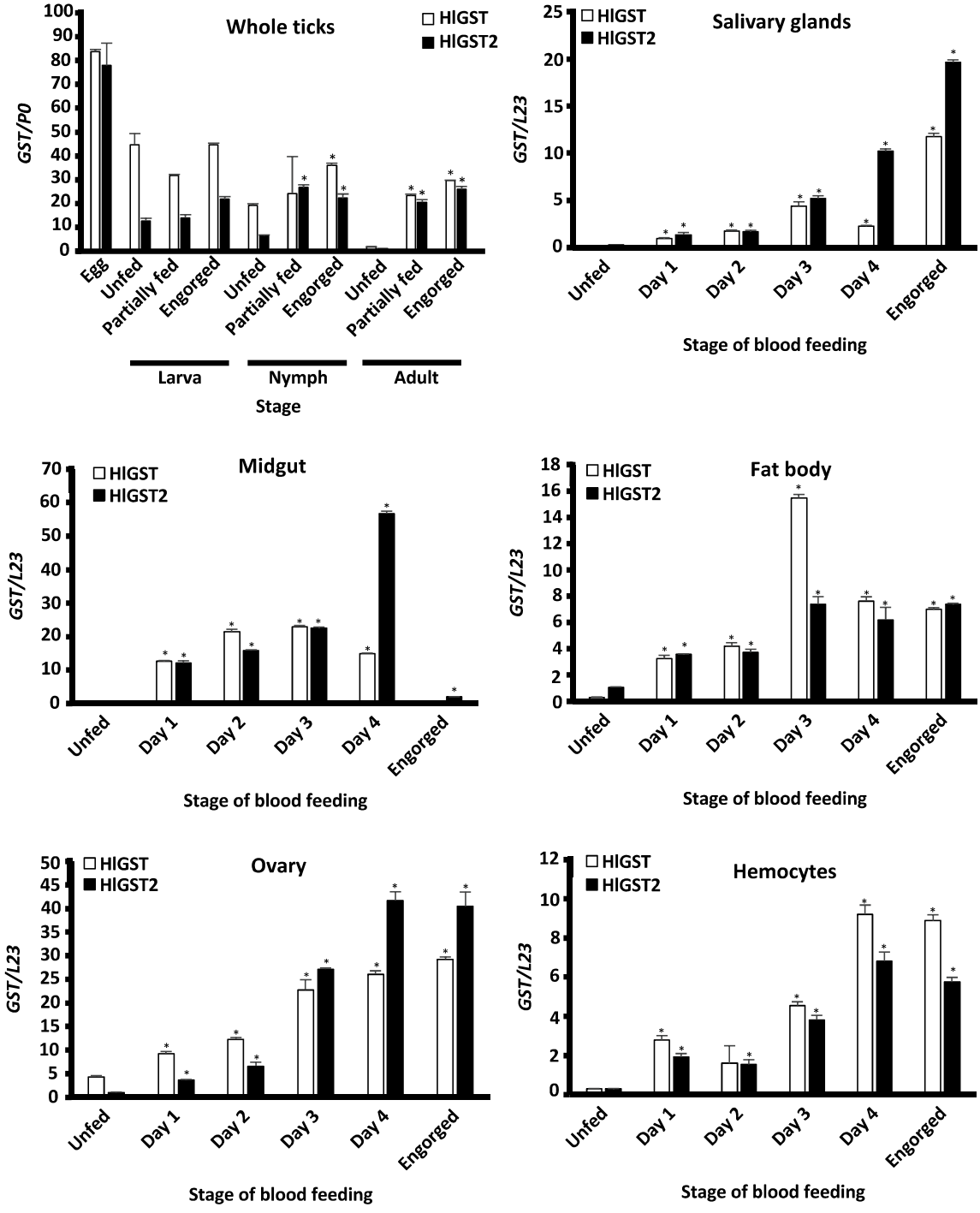

Fig. 1.8 Transcription profiles of *GST* genes in different stages and tissues of ticks during blood-feeding. Total mRNA was prepared from different stages and tissues after dissection. *P0* and *L23* primers were used as controls for whole ticks and tissues, respectively. Error bar represents the mean ± standard deviation. $^{*}P < 0.05$, significantly different by Student's t-test as compared to the unfed at the same stage.

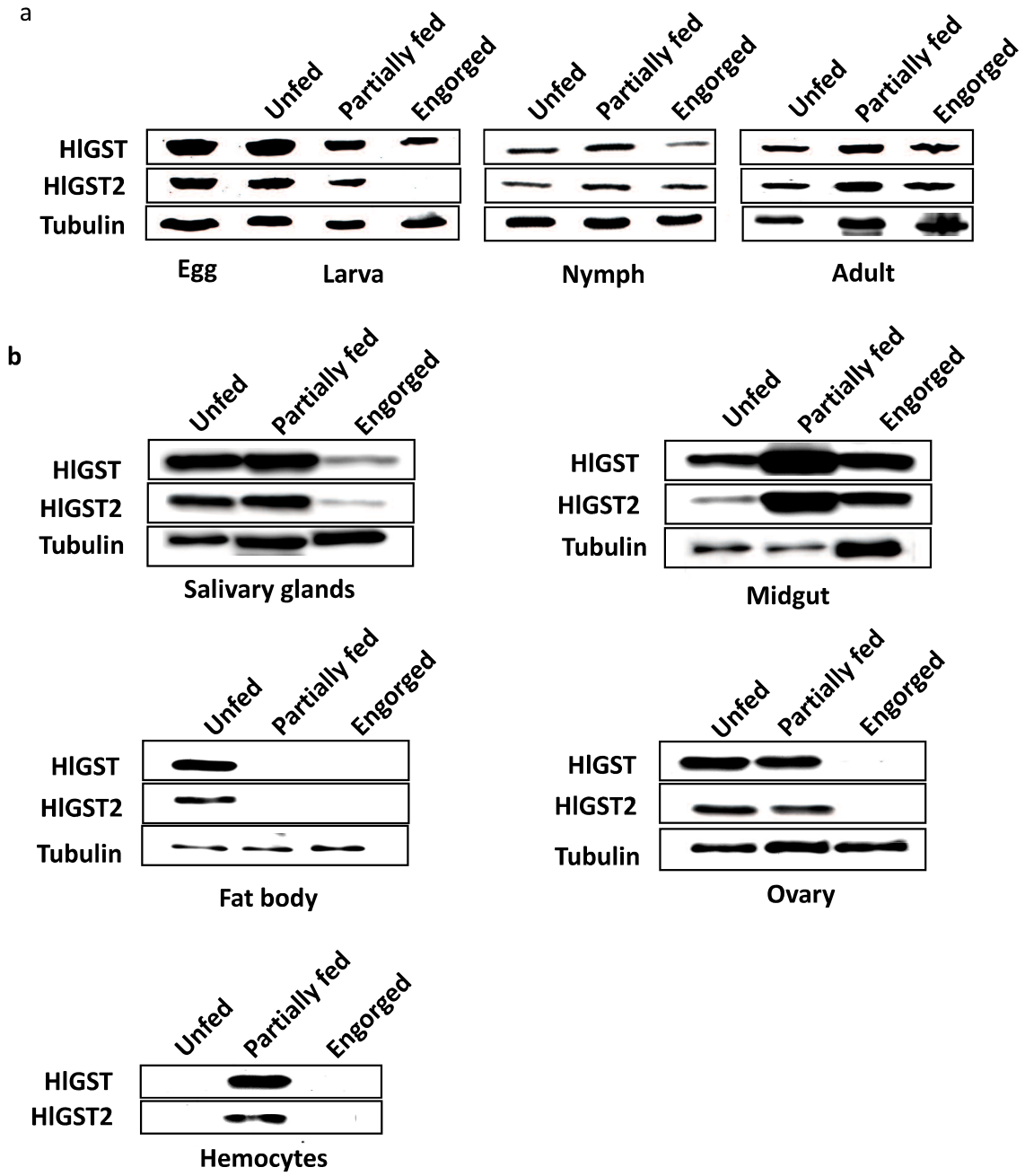

Fig. 1.9 Expression profiles of GSTs in different tick stages (**a**) and organs (**b**) during blood-feeding. Proteins were prepared from different stages and tissues after dissection. Antiserum against tubulin was used as a control for Western blotting. Western blotting results are shown as representative data of three separate experiments showing the same trend. Since no band can be seen using the tubulin antisera on hemocytes, the protein concentration was determined using Micro BCA and maintained at 390 ng before loading for Western blotting

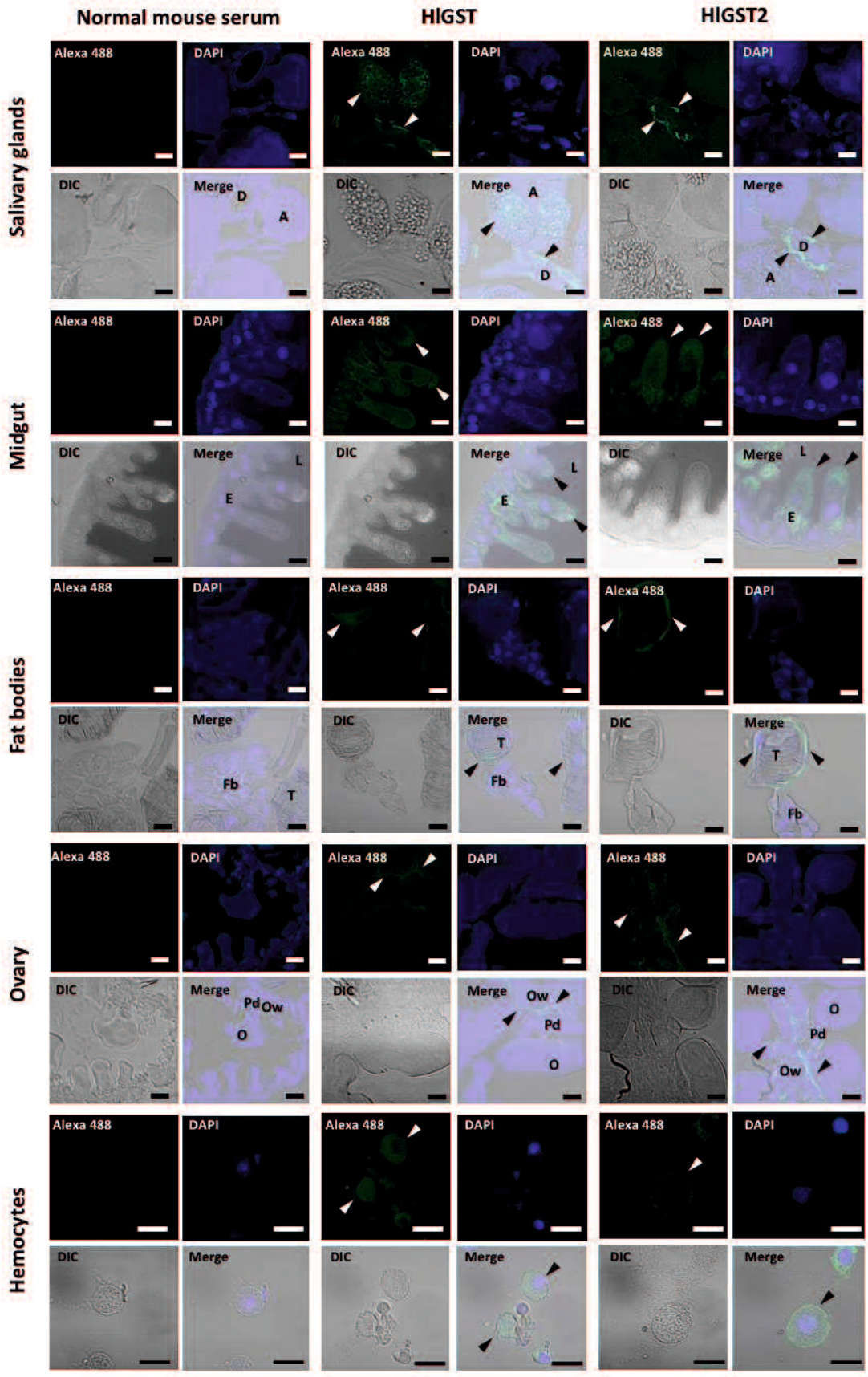
Normal mouse serum
HlGST
HlGST2
Salivary glands
Midgut
Fat bodies
Ovary
Hemocytes
Alexa 488
DAPI
DIC
Merge
D
A
L
E
Fb
T
Pd
Ow
O

Fig. 1.10 Localization of GSTs in tissues of partially fed adult ticks. Immunofluorescent antibody test (IFAT) was used to determine the localization of the GSTs in the different tissues of ticks. Antiserum against HlGST or HlGST2 was used for the primary antibody, anti-mouse IgG conjugated with Alexa 488 was used for the secondary antibody, and nuclei were visualized using DAPI. Normal mouse serum was used for a control. The tissues were visualized using confocal microscope. *Abbreviations*: Salivary glands (A, acinus; D, salivary ducts); Midgut (E, enterocytes; L, lumen; Fat bodies (T, tracheal complex; Fb, fat body cells); Ovary (O, oocyte; Pd, pedicel; Ow, ovarian wall). Arrows show positive GST fluorescence. *Scale-bars*: 20 μm

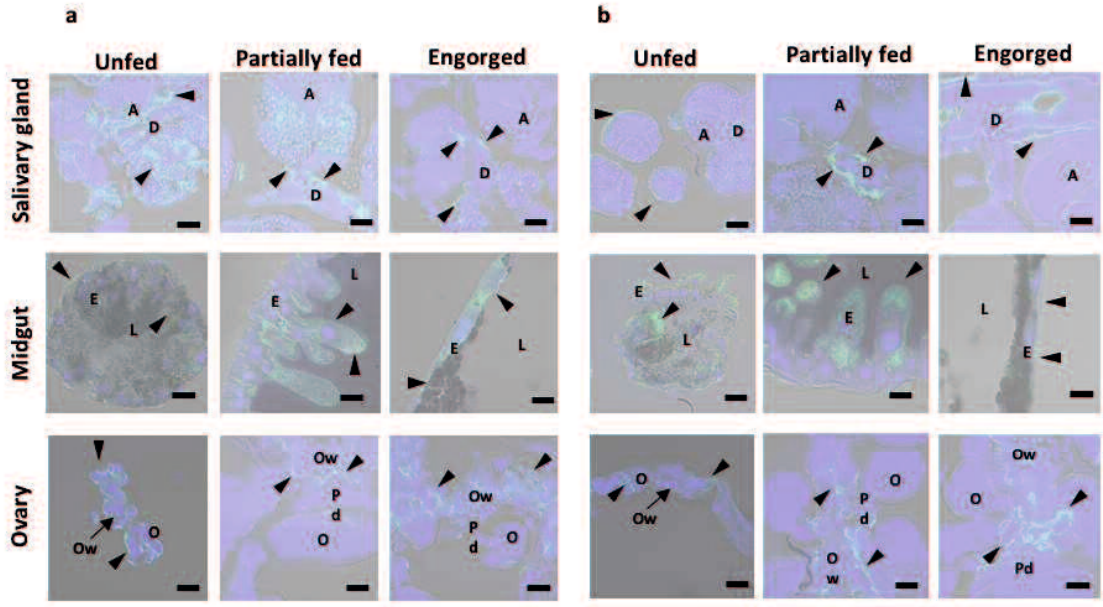

Fig. 1.11 Examination of HlGST **(a)** and HlGST2 (**b**) in selected tissues during blood-feeding. The salivary glands, midgut, and ovary were observed during blood-feeding of adult ticks by indirect immunofluorescent antibody test (IFAT) using a confocal laser scanning microscope**.** Antiserum against HlGST or HlGST2 was used for the primary antibody, anti-mouse IgG conjugated with Alexa 488 was used for the secondary antibody, and nuclei were visualized using DAPI. Normal mouse serum was used for a control. *Abbreviations*: Salivary glands (A, acinus; D, salivary ducts); Midgut (E, enterocytes; L, lumen); Ovary (O, oocyte; Pd, pedicel; Ow, ovarian wall). Arrows show the positive fluorescence of GST. *Scale-bars*: 20 μm

CHAPTER 2

Elucidation of the role of *Haemaphysalis longicornis* GSTs in acaricide detoxification

This work was published as:

Hernandez EP, Kusakisako K, Talactac MR, Galay RL, Hatta T, Fujisaki K, Tsuji N, Tanaka T. (2018). Glutathione S-transferases play a role in the detoxification of flumethrin and chlorpyrifos in *Haemaphysalis longicornis*. *Parasit Vectors*, **11**, 460.

2.1 Introduction

Presently, tick control has relied mainly upon the application of acaricides such as amitraz, synthetic pyrethroids and organophosphates [36,58]. The continuous use of acaricides has some ill effects, such as the development of resistance against these acaricides [82]. One factor that has contributed to the development of acaricide resistance is the improper application of acaricides, with a particular emphasis on sublethal doses [35].

Amitraz is a formamidine acaricide that has been around since the 1960s. It acts as an agonist of the octopaminergic receptors of arthropods, leading to the stimulation of monoamine oxidases and G proteins. This stimulation leads to the synthesis of cAMP and cGMP, and could alter the behavior of the arthropods [83]. On the other hand, organophosphates are acetylcholinesterase inhibitors. Their action results in acetylcholine continuous stimulation, causing hyperactivity and, eventually, the death of the arthropods. Organophosphates possess a broad spectrum of activity against insects and acarians [83]. Pyrethroids are esters capable of opening Na^+ channels, resulting in the depolarization of nerve cell membranes. The effect on arthropods involves two phases. The first phase is the reversible "knockdown" effect, wherein arthropods cease all movements and act as if they are dead. This is caused by pyrethroids acting on the cerebral ganglia. Arthropods

may still wake-up, and then go to the second phase, wherein the pyrethroids may affect peripheral nerves. This could result in brief, rapid and inconsistent movements of arthropods, perhaps leading eventually to death. The pyrethroids permethrin, cypermethrin and deltamethrin are both acaricides and insecticides, while flumethrin is mainly an acaricide [83].

Until now, the exact mechanisms of acaricide metabolism by the ticks are not fully understood. Three metabolic pathways are believed to play roles in this detoxification process: carboxylesterases, monooxygenases and glutathione S-transferases [35]. Glutathione S-transferases (GSTs) are multifunctional enzymes that are responsible for the metabolism and detoxification of both xenobiotic and physiological substances. Metabolism involves the catalysis of thiol additions of the reduced glutathione to organic compounds through their electrophilic centers. The formation of more water-soluble conjugates would facilitate their elimination [84]. The transport of molecules is facilitated by an ATP-requiring active transport system through the multidrug resistance-related protein (MRP) [35].

In the previous chapter I have identified two GST molecules of *H. longicornis* [39]. GSTs act on a wide variety of substrates, and each GST isoenzyme may function very differently from the others, wherein not all GSTs are involved in the detoxification

of acaricides [85,86]. Therefore, it is important to determine the role of the GSTs of ticks in acaricide metabolism. Targeting specific GSTs that impede the ability of the arthropod to survive acaricide application could be included in the development of a tick control plan [87]. In this study, I determined the possibility of the interaction of recombinant GSTs and several acaricides. I also observed the ability of sublethal doses of acaricides to induce GST gene and protein expression. Finally, I established the significance of GSTs in the metabolism of sublethal doses of acaricides through RNA interference (RNAi) experiments.

2.2 Materials and methods

2.2.1 Ticks and experimental animals

The parthenogenetic Okayama strain and the bisexual Oita strain of *H. longicornis* were used in the experiments throughout this study. In Japan, no evidence of resistance against acaricides was reported in this tick species. Ticks and rabbits were maintained as previously described in Chapter 1.

2.2.2 Chemicals

Organophosphate acaricides (ethion, coumaphos, chlorpyrifos and diazinon), pyrethroids (cypermethrin and flumethrin), an avermectin (ivermectin), and a formamidine compound (amitraz) were evaluated for their interaction with the GSTs of *H. longicornis*. Ethion, chlorpyrifos, diazinon, cypermethrin and amitraz were purchased from Wako Pure Chemical Industries, Ltd. (Osaka, Japan). Coumaphos, ivermectin and flumethrin were purchased from Sigma-Aldrich (St. Louis, MO, USA).

.

2.2.3 Interaction of recombinant GSTs with acaricides

The inhibition activity of recombinant GSTs was measured according to the methods of Habig and da Silva [53,58], using 1-chloro-2,4-dinitrobenzene (CDNB) (Sigma-Aldrich) as a substrate. The recombinant GSTs used in this study were expressed as described in Chapter 1. Two-hundred microliters of the reaction mixture consisting of varying concentrations of CDNB (0.125, 0.25, 0.5, 1 and 2 mM) dissolved in methanol, 5 mM glutathione, 0.1 mM of acaricide dissolved in methanol, and 120 μM recombinant GST in 100 mM Tris-HCl (pH 7.5) or without recombinant GST for the blank was tested in a 96-well plate. The methanol concentration was maintained at 5%. Equine liver GST and recombinant *H. longicornis* 2-cys-peroxiredoxin [88] were used as the positive and

negative controls, respectively. Absorbance (A_{340nm}) was measured each minute in an SH-9000 microplate reader (Corona Electric, Ibaraki, Japan) at 25 °C for 5 min. The extinction coefficient of 9.6 $mM^{-1}cm^{-1}$, corrected for the 96-well microplate light path, was used. Each assay was done in triplicate, and the results were expressed as the mean of three separate experiments. Kinetic constants K_m and V_{max} were calculated from the double-reciprocal plot of 1/v *versus* the 1/[S] or Lineweaver-Burk plot in which V_{max} = 1/y-intercept of the regression line and $K_m = V_{max} \times$ slope of the regression line.

2.2.4 Determination of acaricide sublethal dose

The following acaricides were dissolved in methanol at 4 dilutions: flumethrin (0.4 μM, 4 μM, 40 μM and 400 μM), chlorpyrifos (0.01 mM, 0.1 mM, 1 mM and 10 mM), and amitraz (0.01 mM, 0.1 mM, 1 mM and 10 mM). These concentrations were based on previous studies [35,89].

For exposure studies, the methods of Duscher [35] were used with some modifications. Briefly, 0.5 ml of each dilution was spotted onto a 10 × 5 cm piece of filter paper in scattered dots and dried under the fume hood for at least 2 h. Each group of 10 parthenogenetic females, nymphs and larvae, as well as bisexual male and female ticks, was placed in the acaricide-impregnated filter paper and exposed for 48 h. Mortality was

checked after 48 h. For the parthenogenetic larvae and nymphs, further 10-fold dilutions were made to determine the sublethal dose. The maximum sublethal dose in this experiment is the highest dose that has either failed to cause any mortality or caused just a single mortality out of all the ticks tested [35].

2.2.5 GST gene and protein expression analysis of parthenogenetic female ticks exposed to flumethrin, chlorpyrifos and amitraz

Parthenogenetic female ticks were exposed to different sublethal concentrations of flumethrin (0, 0.4, 4 and 40 μM), chlorpyrifos (0, 0.01, 0.1 and 1 mM), and amitraz (0, 0.01, 0.1 and 1 mM). Total RNA and real-time RT-PCR was performed as in accordance to the procedure previously described in Chapter 1.

The protein was also extracted from the abovementioned parthenogenetic female ticks exposed to flumethrin, chlorpyrifos and amitraz. Whole tick samples were homogenized and the tick protein was subjected to Western blot analysis using the same protocol described in Chapter 1.

2.2.6 RNA interference

RNA interference using double-stranded RNA (dsRNA) was performed to determine the effect of GST on survival upon acaricide exposure. dsRNA was synthesized using the procedures described in Chapter 1 using the specified gene primers (Table 2.1). *HlGST*, *HlGST2*, or *HlGST 1/2* dsRNA (0.5 µl) dissolved in high purity water was injected to the hemocoel of unfed adult ticks through the fourth coxa at 1µg/tick concentration [39]. A total of 35 ticks per group were injected with dsRNA. The control group was injected with *EGFP* dsRNA. After injection, the ticks were held for 24 h in a 25 °C incubator to check for mortality resulting from injury during injection. The ticks were then kept in vials sealed with cotton plug, placed in a glass chamber, and maintained at 25 °C and 80–85% relative humidity in an incubator for another 72 h. For larvae and nymphs, the dsRNA immersion method described by Galay et al. [90] was performed. Briefly, a total of 35 larvae or nymphs were immersed in 40 µl of *HlGST*, *HlGST2*, or *HlGST 1/2* dsRNA dissolved to a concentration of 0.5 µg/µl in high purity water for 12 h. After 12 h, the dsRNA solution was removed, and the ticks were checked for mortality resulting from immersion. Ticks were also kept in vials sealed with cotton plug, placed in a glass chamber, and maintained at 25 °C and 80–85% relative humidity in an incubator for another 72 h. Total RNA was extracted from 5 ticks of each developmental stage and

sex, and their cDNA was synthesized. The cDNA was subjected to RT-PCR with a Hot Start Pol system (Jena Bioscience, Jena, Germany) using *GST*-specific primers, such as HlGST RT forward and HlGST RT reverse primers, and HlGST2 RT forward and HlGST2 RT reverse primers (Table 2.1), following the manufacturer's instructions. The PCR cycle profile was as follows: 94 °C for 8 min, 30 cycles of a denaturation step at 94 °C for 30 s, an annealing step at 68 °C for 60 s, and an extension step at 72 °C for 60 s. The PCR products were run in 1.5% TAE agarose gel and stained with ethidium bromide in TAE buffer. *Actin* was used as a loading control. The absence of bands corresponding to *HlGST* and *HlGST2* genes in their corresponding GST knockdown group demonstrates that silencing was successful (Fig. 2.1).

After confirmation of the knockdown, ticks were then exposed to sublethal doses of acaricides using the method described above. Mortality was checked after exposure. Ticks lying on their backs that could not turn over were considered dead.

2.2.7 Statistical analysis

Welch's t-test was used to analyze data from the enzymatic inhibition, real-time RT-PCR of ticks, and tick survival studies. A significant difference is defined as $P < 0.05$. All experiments were done at least twice.

2.3 Results

2.3.1 Interaction of recombinant GSTs with acaricides

Enzyme kinetic analysis in the presence or absence of acaricides was used to determine their ability to inhibit the activity of recombinant GST to catalyze the conjugation of CDNB to glutathione (GSH). The effect of acaricide interaction was determined by the change in the kinetic constants V_{max} and K_m, in accordance with the procedure of Mathews and van Holde [91]. An inhibition that causes an increase in the K_m without a change in the V_{max} is a competitive type of inhibition. An inhibition in which the K_m is not affected by decreased V_{max} is a noncompetitive type of inhibition. An inhibition in which the V_{max} and K_m are decreased is an uncompetitive type of inhibition. In this experiment, flumethrin and cypermethrin showed uncompetitive inhibition of recombinant HlGST. On the other hand, chlorpyrifos and cypermethrin showed noncompetitive inhibition of recombinant HlGST2 (Table 2.2). Other acaricides, with the exception of coumaphos, did not show significant changes in the V_{max} and K_m. Coumaphos significantly decreased the K_m of recombinant HlGST, indicating the apparent activation of the enzyme. These results demonstrated that the interactions of the recombinant GSTs with acaricides depend on the variety of acaricide.

2.3.2 Sublethal dose of flumethrin, chlorpyrifos and amitraz on different stages and strains of H. longicornis

Based on the results of enzyme kinetic analysis, flumethrin and chlorpyrifos were selected to analyze the importance of GSTs in their metabolism. Amitraz was also selected as a representative of the formamidine group. For adult parthenogenetic Okayama and bisexual Oita strains of ticks, the dilution of 40 μM proved to be the highest sublethal dose of flumethrin (Table 2.3), while 1 mM was the highest sublethal dose of chlorpyrifos (Table 2.4) and amitraz (Table 2.5). For nymphs, the dilution of 4 μM proved to be the highest sublethal dose of flumethrin (Table 2.3), while 100 μM was the highest sublethal dose of chlorpyrifos (Table 2.4) and amitraz (Table 2.5). For larvae, the dilution of 4 nM proved to be the highest sublethal dose of flumethrin (Table 2.3), while 100 nM was the highest sublethal dose of chlorpyrifos (Table 2.4) and amitraz (Table 2.5).

2.3.3 Effect of flumethrin, chlorpyrifos and amitraz on the gene and protein expression of GSTs of parthenogenetic ticks

The effect of flumethrin, chlorpyrifos and amitraz on the mRNA expression level of parthenogenetic female ticks were also tested (Fig. 2.2a). Exposure to 4 μM and 40 μM flumethrin resulted in the overexpression of *HlGST*. *HlGST2* genes at 0.4 μM and 40 μM

flumethrin exposure did not show any significant increase in mRNA expression, but they showed a significant increase at 4 μM flumethrin exposure. Chlorpyrifos exposure did not result in any significant change in *HlGST* gene expression. On the other hand, the *HlGST2* gene was overexpressed when ticks were exposed to 1 mM chlorpyrifos. Although amitraz exposure did not cause overexpression in either GST, *HlGST* showed a significant decrease in expression at a concentration of 0.01 mM, while it increased significantly at a 0.1 mM concentration. *HlGST2* genes did not show any significant change when ticks were exposed to amitraz. These results demonstrated that flumethrin and chlorpyrifos trigger the overexpression of *HlGST* and *HlGST2* genes, respectively. This might then indicate their possible role in the metabolism of these acaricides.

GST proteins of adult parthenogenetic *H. longicornis* ticks exposed to sublethal doses of flumethrin, chlorpyrifos, and amitraz were detected by Western blot analysis (Fig. 2.2b). The expression of HlGST protein was induced with exposure to 0.4 μM, 4 μM and 40 μM flumethrin. The protein expression of HlGST2 increased in a dose-dependent manner. Chlorpyrifos and amitraz at sublethal doses (0.01, 0.1 and 1 mM) did not cause any significant change in the expression of GST proteins. These results demonstrate that acaricides utilize GST proteins differently.

To be able to determine whether larval GSTs are induced in the same manner as the parthenogenetic female, parthenogenetic larvae exposed to sublethal doses of flumethrin (0, 0.4 and 4 nM) and chlorpyrifos (0, 10 and 100 nM) were checked for their gene and protein expression. Similar upregulation of *HlGST* genes and proteins was observed upon larval exposure to sublethal doses of flumethrin (Fig. 2.3). Unlike in adults, both the *HlGST2* gene and protein were upregulated upon larval exposure to a sublethal dose of chlorpyrifos (Fig. 2.3). This indicates that the utilization of GSTs could vary between tick stages.

2.3.4 Effect of GST knockdown on different stages of parthenogenetic ticks upon exposure to flumethrin and chlorpyrifos

To further establish the importance of GST in acaricide detoxification, *GST* knockdown experiments were performed, and *GST* knockdown ticks were then exposed to different sublethal doses of flumethrin and chlorpyrifos. Nymphs and adults showed no significant increase in mortality in *GST* knockdowns as compared to *EGFP* knockdown groups (Figs. 2.4 and 2.5). The knockdown of *HlGST* in larvae resulted in the death of almost all larvae tested in 4 nM flumethrin (Fig. 2.4a). Additionally, a significant decrease in survival was also observed when both *HlGST* and *HlGST2* were knocked

down and larvae were exposed to 0.4 nM flumethrin as compared to *HlGST* knockdown alone. On the other hand, the knockdown of *HlGST2* and both *HlGST* and *HlGST2* caused a significant increase in the mortality of larvae exposed to 10 μM and 100 μM chlorpyrifos (Fig. 2.5a). These results showed that HlGST is vital for the survival of larval ticks against sublethal doses of flumethrin, while HlGST2 is important in larval tick survival against chlorpyrifos.

2.3.5 Effect of GST knockdown on different sexes of ticks upon exposure to flumethrin and chlorpyrifos

In mammals, as well as insects, sexual differences in GST expression have been observed [32,46,92]; therefore, gene knockdown experiments with subsequent exposure to acaricides were also performed with male and female *H. longicornis* ticks to determine whether sex is a factor in tick survival against flumethrin and chlorpyrifos. Results have shown that the knockdown of *HlGST* and *HlGST2* with subsequent exposure to sublethal doses of flumethrin leads to a significant increase in the mortality of male ticks (Fig. 2.4d). To check whether males and females have the same induction response, real-time RT-PCR and Western blot analysis were performed to check the expression levels of HlGST and HlGST2. Interestingly, although both *GST* genes are induced upon exposure to

flumethrin, protein expressions were constant in male ticks (Fig. 2.6). On the other hand, female ticks showed no induction in either gene or protein expression. These results showed that HlGST is vital for the survival of male ticks against sublethal doses of flumethrin. These results also demonstrated that different strains of ticks have different induction responses to acaricides.

2.4 Discussion

The predominant tick-control measure is the use of acaricides. Ticks make use of several mechanisms to metabolize these compounds. Therefore, several factors could be considered in the development of new tick-control strategies, such as the type of acaricide and its schedule of application. It is then important to understand the mechanism through which ticks metabolize these substances. Interference with these mechanisms would make the tick more prone to an acaricide and, eventually, lead to a more efficient tick control method [35,93].

In this study, the role of two kinds of GSTs in the detoxification of several acaricides was investigated. I previously identified and expressed two mu-class GSTs from the hard tick *H. longicornis* [39], on which I used expressed recombinant GSTs to perform enzyme kinetic analysis in the presence of acaricides. The inhibition of GST

activity by acaricides or insecticides has been observed previously [58,94]. Differences in the type of inhibitions demonstrated that each GST isoenzyme has a specific profile of interaction with chemical compounds, even though the same chemical compounds would have different interactions with GST isoenzymes [58].

In cases of uncompetitive inhibition, inhibitors such as flumethrin and cypermethrin (Table 2.2) would only bind to an enzyme-substrate complex. This binding could also result in an irreversible interaction that may inactivate the enzyme [91]. This inhibition also could be a result of the combination of GST and acaricide rather than conjugation of the acaricide with a reduced glutathione. This kind of binding of GSTs with pyrethroids was also observed in insects such as *Tenebrio* sp. and *Aedes* sp. Pyrethroids are believed to bind to the enzyme's active site but did not yield a conjugated product. This suggests that the enzyme acts as a binding protein rather than a conjugating protein [95,96]. This type of combination reaction was also observed in other detoxification enzymes, such as esterase. *Tetranychus cinnabarinus* esterase (TCE2) protein combined with abamectin rather than hydrolyzing it. It is believed that this binding decreased or delayed the noxious compound from reaching its target site; therefore, it is still considered an important mechanism in the metabolism of abamectin [97].

Noncompetitive inhibition occurs when an inhibitor, such as cypermethrin or chlorpyrifos (Table 2.2), binds to a non-substrate binding site. The presence of a non-substrate binding site was also observed in the pi class of GSTs [84]. In this class of GSTs, the presence of low-affinity and high-affinity binding sites of the enzyme for bilirubin has been observed. Also, the inhibition of GST activity by bromosulfophthalein was attributed to the non-substrate binding site [84]. Moreover, the noncompetitive inhibition of flumethrin was also observed in the recombinant *Rhipicephalus* (*Boophilus*) *microplus* GST [58].

In this study, recombinant HlGST was activated by coumaphos through the lowering of the K_m (Table 2.2). This kind of activation has also been observed in the recombinant *R. microplus* GST, wherein its activity was activated by coumaphos, the biological significance of which is still uncertain and could be the subject of a future study [58]. Since the *in vitro* reaction showed a potential role of GSTs in interacting with acaricides, several types of acaricides that have interacted with GSTs were testedor their effect on the GST gene and protein expression levels of ticks exposed to acaricides.

Dose-dependent gene expression that led to overexpression was observed on the *HlGST* gene when adult ticks were exposed to sublethal doses of flumethrin (Fig. 2.2a). Although pyrethroids are not supposed to be substrates of GSTs, the enzyme kinetic

analysis has shown the ability of recombinant HlGST to bind with flumethrin. This binding or sequestering mechanism of GSTs could give passive protection by either decreasing the level of free pyrethroids or facilitating the binding of other enzymes with it [96,98]. This binding could be facilitated by alkyl or aryl hydrogen groups in the pyrethroids that could interact with GSTs. Also, the role of GST in detoxifying lipid peroxidation products caused by pyrethroids should be considered in determining the role of GST in the metabolism of an acaricide [99]. The overexpression of *GST* genes of *H. longicornis* upon exposure to flumethrin was also observed by Hatta et al. [89]. The overexpression of mu-class *GST* genes was also observed in mites after exposure to pyrethroids [98,100]. Although the larva has a higher basal GST expression as compared with the adult [39], the ability of flumethrin to induce *HlGST* gene and protein expression remains the same. Interestingly, when the bisexual strain of *H. longicornis* was used, a different expression pattern was observed (Fig. 2.6a). No induction of *GST* genes was observed in the female bisexual strain as compared with the parthenogenetic *H. longicornis.* In the case of bisexual males, the induction of gene expression was observed for both *HlGST* and *HlGST2* genes. This different expression of GSTs among arthropod strains was also observed in *Anopheles gambiae*, in which two strains (G3 and ZANDS) demonstrated different expressions in response to DDT. It is believed that GST

expression is greatly influenced by environmental factors. Environmental factors, especially those that could confer resistance to a pesticide, include temperature, the type and dose of pesticide to which the arthropod has been exposed, and even the solvent quality used to dilute the pesticide [101]. The continuous effects of these environmental factors have already resulted in changes at the genetic level [86,102]. In the case of sex, cDNA analysis showed no difference between parthenogenetic, male and female ticks. It should be noted that male and female ticks have demonstrated different gene expression patterns upon exposure to sublethal doses of flumethrin (Fig. 2.6a). Although the exact mechanism of the difference in male and female GST gene induction still remains unknown, differences in GST activity have been observed previously in mosquitoes [46]. In the locust, different *GST* gene expressions were also observed between spermaries and ovaries [92]. Male and female ticks could have different *GST* gene composition levels. In this way, when ticks are exposed to flumethrin, a *GST* with a higher activity against flumethrin would result in increased transcription. Therefore, if there is another unknown GST that has higher activity than the identified *GST*s, the unknown GST could have proliferated instead of the identified ones. Also, if there is an unknown GST gene present in the female and absent in the male, it would result in different transcriptions in the known *GST* genes. On the other hand, when mosquitoes were exposed to pyrethroids, the

overexpression of multiple *cytochrome P450* genes was observed aside from the upregulated *GST* genes [103,104].

The *HlGST2* gene showed overexpression at the highest sublethal dose of chlorpyrifos (Fig. 2.2a). However, it is well known that organophosphates are metabolized by cytochrome P450 monooxygenases and hydrolases. Specifically, chlorpyrifos is activated to chlorpyrifos oxon by cytochrome P450 enzymes before being deethylated or dearylated. The metabolism of chlorpyrifos could yield metabolites that could be subjected to GSH conjugation by GSTs [85]. Therefore, GSTs could have an indirect role in organophosphate detoxification. In *R.* (*B.*) *microplus*, the overexpression of *GST* was observed when ticks were exposed to coumaphos [105]. On the other hand, chlorpyrifos has shown the ability to overexpress the *GST* gene of the migratory locust, cotton leaf worm and rice plant hopper [106–108]. Interestingly, *HlGST2* genes appear to be maintained at lower concentrations of chlorpyrifos (Fig. 2.2a). The noninduction of *HlGST2* at low doses of chlorpyrifos could be because of the organism's ability to specifically produce the appropriate *GST* genes depending on its needs. Different responses of GSTs to chlorpyrifos were also observed in migratory locusts [106]. On the other hand, amitraz did not show any effect on the *GST* gene expression level. Since amitraz is considered to be an agonist in the octopaminergic system of arthropods [83],

this mimicry could have resulted in its non-recognition as a foreign or xenobiotic compound and, therefore, not a metabolite of the GSTs.

In accordance with the *GST* gene expression level, the protein expression level of HlGST2 also increased depending on the concentration of flumethrin (Fig. 2.2b). This also held true in larvae of ticks exposed to sublethal doses of chlorpyrifos. When ticks were exposed to a sublethal dose of flumethrin, HlGST protein initially increased but appeared to maintain its expression when the dosage of flumethrin was increased, even though gene expression increased dramatically (Fig. 2.2b). On the other hand, no difference was observed in the protein expression level regardless of the concentration when adult ticks were exposed to sublethal doses of chlorpyrifos (Fig. 2.2b). It has always been believed that GST proteins are transcriptionally regulated [109]. Based on our results and previous studies, GST not only functions as a conjugate with GSH but also as a binding protein, wherein they "sacrifice" themselves by binding covalently with reactive compounds [110]. The fate of the GST conjugates is yet to be demonstrated. They could possibly be released from the cytoplasm, as some studies have shown the ability of GST to be secreted or to move across the plasma membrane through the facilitation of MRP [32,67]. This could be why non-substrates that bind with GST, such as flumethrin with HlGST or chlorpyrifos with HlGST2, did not have a drastic increase

in protein expression, as GST proteins are being released from the cell after being bound to flumethrin or chlorpyrifos.

To further understand the role of GSTs in flumethrin and chlorpyrifos metabolism, RNAi was performed on GST genes, and ticks at different stages were exposed to sublethal doses of the acaricides. No significant differences in mortality were observed in the knockdown groups of adult female and nymph ticks exposed to sublethal doses of flumethrin and chlorpyrifos (Figs. 2.4 and 2.5). Other GST isoenzymes could have possibly compensated for the silenced *GST* [78]. Several tick species have demonstrated the presence of multiple isoenzymes of GSTs. Thirty-five genes of GSTs, of which 14 belong to the mu-class GST were shown in an *in silico* analysis of the *Ixodes scapularis* gene database [57]. Multiple GSTs have also been found in *Dermacentor variabilis* and *Rhipicephalus* (*Boophilus*) *annulatus* [40,58]. Interestingly, the *HlGST* knockdown in male ticks resulted in increased susceptibility to flumethrin (Fig. 2.4d). This could mean that HlGST could be the main GST in the male tick's detoxification mechanism against flumethrin. However, further testing and studies need to be conducted on the different detoxification mechanisms between male and female ticks. Notably, the larval stage of ticks also showed increased susceptibility to the effects of sublethal doses of flumethrin and chlorpyrifos. The importance of the GST system at the early stage of

development was also observed in insects such as *Tenebrio* and *Anopheles,* as well as the red mite *Panonychus*, wherein increased expression and/or activity was observed at the younger stage of development as compared with the adult [46,98,111,112]. The results in Chapter 1 have also shown relatively higher GST protein expression in the unfed larval stages of ticks as compared to the unfed nymph and adult *H. longicornis* [39]. Since the younger stages do not have a well-developed system of protection, such as integuments, it is possible that the GST system is vital for protecting larvae by detoxification.

Flumethrin may not be readily conjugated to glutathione by GSTs; however, GST could bind to flumethrin to decrease its ability to reach the tick nerve cell membrane. This, in turn, could result in a reduced toxic effect of flumethrin. The knockdown of *HlGST* in larvae and adult male ticks also could have resulted in increased intracellular flumethrin, eventually leading to cellular toxemia. The knockdown of GST genes in *Rhipicephalus sanguineus* also leads to increased mortality upon exposure to a sublethal dose of pyrethroids [35]. In mites, exposure to pyrethroids after GST inhibition also resulted in increased susceptibility to acaricides [100]. Higher mortality was also observed when both *GST*s were knocked down, as compared to the knockdown of *HlGST* alone, when larvae were exposed to a sublethal dose of flumethrin. This could possibly show the ability of HlGST2 to compensate, to a certain degree, for the loss of HlGST. On

the other hand, the metabolism of chlorpyrifos leads to the production of toxic metabolites [85]. These metabolites could have increased when *HlGST2* is knocked down in larvae. The abundance of these metabolites could have resulted in intracellular toxicity and, eventually, the death of ticks. The same increase in susceptibility to chlorpyrifos upon *GST* knockdown has also been observed in migratory locusts [106].

In summary, this study has demonstrated that HlGST could play an important role in the detoxification of pyrethroids such as flumethrin, wherein the inhibition of enzymatic activity was observed. *HlGST* gene expression was also induced by sublethal doses of flumethrin, and the knockdown of *HlGST* resulted in the increased susceptibility of larvae and male ticks to flumethrin. On the other hand, HlGST2 plays an important function in the metabolism of organophosphates, such as chlorpyrifos. Chlorpyrifos inhibited the GST activity of recombinant HlGST2. *HlGST2* gene induction upon exposure to sublethal doses of chlorpyrifos was also observed. More importantly, larval susceptibility to chlorpyrifos significantly increased upon *HlGST2* knockdown. The data also showed that GSTs have a more important role in larval survival as compared to ticks at other stages upon exposure to sublethal doses of acaricides. I have also demonstrated that environmental factors as well as GST pool composition could play a role in the ability of acaricides to induce GST gene expression as observed in male and female ticks.

Tables and Figures in CHAPTER 2

Table 2.1 Gene-specific primers used in this study. Italics denotes RNA polymerase promoter sequences

Primer	Sequence [5'→3']
HlGST real-time forward	CTTCTTGGATCTTGGCGGGT
HlGST real-time reverse	CGATGTCCCAGTAGCCGAG
HlGST RT forward	ACGTGAAGCTCACCCAGAGCAT
HlGST RT reverse	AAGCTAGCCATGTCGCCGTTGA
HlGST RNAi forward	GCCTGGCTCAAGGAGAAACACA
HlGST RNAi reverse	ACAAAGGCCTTCAGGTTGGGGA
HlGST T7 forward	*TAATACGACTCACTATAGG*GCCTGGCTCAAGGAGAAACACA
HlGST T7 reverse	*TAATACGACTCACTATAGG*ACAAAGGCCTTCAGGTTGGGGA
HlGST2 real-time forward	CCCTTCCGGGAATGAAGGAG
HlGST2 real-time reverse	GATCGCTCAGCAGTCGTCAG
HlGST2 RT forward	ACGTCAAGCTGACGCAGAGCAT
HlGST2 RT reverse	ATGGGCCAAGCCTTGAAGCGAT
HlGST2 RNAi forward	AGGATAAAAGGTACGGCTTCGGCA
HlGST2 RNAi reverse	TTTCACGATCTGGAGAGCCTCGTA
HlGST2 T7 forward	*TAATACGACTCACTATAGG*AGGATAAAAGGTACGGCTTCGGCA
HlGST2 T7 reverse	*TAATACGACTCACTATAGG*TTTCACGATCTGGAGAGCCTCGTA
P0 real-time forward	CTCCATTGTCAACGGTCTCA
P0 real-time reverse	TCAGCCTCCTTGAAGGTGAT
L23 real-time forward	CACACTCGTGTTCATCGTCC
L23 real-time reverse	ATGAGTGTGTTCACGTTGGC
Actin real-time forward	ATCCTGCGTCTCGACTTGG
Actin real-time reverse	GCCGTGGTGGTGAAAGAGTAG
Actin RT forward	CCAACAGGGAGAAGATGACG
Actin RT reverse	ACAGGTCCTTACGGATGTCC
Tubulin real-time forward	TTCAGGGGCCGTATGAGTAT
Tubulin real-time reverse	TGTTGCAGACATCTTGAGGC
EGFP T7 forward	*TAATACGACTCACTATAGG*GACGTAAACGGCCACAAGTT
EGFP T7 reverse	*TAATACGACTCACTATAGG*TGCTCAGGTAGTGGTTGTCG

Table 2.2 Enzyme kinetic constants of recombinant GSTs in the presence of different acaricides

Acaricide	Class	Recombinant HlGST			Recombinant HlGST2		
		V_{max}	K_m	Inhibition	V_{max}	K_m	Inhibition
None		11.70 ± 1.92	0.82 ± 0.14		14.72 ± 0.56	0.61 ± 0.20	
Flumethrin	Synthetic pyrethroids	4.26 ± 0.30*	0.48 ± 0.07*	UC	5.85 ± 0.73	1.70 ± 0.92	None
Cypermethrin	Synthetic pyrethroids	3.61 ± 1.65*	0.38 ± 0.04*	UC	2.20 ± 0.64*	0.36 ± 0.12	NC
Chlorpyrifos	Organophosphates	9.52 ± 4.21	0.55 ± 0.24	None	8.00 ± 1.08*	0.35 ± 0.25	NC
Ethion	Organophosphates	8.36 ± 0.87	0.58 ± 0.15	None	15.55 ± 1.02	0.37 ± 0.07	None
Coumaphos	Organophosphates	6.35 ± 2.40	0.48 ± 0.10*	None	9.68 ± 3.38	1.17 ± 0.31	None
Diazinon	Organophosphates	18.38 ± 5.43	1.51 ± 0.78	None	26.13 ± 5.33	1.59 ± 0.58	None
Amitraz	Formamidine	15.04 ± 1.66	0.87 ± 0.25	None	10.10 ± 2.55	0.51 ± 0.09	None
Ivermectin	Avermectin	10.94 ± 5.10	0.74 ± 0.36	None	14.64 ± 3.47	0.74 ± 0.31	None

Abbreviations: UC, uncompetitive inhibition; NC, noncompetitive inhibition

*$P < 0.05$ *vs* no acaricide

Table 2.3 Tick survival (in %) after exposure to different doses of flumethrin. The table is representative of three separate experiments showing approximately the same result

	0	**0.4 nM**	**4 nM**	**40 nM**	**400 nM**	**4 µM**	**40 µM**	**400 µM**
Larva	90	100	90[a]	10	10	10	0	10
Nymph	100	nt	nt	Nt	90	90[a]	50	10
P-adult	100	nt	nt	Nt	100	100	100[a]	80
M-adult	100	nt	nt	Nt	100	100	100[a]	80
F-adult	100	nt	nt	Nt	100	100	100[a]	70

Abbreviations: P-adult, parthenogenetic adult; M-adult, adult male; F-adult, adult female; nt, not tested

[a]Maximum sublethal dose

Table 2.4 Tick survival (in %) after exposure to different doses of chlorpyrifos. The table is representative of three separate experiments showing approximately the same result

	0	**1 nM**	**10 nM**	**100 nM**	**1 µM**	**10 µM**	**100 µM**	**1 mM**	**10 mM**
Larva	100	100	90[a]	80	0	0	0	0	0
Nymph	100	nt	nt	nt	100	100	90[a]	0	0
P-adult	100	nt	nt	nt	nt	100	100	100[a]	0
M-adult	100	nt	nt	nt	nt	100	100	100[a]	0
F-adult	100	nt	nt	nt	nt	100	100	100[a]	0

Abbreviations: P-adult, parthenogenetic adult; M-adult, adult male; F-adult, adult female; nt, not tested

[a]Maximum sublethal dose

Table 2.5 Tick survival (in %) after exposure to different doses of amitraz. The table is representative of three separate experiments showing approximately the same result

	0	**1 nM**	**10 nM**	**100 nM**	**1 µM**	**10 µM**	**100 µM**	**1 mM**	**10 mM**
Larva	100	90	100[a]	80	0	0	0	0	0
Nymph	100	nt	100	100	100	90[a]	80	50	0
P-adult	100	nt	nt	nt	nt	100	100	90[a]	0
M-adult	100	nt	nt	nt	nt	100	100	100[a]	0
F-adult	100	nt	nt	nt	nt	100	100	90[a]	0

Abbreviations: P-adult, parthenogenetic adult; M-adult, adult male; F-adult, adult female; nt, not tested

[a]Maximum sublethal dose

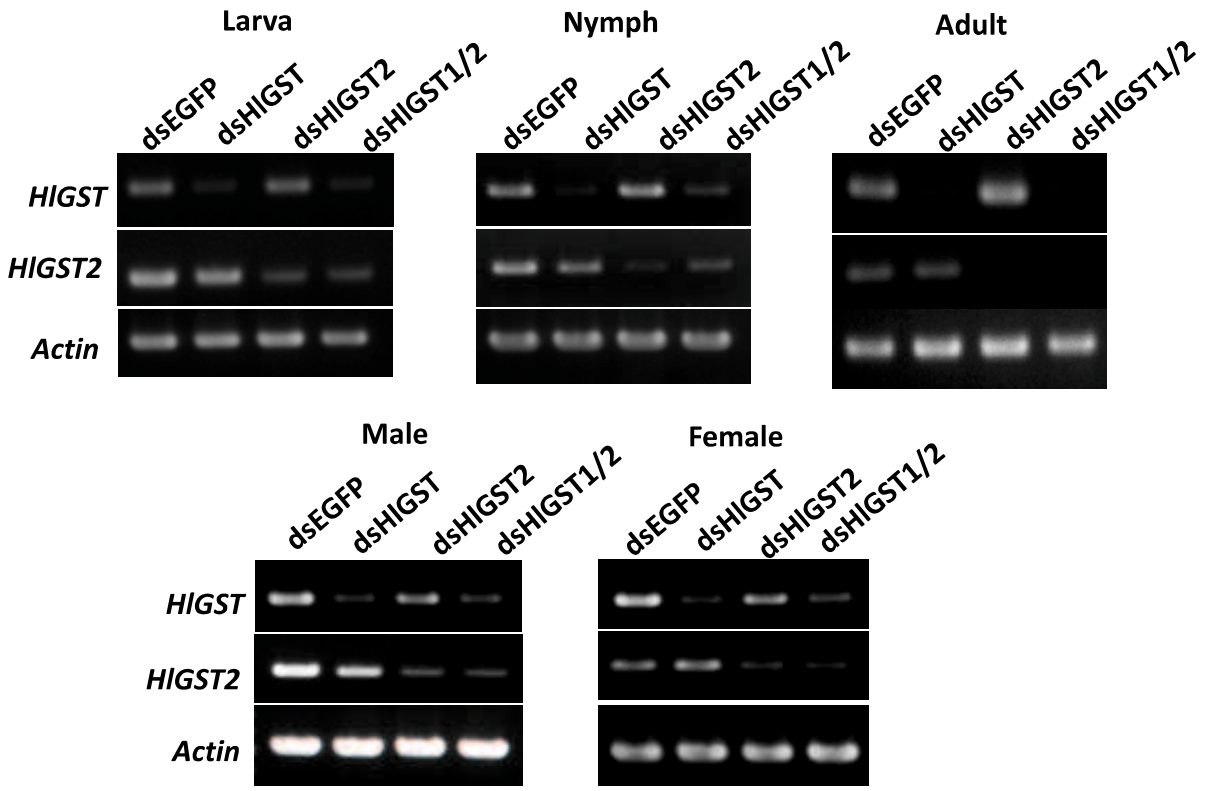

Fig. 2.1 RT-PCR of knockdown ticks. Total RNA was extracted from whole *GST* and *EGFP* knockdown ticks 4 days post-injection/immersion to dsRNA. cDNA was synthesized and subjected to RT-PCR. PCR products were run on 1.5% TAE agarose gel and stained with ethidium bromide. *Actin* was used as a loading control.

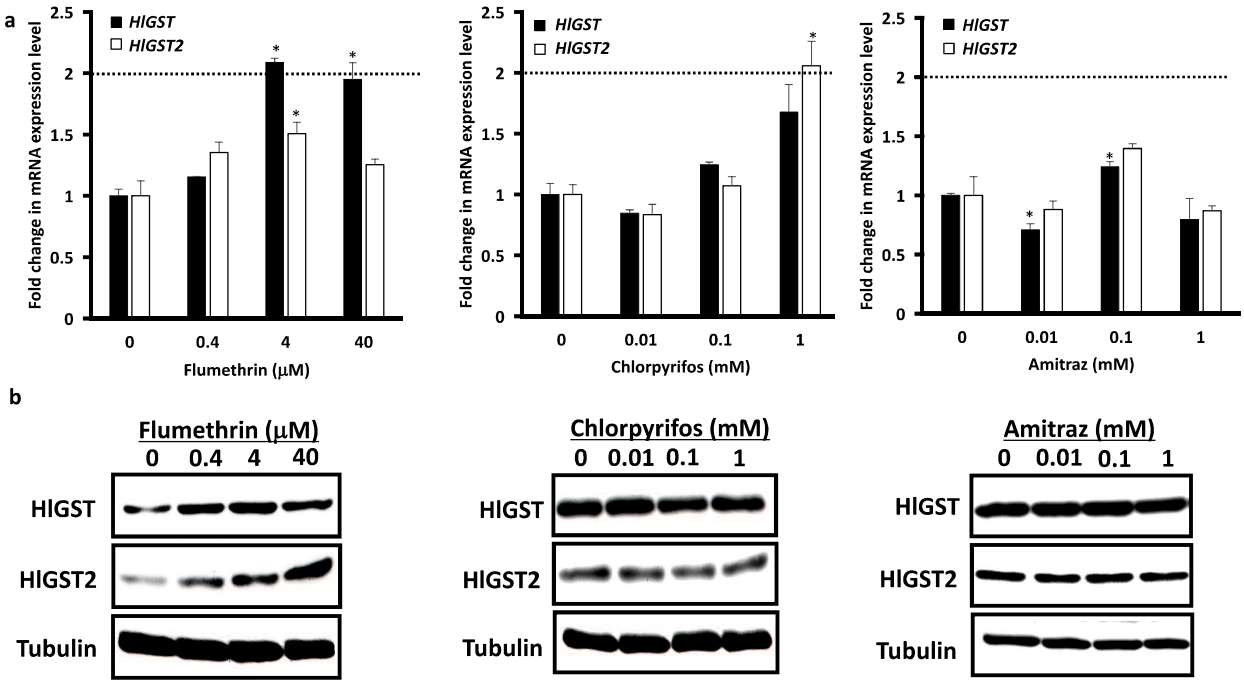

Fig. 2.2 Gene (**a**) and protein (**b**) expression of GSTs of adult parthenogenetic ticks exposed to sublethal doses of flumethrin, chlorpyrifos and amitraz. **a** Total mRNA was extracted from adult ticks and transcribed to cDNA before real-time RT-PCR. *P0* primers were used as controls. The error bar represents the mean ± standard deviation. **P* < 0.05: significantly different by Welch's t-test as compared to no treatment. The dotted line indicates overexpression. Overexpression is determined if there is at least a 2-fold increase in expression level, as shown by Bhattacharjee et al. [78]. **b** Proteins were prepared from adult ticks exposed to sublethal doses of flumethrin, chlorpyrifos and amitraz. Antiserum against tubulin was used as a control for Western blot analysis. Western blot analysis results are shown as representative data of three separate experiments showing the same trend

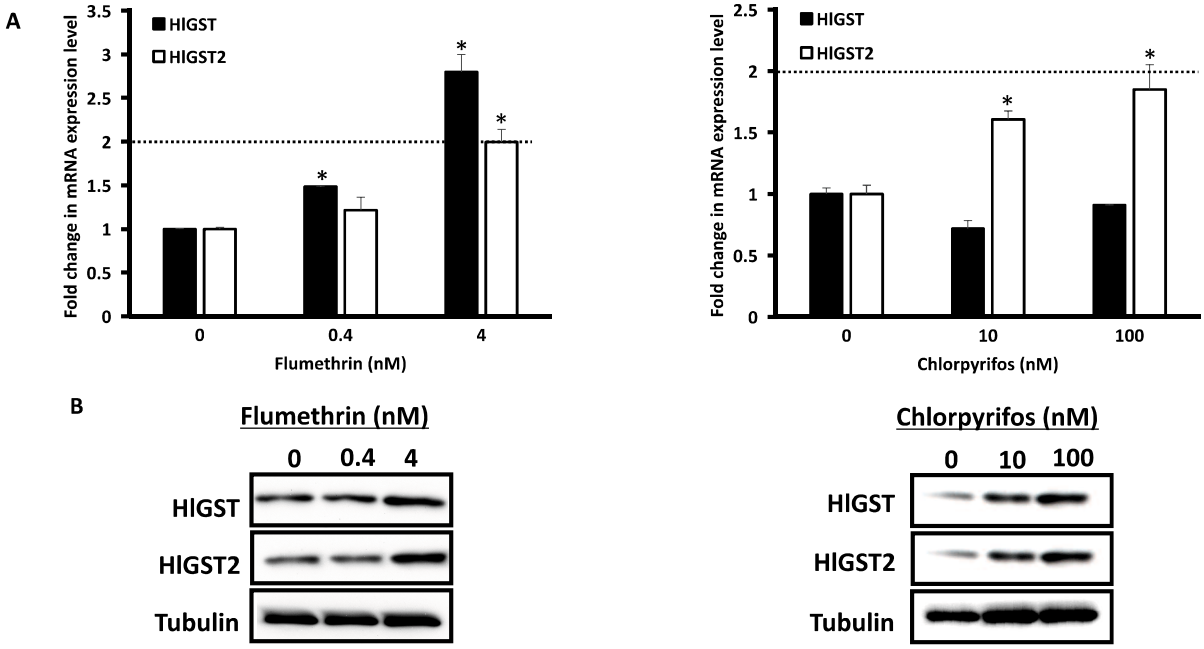

Fig. 2.3 Gene (**A**) and protein (**B**) expressions of larval ticks upon exposure to sublethal doses of flumethrin and chlorpyrifos. Ticks were exposed to sublethal doses of flumethrin and chlorpyrifos for 48 h. **a** Total mRNA was extracted from ticks, and cDNA was then transcribed for real-time RT-PCR. *P0* primers were used as a control. The error bar represents the mean ± standard deviation. **P* < 0.05: significantly different by Welch's t-test as compared to no treatment. The dotted line indicates overexpression. Overexpression is determined if there is at least a twofold increase in expression level, as shown by Bhattacharjee et al. [78]. **b** Proteins were prepared from ticks exposed to sublethal doses of acaricides. Antiserum against tubulin was used as a control for Western blot analysis. Western blot analysis results are shown as representative data of three separate experiments showing the same trend

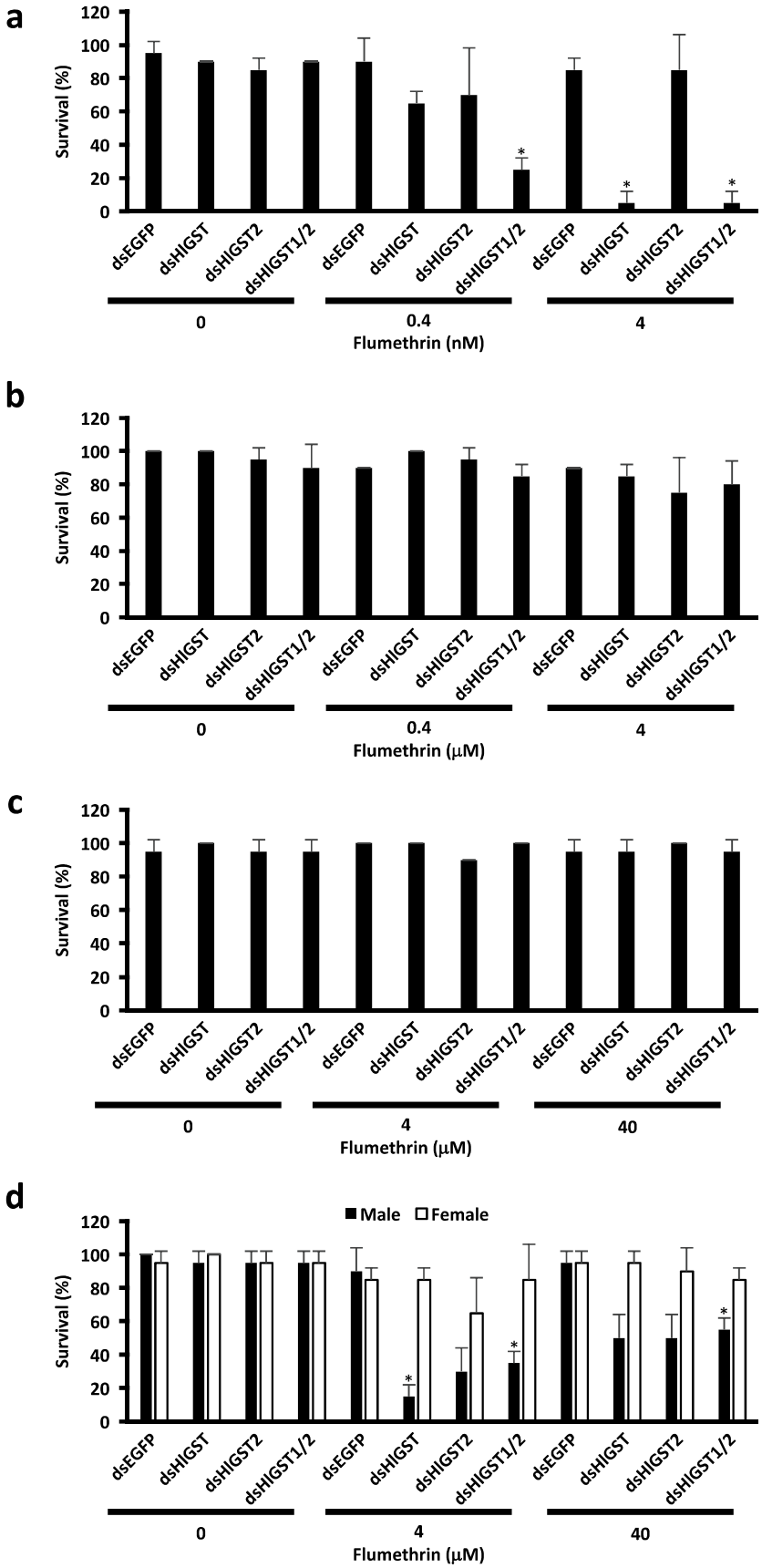
a
Survival (%)
120
100
80
60
40
20
0
dsEGFP
dsHIGST
dsHIGST2
dsHIGST1/2
0
0.4
4
Flumethrin (nM)
b
Survival (%)
Flumethrin (μM)
c
Survival (%)
0
4
40
Flumethrin (μM)
d
Male
Female
Survival (%)
0
4
40
Flumethrin (μM)

Fig. 2.4 Tick survival upon exposure to sublethal doses of flumethrin. Parthenogenetic larva (**a**), nymph (**b**), adult (**c**) and bisexual adult (**d**) ticks were exposed to sublethal doses of flumethrin for 48 h. Ticks lying on their backs that could not turn over were considered dead. *$P < 0.05$: significantly different by Welch's t-test as compared to the *EGFP* knockdown of the same acaricide concentration

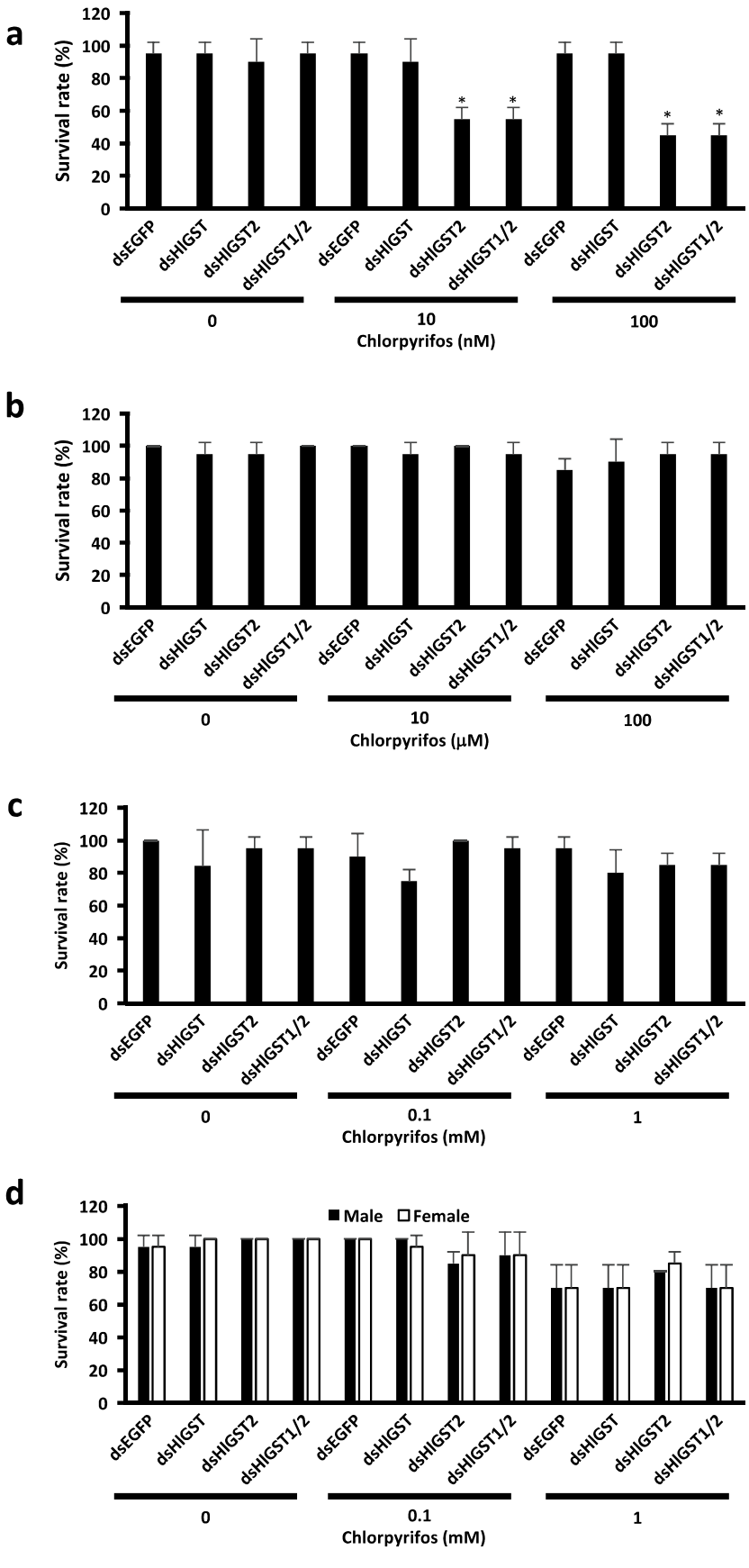
a
Survival rate (%)
120
100
80
60
40
20
0
dsEGFP
dsHIGST
dsHIGST2
dsHIGST1/2
0
10
100
Chlorpyrifos (nM)
b
Survival rate (%)
Chlorpyrifos (μM)
c
Survival rate (%)
0.1
1
Chlorpyrifos (mM)
d
Male
Female
Survival rate (%)
Chlorpyrifos (mM)

Fig. 2.5 Tick survival upon exposure to sublethal doses of chlorpyrifos. Parthenogenetic larva (**a**), nymph (**b**), adult (**c**) and bisexual adult (**d**) ticks were exposed to sublethal doses of chlorpyrifos for 48 h. Ticks lying on their backs that could not turn over were considered dead. *$P < 0.05$: significantly different by Welch's t-test as compared to the *EGFP* knockdown of the same acaricide concentration

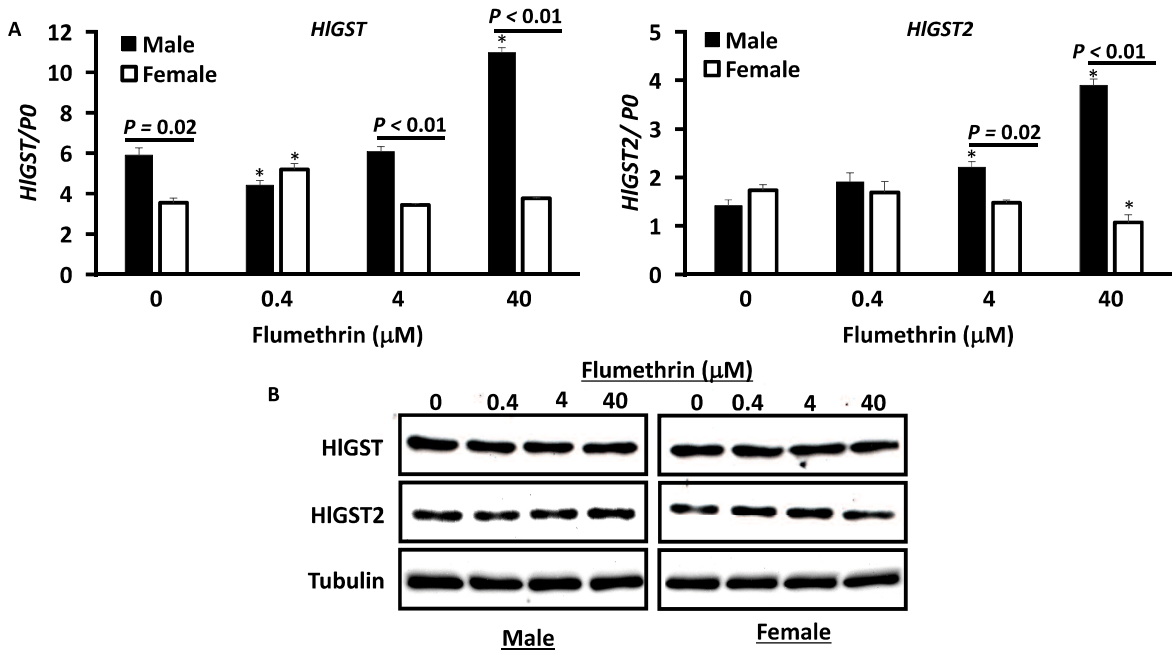

Fig. 2.6 Gene (**A**) and protein (**B**) expressions of HlGST of male and female ticks upon exposure to sublethal doses of flumethrin. Ticks were exposed to sublethal doses (0, 0.4, 4 and 40 μM) of flumethrin for 48 h. **a** Total mRNA extracted from ticks was transcribed to cDNA for real-time RT-PCR. *P0* primers were used as controls. The error bar represents the mean ± standard deviation. **P* < 0.05: significantly different by Welch's t-test as compared to no treatment. **b** Proteins were prepared from ticks exposed to sublethal doses of acaricides. Antiserum against tubulin was used as a control for Western blot analysis. The Western blot analysis results are shown as representative data of three separate experiments showing the same trend

CHAPTER 3

Expression analysis of glutathione S-transferases and ferritins during the embryogenesis of the tick *Haemaphysalis longicornis*

This work will be published as:

Hernandez, E.P., Shimazaki, K., Niihara, K., Umemiya-Shirafuji, R., Fujisaki, K., and Tanaka, T. (2019). Expression analysis of glutathione S-transferases and ferritins during the embryogenesis of the tick *Haemaphysalis longicornis*.

3.1 Introduction

The hard tick *Haemaphysalis longicornis* has been gaining attention recently because it is a vector of several pathogen-causing diseases. These ticks, originally known to be native to Eastern Asia and to have been established in Australia and New Zealand, are now also reported in multiple places in North America [1,113]. They are obligate blood-feeding arthropods that need to feed on blood in almost all developmental stages, except during embryonic and larval development. Embryogenesis is a crucial stage in the life cycle of these ticks [114]. Due to the lack of blood during this crucial process, the egg mainly relies on the yolk to furnish it with the energy and nutrition required for development [115].

Glutathione S-transferases (GSTs) are enzymes that act in the excretion of physiologic and xenobiotic substances, protecting cells against chemical toxicity and stress. Aside from this, they are involved in the catalysis of products of oxidative stress [33]. A previous study revealed that GST activities increase during embryonic and larval development, but the exact GST molecule contributing to this increase remains unknown [14]. In the previous chapters, the two GST molecules (HlGST and HlGST2) of *H. longicornis* were identified and characterized during blood feeding and acaricide exposure, but their role during embryonic development is yet to be determined [34,39,44].

Iron molecules are important in many metabolic processes, including energy metabolism and DNA replication, which is important in the embryogenesis of mammals and may also be applicable to other species [116] . However, the Fe^{2+} form has been shown to catalyze the Fenton reaction to produce reactive oxygen species (ROS), which damage cells [117]. Ferritin in ticks has an intracellular type (Fer1) and a secretory type (Fer2) [7,23]. Fer1 has the function of retaining Fe^{3+} transformed from the toxic Fe^{2+} as an antioxidant molecule; conversely, Fer2 transports Fe^{3+} from the midgut to the ovary, suggesting that it plays an important role as an antioxidant and in embryogenesis [8]. Furthermore, silencing the *Fer2* gene has been shown to cause a decreased hatching rate and the formation of abnormal eggs [23].

Antioxidant molecules are currently being explored as target molecules for tick control. Aside from these, molecules of embryonic origin are also looked upon as potential targets. Previous studies have shown that malondialdehyde (MDA), which is an index of lipid peroxidation and oxidative stress, has an increasing expression during embryonic development [14]. This could be an indication that during embryonic development, oxidative stress occurs in the tick that could result in lipid peroxidation. The occurrence of oxidative stress may be related to the acquired maternal iron. In this study, I attempted to identify the possible roles of the antioxidant molecules GST and Fer

during embryonic development by analyzing their expression and correlating their possible functions during the various events of embryonic development.

3.2 Materials and methods

3.2.1 Ticks and experimental animals

In this study, the parthenogenetic Okayama strain of *H. longicornis* was used in all experiments. Ticks and rabbits were maintained as previously described in Chapter 1. Engorged female ticks were collected and placed on 24-well plates and placed in a humid chamber in a 25 °C incubator. During egg laying, the eggs were collected daily for at least one week, placed in a separate 24-well plate, and kept in the same incubator.

3.2.2 Total RNA extraction and real-time PCR analysis

Total RNA was extracted from eggs on different days during oviposition (days 0, 5, 10, 15, and 20) [14]. Egg samples were homogenized using an automill (Tokken, Chiba, Japan) and were added to TRI Reagent® (Molecular Research Center, OH, USA). RNA extraction was performed following the manufacturer's protocol. Subsequently, single-strand cDNA was prepared by reverse transcription using the ReverTra Ace® qPCR RT Master Mix (Toyobo, Osaka, Japan), following the manufacturer's protocol.

Transcription analysis of *HlGST*, *HlGST2*, *HlFer1*, and *HlFer2* genes was performed through real-time PCR using the protocol described in Chapter 1 using the specified gene primers (Table 3.1).

3.2.3 Protein extraction and Western blot analysis

Protein was extracted from eggs on different days post-oviposition. Egg samples were homogenized using an automill (Tokken) and then suspended in PBS treated with Complete Mini Proteinase Inhibitor Cocktail Tablets (Roche, Mannheim, Germany). After sonication and recovery of the supernatant, the egg protein concentration was measured using a Micro BCA kit (Thermo Scientific, Rockford, IL, USA). Western blotting was performed in accordance to the procedure described in Chapter 1.

3.2.4 Thiobarbituric acid reactive substances (TBARS) assay

To measure the levels of oxidative stress, a TBARS assay was performed using the method described by Hu et al. [118]. Briefly, egg homogenates were added to two volumes of 7.5% trichloroacetic acid and mixed. The mixture was centrifuged at 1000 × *g* for 10 min. A supernatant was added to half the volume of 0.7% 2-thiobarbituric acid

and boiled for 10 min. The mixture was cooled, and TBARS were measured at $OD_{532\ nm}$. The extinction coefficient of 156,000 $M^{-1}cm^{-1}$ was used for calculation.

3.2.5 Iron assay

To measure the ferrous and ferric iron concentrations of the egg homogenates, a Quantichrome™ iron assay kit was used following the manufacturer's protocol for a 96-well plate (BioAssay Systems, Hayward, CA, USA).

3.2.6 Embryonic fixation and scaling

For embryonic fixation and scaling, the protocol by Santos et al. (119) was followed with some modifications. Briefly, approximately 100 mg of eggs were separated for fixation and placed in a 1.5 ml tube. The eggs were washed for 8 min with a solution containing 1.5% sodium hypochlorite and 5% sodium carbonate. Subsequently, the eggs were washed with Milli-Q water three times. One milliliter of Milli-Q water was added to the tube, which was then heated at 90 °C for 2 min using a heat block. Immediately following this heating procedure, the tube containing the eggs was left on ice for 2 min, causing the cracking of the eggshells. Shortly thereafter, a fixation solution containing heptane and 4% paraformaldehyde in PBS (1:1) was added. The eggs remained suspended

between the phases of the fixation solution, which was rotated at room temperature for 1 h. The lower phase containing the paraformaldehyde was removed, 100% methanol was added to the solution, and the tube was vigorously shaken for 2 min. Eggs that had lost their shells sank toward the bottom of the tube, whereas eggs that retained their shells remained at the interface between the phases of the solution. The eggs were washed three times with methanol, then washed three times with PBS buffer. One milliliter of 20% sucrose solution was added and put in a shaker at 4 °C for 24–48 h. After removing the sucrose solution, 1 ml of SCALEVIEW A-2 (Olympus, Tokyo, Japan) was added and put in a shaker at 4 °C for 7 days. The eggs were then observed under a fluorescence microscope and classified based on the system by Santos et al. [119] (Fig. 3.1).

3.2.7 Differential egg count during oviposition

Scaled eggs during the different days of oviposition were classified. One hundred random eggs were observed and tallied based on the classification system by Santos et al. [119]. Since it is difficult to distinguish between stages 12–14 of the embryo during counting, these stages were grouped as one.

3.2.8 Statistical analysis

Statistical analyses were performed using STATA 15.0 software. Since the data is not normal and the variances are not equal, a Kruskal–Wallis rank test with Bonferroni multiple comparison tests was applied. Statistical significance was set as $^{*}P<0.05$.

3.3 Results

3.3.1 Transcription profiles of GST and ferritin genes during embryogenesis

Real-time PCR was performed to analyze the transcription profiles of *HlGST*, *HlGST2*, *Fer1*, and *Fer2* in different embryonic stages (Fig. 3.2). *HlGST* and *HlGST2* genes showed the highest expression levels during day 1 post-oviposition. At day 5 post-oviposition, the expression of the *GSTs* decreased, especially *GST2*, which decreased significantly. This was followed by an increase on day 10. After day 10 post-oviposition, both *GST1* and *GST2* genes decreased in expression and continued to decrease at day 20 post-oviposition, wherein the *GST1* was significantly decreased at day 20 in comparison to day 1 and day 10. Conversely, *Fer1* and *Fer2* gene expression significantly increased from day 1 to day 15, followed by decreased expression at day 20 post-oviposition. These results indicate that embryogenesis affects the transcription profiles of oxidative stress–related genes, including *GSTs* and *ferritins.*

3.3.2 Protein expression profiles GSTs and ferritins during embryogenesis

Western blot analysis was performed to detect HlGST, HlGST2, Fer1, and Fer2 during embryonic development (Fig. 3.3). Both HlGST and HlGST2 proteins increased during the embryogenesis. Conversely, Fer2 protein expression appeared to be constitutively expressed from days 1–20 post-oviposition. On the other hand, the Fer1 protein was not detected in any developmental stages. These results show that embryogenesis affects the GST and ferritin protein expressions. The GST proteins appear to be transcriptionally regulated; however, the ferritin proteins are not.

3.3.3 MDA concentration of embryos at different stages

As GSTs and ferritins are related to oxidative stress, a TBARS assay was performed to measure the levels of oxidative stress by measuring the MDA concentration at different embryonic stages (Fig. 3.4a). The levels of MDA appeared to increase during the course of development, with a significant increase from day 1 to day 15 post-oviposition. This result indicates that embryonic development entails oxidative stress.

3.3.4 Ferrous iron concentration of embryos during embryogenesis

Since ferritins are among the major molecules used to regulate the ferrous iron concentration in ticks, an iron assay was performed to measure the ferrous iron concentration during the course of embryogenesis (Fig. 3.4b). The ferrous iron concentration in the eggs appeared to be maintained from days 1–20 post-oviposition, as no significant change in ferrous iron concentration was observed. These results suggest that the tick embryos have a mechanism to maintain the ferrous iron concentration during development.

3.3.5 Developmental staging of the embryo

The ratio of each developmental stage at each time point was determined via DAPI staining on the embryo after its fixation and scaling; it was observed under a fluorescence microscope to determine the events occurring in the embryo during that specific time point (Table 3.2). At day 1 post-oviposition, 98% of the eggs belonged to stage 1, wherein the embryo has been cellularized. At day 5 post-oviposition, 1–21% of the eggs belonged to stage 2, 16–34% to stage 3, 34–51% to stage 4, and 9–20% to stage 5. In stages 2 and 3, cellular proliferation intensifies, while in stages 4 and 5, the formation and migration of cumulus cells take place (Fig. 3.1). At day 10 post-oviposition, 4–39%

of the eggs belong to stage 9, in which the ventral furrow is formed (Fig. 1). Also on this day, 49–58% of the eggs are at stage 10 of development, wherein the ventral sulcus closes and the appendages increase in size (Fig. 3.1). At this stage, a germ band was also identified (Fig. 3.1). At day 15 post-oviposition, 80–98% of the eggs belong to stage 11, wherein there is a continuous increase in the limb buds and the germ band becomes shorter and broad (Fig. 3.1). The fourth leg, as well as the ventral furrow, also starts to regress at this stage. Finally, at day 20 post-oviposition, 85–98% of the eggs belong to a combination of stages 12–14, wherein there is dorsal closure and the eggs are almost hatched (Fig. 3.1). These results imply that DAPI staining, together with the scaling of eggs, could be a useful tool to visualize the events occurring during embryogenesis.

3.4 Discussion

Embryogenesis refers to the period of development from fertilization to the differentiation of tissues. Embryogenesis is a product of well-controlled molecular- and cellular-programmed proliferation and differentiation of cells [120]. This complex process of development requires energy from adenosine triphosphate (ATP) through glycolysis or oxidative phosphorylation. In the hard tick *Rhipicephalus* (*Boophilus*) *microplus*, the same energy demand was observed during embryogenesis [121,122].

The female *H. longicornis*, after the completion of feeding, detaches from the host and initiates oviposition afterward. In previous literature, hatching was observed beginning on day 17 after egg laying [123], while during the course of this study, hatching commenced from around day 20 post-oviposition. The phospholipoglycoprotein in the yolk or the vitellin, acquired during oogenesis as vitellogenin, would be an energy source during embryogenesis through mitochondrial respiration and oxidative phosphorylation [124]. However, the use of oxygen as part of the substrate for energy poses a potential hazard, as it could result in the production of ROS and may cause the modification of several macromolecules, some of which are lipids, proteins, DNA, and RNA. Therefore, embryonic cells must have a mechanism to protect the cells from ROS and oxidative stress [120]. In *R. microplus*, an increasing oxygen consumption was observed during embryogenesis [14]. In this study, increasing levels of MDA, which is an indicator of lipid peroxidation, were observed from day 1 to day 15 post-oviposition (Fig. 3.4a). In *R. microplus* eggs, increasing levels of MDA were also observed during the progression of embryogenesis [14]. This could further indicate that embryogenesis results in oxidative stress in ticks, and ticks possess a mechanism to maintain the redox balance in order to survive.

In ticks, maintenance of the redox balance is achieved through a complex antioxidant system composed mostly of enzymes [20,125,126]. Included in the plethora of enzymes are the GSTs. The utilization of GSTs during periods of oxidative stress, such as blood feeding, was expressed by the increased gene and/or protein expression of these molecules [39–41].

During embryogenesis, *R. microplus* GST activity was observed to increase from day 1 to day 20 after oviposition [14]. In my study, both GST1 and GST2 proteins increased as embryogenesis occurred from day 1 to day 20 (Fig. 3.3). On the other hand, the *GST1* and *GST2* gene expression appeared to peak at day 1 and day 10 post-oviposition (Fig. 3.2a and b). The high *HlGST* gene expression on day 1 post-oviposition could be derived from the deposited maternal mRNA. After fertilization, there is a period of transcriptional silence. During this period of quiescence, the embryonic genome in the nucleus is not yet expressed; therefore, the development occurring at this period, such as cellularization, is directed by cytoplasmic factors wherein the majority are maternal mRNA [127]. This could indicate the crucial role of GSTs during the early stages of development, as maternally derived mRNAs are molecules important to early embryonic development [128]. The decrease in the expression of *HlGST* and *HlGST2* genes at day 5, wherein continuous cellularization is occurring, could be attributed to the gradual

decrease of the maternal mRNA in this period. Upregulated *GST* genes were observed on day 10. During this stage, the germ band is already formed, with the distinction of each area. This indicates that cellular differentiation among organs could have already occured. At day 9 post-oviposition in *Hyalomma dromedarii*, the tick embryo's basic protein is at its highest level. This indicates that the embryo during this stage has the necessary amount of protein or mRNA to synthesize new molecules on its own [129]. After the increase at day 10 post-oviposition, a decrease in *GST* gene expression was observed from day 15 to day 20. Interestingly, the same expression pattern in zebra fish was observed in its mu-class GSTs (the same class of HlGST and HlGST2), wherein there is an increase in *GST* gene expression during the initial stages followed by decreasing *GST* gene expression in the later stages of development [130]. In a study by Campos et al. [122], mitochondrial exopolyphosphatase (PPX) activity in *R. microplus* was correlated to energy production in the mitochondria in embryos. An increase in PPX activity was shown after the day 4 oviposition, and the increase continued until its peak at day 7; it then decreased during days 12–18 of development. Therefore, oxidative phosphorylation increased during this period. This could also indicate an increase in oxidative stress from the redox reaction. This could trigger the transcription of these GSTs [33]. It is also possible that another closely related *GST* gene that is more suitable to the events occurring at day 15 and day

20 after oviposition is favorably expressed. This is the period when distinct organs and features of the ticks can already be identified and the embryos are in preparation for hatching, since *I. scapularis* has more than 30 identified GST transcripts [57]. The downregulation of a GST gene in favor of another GST gene has also been observed in the locust during chlorpyrifos exposure [106].

Although my study indicates the possible roles of HlGST and HlGST2 during embryogenesis, previous studies have shown that when *GST* genes were knocked down in eggs, no significant difference was observed in terms of hatching in comparison with the control group [39]. This indicates the capability of other GSTs to functionally compensate for the loss of another closely related GST. One example of this is the functional compensation of *GST-Mu2* when the *GST-Mu1* gene was knocked down in HeLa cells [78].

Aside from mRNA and yolk nutrients that are maternally derived, other nutrients, such as iron, are acquired by the embryo from the adult female tick. Iron is transported to the embryo using iron-binding proteins such as ferritins and transferrins [9,117]. In this study, I checked the expression levels of the identified ferritins (*HlFer1* and *HlFer2*) in *H. longicornis*. Both *ferritins* have a low mRNA expression at the initial stage of embryogenesis (day 1 and day 5) and were upregulated from day 10 to day 15 and

downregulated at day 20 (Fig. 3.2c and d). This further strengthens the hypothesis that the embryo-derived mRNA is expressed abundantly beginning on day 10 post-oviposition. This could also be an indication of organogenesis during this period, especially at day 15, when the expression of ferritin genes, especially *HlFer2*, is highest. Incidentally, the organogenesis in *Hy. dromedarii* also occurs at day 15 post-oviposition [129]. In the study of Galay et al. [23], the Fer2 is sourced from the midgut and secreted as a protein into the hemolymph, wherein it would be transported to other organs, including the ovaries and oocytes. This is further supported by Western blotting results, wherein, even with the very low *HlFer2* gene expression at days 1–5 post-oviposition, the HlFer2 protein is still constantly expressed throughout the embryogenesis (Fig. 3.3). This could indicate that the HlFer2 protein detected at the earlier stages, before organogenesis, such as from day 1 to day 5, is the maternally derived Fer2 protein that was taken in by the ovary and oocytes. No Fer1 protein was detected, even with the upregulation of gene expression at day 10 and day 15 (Fig. 3.3). This could be because the intracellular ferritin expression, including that of HlFer1, in tick cells is regulated by the interaction of IRE in the *ferritin* mRNA with an iron-regulatory protein (IRP). On the other hand, IRP activity is dependent on the ferrous iron concentration in its environment [24]. Since no drastic change in the

concentration of ferrous iron was observed during the embryogenesis, there is no induction of the protein expression of HlFer1.

The nondetection of a HlFer1 protein and the consistency of expression of HlFer2 indicate that HlFer2 could be the dominant protein that helps to maintain iron homeostasis in the embryo. It is also to be noted that the other iron-shuttling protein, transferrin, can be detected in the ovary but not in the eggs [9]. This could further support the importance of HlFer2 in embryogenesis. The knockdown of HlFer2 in adult females, which also resulted in the lack of HlFer2 in the eggs, caused abnormal morphology and lower hatchability in eggs [23]. In *Drosophila*, the mutation of ferritins also resulted in abnormalities and death in embryos due to ectopic apoptotic events [131]. ROS are known to be mediators of apoptosis, and the ferrous iron, through a Fenton reaction, could trigger the production of these ROS [8]. Therefore, the absence of functional ferritin could have resulted in increased ferrous iron that may result in these abnormal apoptotic events.

In this chapter, I showed that ticks could be utilizing oxidative stress–related molecules that were previously indicated during blood feeding, such as GSTs and Fer2. This is manifested by the increasing or constant expression of these molecules during the course of embryogenesis. This is further supported by the effect on egg fertility in knockdown and vaccination studies with these molecules. After vaccination with

recombinant GST1, animals infested with *R*. (*B.*) *microplus* showed a 10% reduction in egg fertility [132]. In *R. appendiculatus*, a 33% reduction in egg fertility was reported (133). On the other hand, the knockdown of Fer2 resulted in an 89% reduction in egg hatching in the *H. longicornis* tick, while vaccination experiments on it resulted in a 20% decrease in egg hatching and a 49% reduction in larval survival [23,134]. In *Ixodes ricinus*, vaccination with Fer2 resulted in an 85% reduction in egg fertility, while a 40% reduction was observed in *R.* (*B.*) *microplus* and a 51% reduction in *R. annulatus* [135]. This study, along with the previous studies, shows that the oxidative stress–related molecules GST and HlFer2 could play a vital role in the embryogenesis of *H. longicornis* ticks.

Tables and Figures in CHAPTER 3

Table 3.1 Gene-specific primers used in this study

Primer	**Sequence (5' → 3')**
GST1 real-time forward	CTTCTTGGATCTTGGCGGGT
GST1 real-time reverse	CGATGTCCCAGTAGCCGAG
GST2 real-time forward	CCCTTCCGGGAATGAAGGAG
GST2 real-time reverse	GATCGCTCAGCAGTCGTCAG
Fer1 real-time forward	ATGGCCGCTACTCAACCCCG
Fer1 real-time reverse	GAACTTGTGGAAGCCCGGCA
Fer2 real-time forward	ATGCTCCCGATCCTGATCTT
Fer2 real-time reverse	GGCCATCTGCATGTAGACCAA
P0 real-time forward	CTCCATTGTCAACGGTCTCA
P0 real-time reverse	TCAGCCTCCTTGAAGGTGAT
L23 real-time forward	CACACTCGTGTTCATCGTCC
L23 real-time reverse	ATGAGTGTGTTCACGTTGGC
Actin real-time forward	ATCCTGCGTCTCGACTTGG
Actin real-time reverse	GCCGTGGTGGTGAAAGAGTAG

Table 3.2 Proportion of the different embryo stages at different days post-oviposition (%)

DPO	Stages											
	1	2	3	4	5	6	7	8	9	10	11	12–14
1	98	1-2	1	0	0	0	0	0	0	0	0	0
5	0-1	1-21	16-34	34-51	9-20	1-12	0	0	0	0	0	0
10	0-1	0-1	1-18	0-9	0-5	2-9	0-2	0-5	4-39	45-58	0-2	0
15	0	0	0	0	0	0	0	1-5	0-11	1-3	80-98	0-2
20	0-1	0-1	1-4	0-1	0	1-2	0	1-3	0-1	1-2	0-2	85-93

DPO: days post-oviposition.

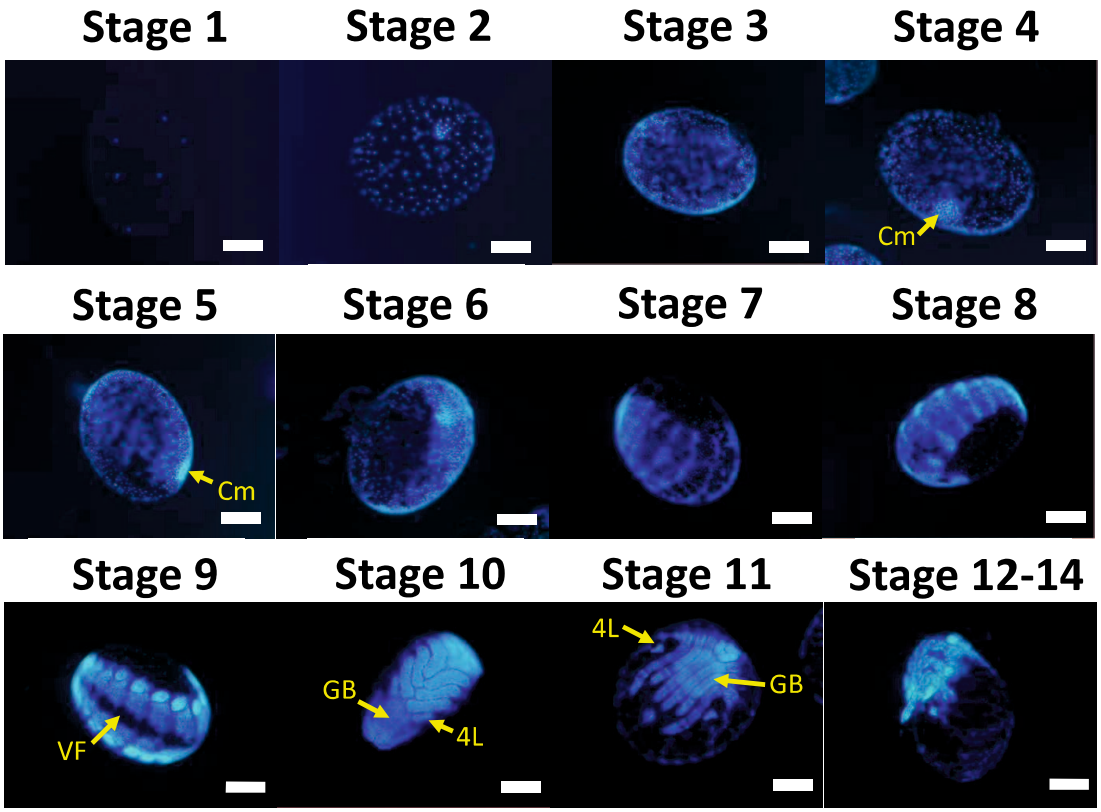

Fig. 3.1 Staging of the embryonic development of *H. longicornis*. Embryos were deshelled and scaled. The embryonic nuclei were stained with DAPI and observed under fluorescence microscopy. The embryos were staged based on the classification system by Santos et al. [119]. Cm: cumulus cells; VF: ventral furrow; GB: germ band; 4L: 4th set of limbs. Scale bars = 200 μm.

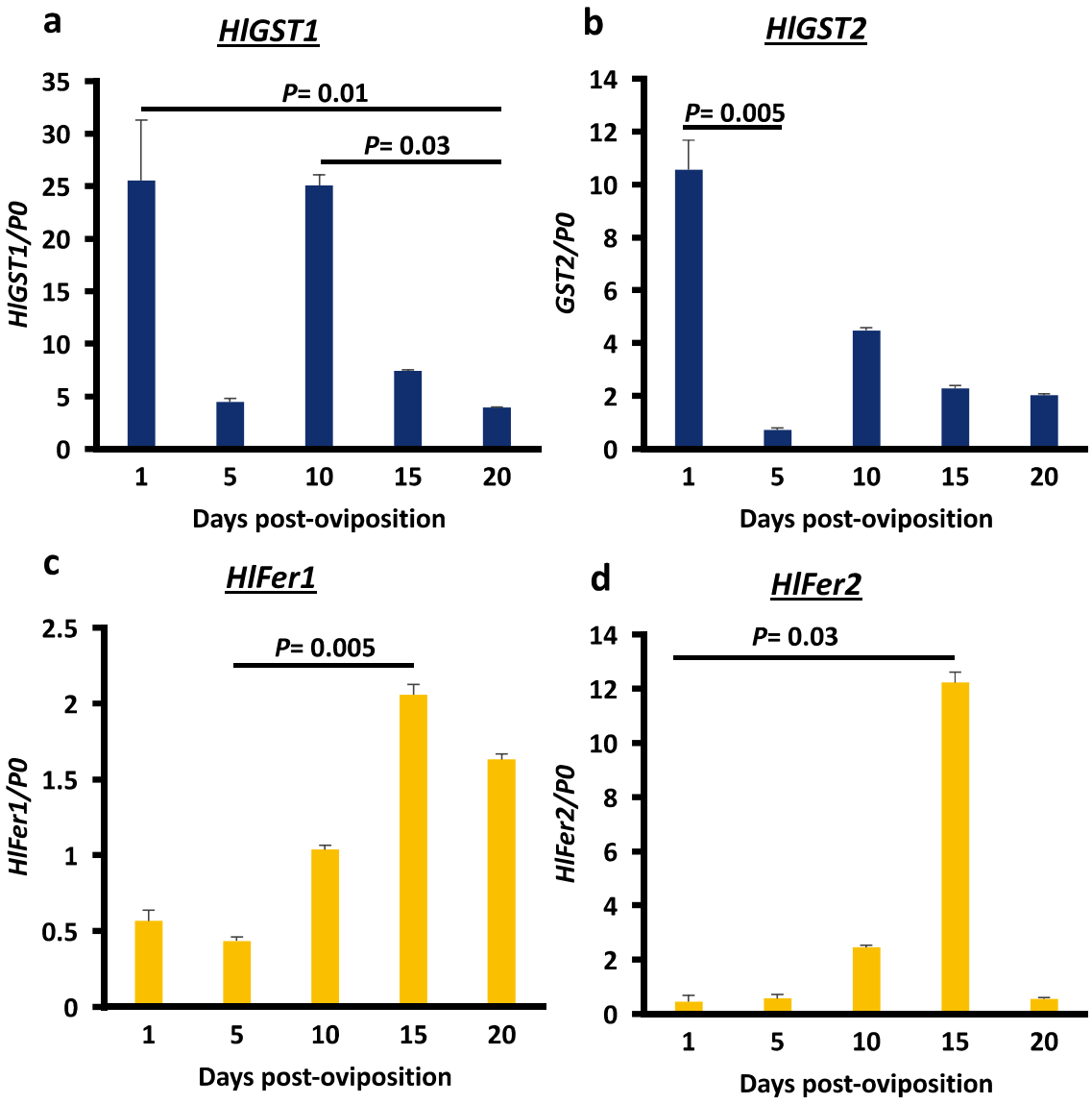

Fig. 3.2 Transcription profiles of (a) *HlGST1*, (b) *HlGST2*, (c) *HlFer1*, and (d) *HlFer2* genes during *H. longicornis* embryogenesis**.** Total RNA was prepared from embryos harvested at different days post-oviposition. *P0* genes were used as the control. Error bar represents the mean ± standard deviation. Significant difference was determined using the Kruskal–Wallis rank test.

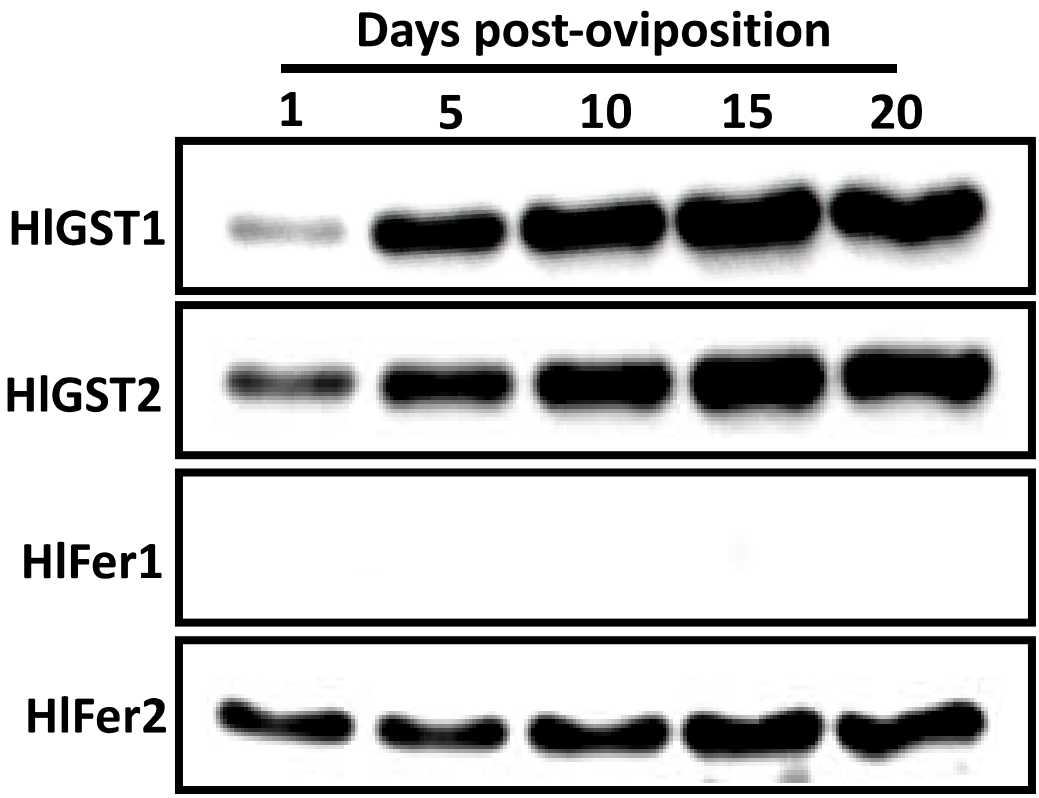

Fig. 3.3 Expression profiles of GSTs and ferritins during *H. longicornis* embryogenesis**.** Proteins were prepared at different days post-oviposition. The results of Western blotting are shown as representative data of three separate experiments showing the same trend. The protein concentration was determined using a Micro BCA kit and maintained at 50 μg per lane before loading for Western blotting.

a

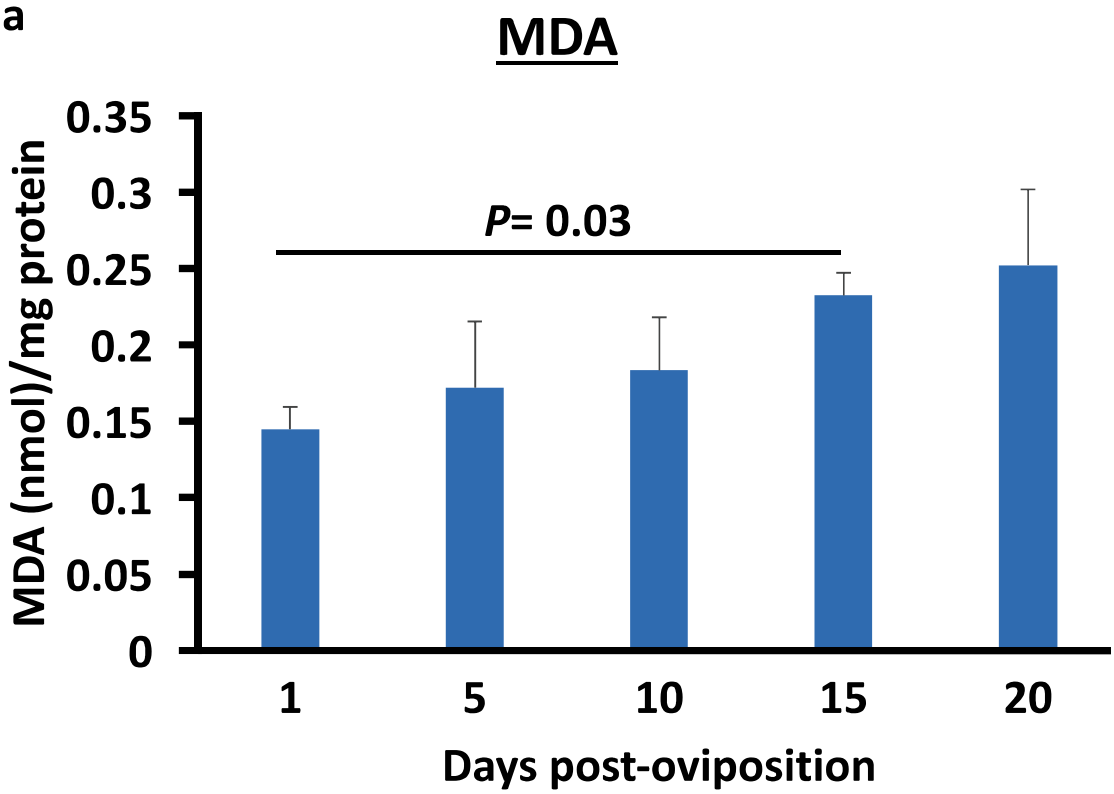
MDA
MDA (nmol)/mg protein
0.35
0.3
0.25
0.2
0.15
0.1
0.05
0
P= 0.03
1
5
10
15
20
Days post-oviposition

b

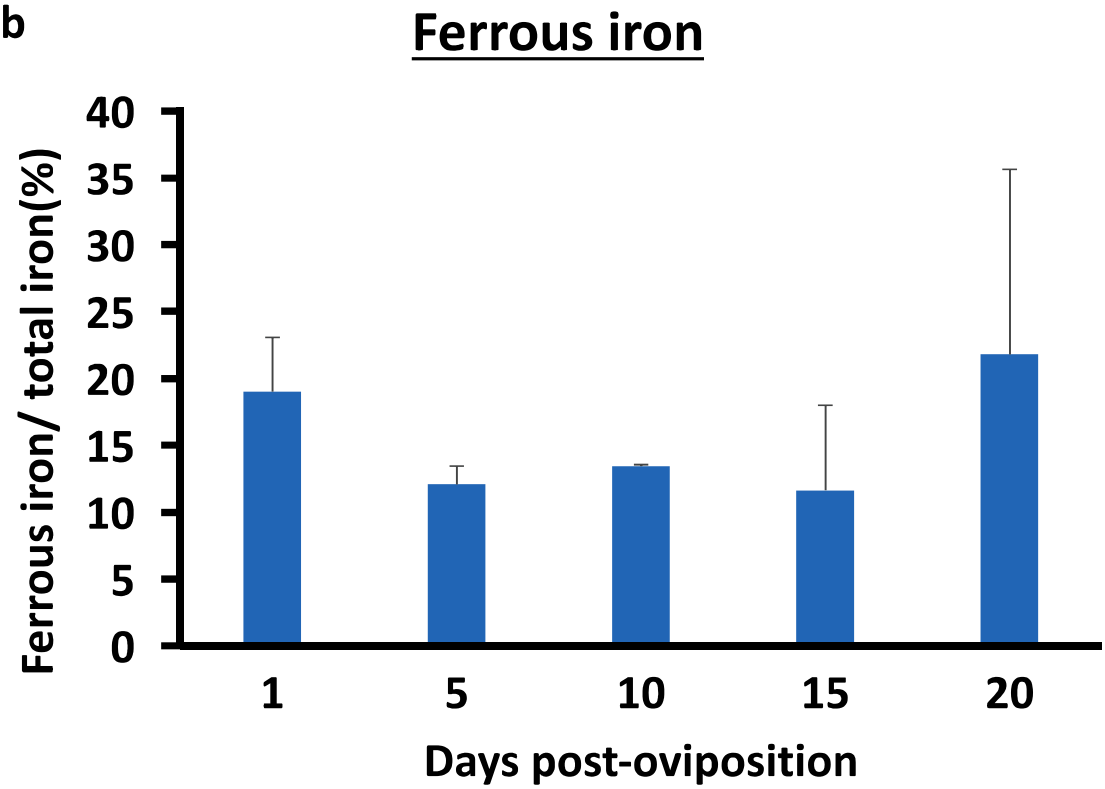
Ferrous iron
Ferrous iron/ total iron(%)
40
35
30
25
20
15
10
5
0
1
5
10
15
20
Days post-oviposition

Fig. 3.4 MDA concentrations (a) during the embryogenesis of *H. longicornis.* MDA concentration was determined by TBARS assay. Significant difference was determined using the Kruskal–Wallis rank test. Ferrous iron (b) percentages during *H. longicornis* embryogenesis. The total iron concentration was determined using an iron assay kit, while the ferrous iron concentration was determined using the same kit without a reducing agent. The ferrous iron percentage is the concentration of ferrous iron divided by the total iron concentration.

CHAPTER 4

Induction of intracellular ferritin expression in an embryo-derived *Ixodes scapularis* cell line (ISE6)

This work was published as:

Hernandez EP, Kusakisako K, Talactac MR, Galay RL, Yoshii K, Tanaka T. (2018). Induction of intracellular ferritin expression in embryo-derived *Ixodes scapularis* cell line (ISE6). *Sci Rep*, **8**, 16566.

4.1 Introduction

Iron is vital to life, for it is important in many metabolic processes of the cells, including oxygen transport and deoxyribonucleic acid (DNA) synthesis, as well as electron transport [136]. On the other hand, excess iron specifically in the ferrous ion (Fe^{2+}) could lead to deleterious effects due to its ability to trigger the Fenton reaction. The Fenton reaction is a result of iron reacting to hydrogen peroxide (H_2O_2), resulting in the generation of hydroxyl radicals. Thus iron must be carefully balanced in cells [137].

Ticks are obligate blood-feeding arthropods. Since tick digestion occurs within the digestive cells, they are more exposed to increased amounts of iron coming from the host blood as compared to other blood-feeding arthropods. Thus, ticks make use of several strategies to control iron levels [8]. One strategy ticks utilise is iron sequestration. Several proteins have been shown to be important in the sequestration of iron. These include two ferritins, such as intracellular ferritin (Fer1) and secretory ferritin (Fer2), and they also include iron regulatory proteins (IRP) to control Fer1 expression [7].

Ferritins are iron-storage proteins found in almost all organisms. The primary function of FER is to store excess iron available in the cellular iron pool. The iron storage process involves the binding and oxidation of Fe^{2+} and the formation of ferric ion (Fe^{3+}) in the core cavity [8]. Fer1 protein expression is regulated by the interaction between IRPs

and iron-responsive elements (IRE) in the *Fer1* mRNA. Thus, these interactions are dependent on the cell's iron availability. During periods of low iron levels, IRP binds to the IRE element in the untranslated region of the *Fer1* mRNA, effectively blocking protein translation. When iron levels increase, Fe-S clusters can form an insert themselves into tick IRPs; the IRPs ar then converted into aconitase and detach from the mRNA iron loop. This results in Fer1 translation so that newly synthesised Fer1 can sequester the free iron to protect the tick cell from oxidative stress [7,138].

Tick cell lines have been used in the study of pathogenic organisms that can be transmitted by ticks [139]. Recently, studies involving immunology and physiology as well as response to oxidative stress utilised tick cell lines [25,139]; for this purpose, the embryo-derived tick cell line from *Ixodes scapularis* (ISE6) is one of the most used tick cell lines. Despite ISE6 cells being widely used, its protein composition still remains unknown. Researchers have attempted to define the origin of ISE6 cells, but were only able to establish that these cells have a neuron-like phenotype while retaining some proteomic characteristics similar to those of another embryo-derived cell line [139].

Since ISE6 cells are known to be embryo derived [139], I hypothesised that they retain certain characteristics of embryonic tissues. In previous studies on *H. longicornis* embryonic tissue, detection was possible for *Fer1* mRNA but not the Fer1 protein, and

for Fer2 protein but not *Fer2* mRNA [23]. Therefore, this study would like to establish a method to induce Fer1 protein expression in ISE6 cells to be used for further understanding the mechanism of iron regulation *in vitro* in ticks.

4.2 Materials and Methods

4.2.1 Culture of cells

The ISE6 cell line from the embryo of *Ixodes scapularis* was grown at 34˚C in L-15B medium (pH 6.4–6.6) with 10% fetal bovine serum (FBS) (Biosera, Dominican Republic), 5% tryptose phosphate broth, and antibiotics [140,141].

4.2.2 Identification of the Ferritin gene of ISE6 cells

BLAST analysis (https://blast.ncbi.nlm.nih.gov/Blast.cgi) of *H. longicornis* ferritin and *I. ricinus* IRP was used to determine their homologue in *I.* scapularis. Using the NCBI database, I determined the gene sequence of the predicted *I. scapularis* ferritins and IRP. From the gene sequence, gene-specific detection primers were designed: forward primers (ISFer1 RT-F, ISFer2 RT-F, IRP RT-F) and reverse primers (ISFer1 RT-R, ISFer2 RT-R, IRP RT-R) (Table 4.1).

Afterward, total RNA was extracted from ISE6 cells. To extract total RNA, one well containing 2.5×10^5 ISE6 cells from a 48-well plate was harvested and transferred

to a 1.5 ml tube. The cells were centrifuged at 630 × *g* for 3 min, wherein the supernatant was removed. The RNA was extracted using TRI Reagent (Molecular Research Center, Cincinnati, OH, USA) following the manufacturer's protocol. cDNA was synthesised from 1 μg of total RNA using ReverTra Ace Master Mix (Toyobo, Osaka, Japan) following the manufacturer's protocol.

4.2.3 RT-PCR analysis

Total RNA was extracted from representative wells using TRI Reagent (Molecular Research Center), and cDNA was synthesised using a ReverTra Ace synthesis kit (Toyobo) following the manufacturer's protocol. RT-PCR was subsequently performed using Hot Start ®PCR Mix (Jena Bioscience, Jena, Germany) following the manufacturer's protocol, using 16S rRNA as a loading control, followed by specific primers for *Fer1*, *Fer2*, or *IRP* genes. The PCR profile for *Fer1, Fer2, and 16s* was as follows: an initial denaturation step at 98^{o}C for 8 min; 25 cycles of the denaturation step at 98^{o}C for 30 sec; an annealing step of 65^{o}C for 60 sec; and an extension step at 72^{o}C for 60 sec. For *IRP,* the PCR profile was as follows: an initial denaturation step at 98^{o}C for 8 min; 40 cycles of the denaturation step at 98^{o}C for 30 sec; an annealing step of 65^{o}C for 60 sec; and an extension step at 72^{o}C for 90 sec. PCR products were run on 1.5% agarose

gel and stained with ethidium bromide for 50 min and viewed using ATTO system WUV-M20 (ATTO, Tokyo, Japan).

4.2.4 Ferrous sulphate treatment of ISE6 cells

ISE6 cells were seeded in a 48-well plate of 250 µl of 0.5 × 10^6 cells/ml and incubated at 34˚C overnight. The culture was removed, and the cells were treated with several concentrations of ferrous sulphate (0, 2, 10, and 20 mM) in culture medium at 34˚C at different time points (0, 12, 24, and 48 h).

4.2.5 In vitro ISE6 cell proliferation and survival assays

After ferrous sulphate treatment, ISE6 cells were used for *in vitro* cell proliferation and survival assays. After washing with phosphate-buffered saline (PBS), the cells were diluted in 200 µl of culture medium. One hundred microliters of cells was transferred to a 96-well plate for cell proliferation assay (MTT assay) and 1.5 ml tubes for cell survival assay (Trypan blue assay).

The cells in a 96-well plate for were incubated at 34˚C overnight before being subjected to an MTT assay using Cell Titer 96® Non-Radioactive Cell Proliferation Assay Kit (Promega, Madison, WI, USA). Briefly, 15 µl of dye solution was added to

each well. The plate was further incubated for 4 h. Then, 100 µl of solubilisation solution/stop mix was added to each well and incubated at 34˚C overnight. Absorbance at 570 nm was determined using a microplate reader (SH-9000 Lab, Corona Electric, Ibaraki, Japan). Ten microliters of cells in a 1.5 ml tube for Trypan blue assay was mixed with the same volume of Trypan blue. The ratio of stained to unstained cells was determined using a haemocytometer.

4.2.6 Western blotting of ISE6 cell lysates

Ferrous sulphate–exposed cells from representative wells were placed in PBS and bath sonicated for 5 min, amplitude 45 (AS ONE, Osaka, Japan), and then centrifuged at 20,600 × *g* at 4˚C for 5 min. Seventy microliters of supernatant was collected. Equal amounts of supernatant and 2 × loading buffer were mixed and placed in boiling water for 5 min, followed by centrifugation at 20,600 × *g* at 4˚C for 5 min. The protein extracts were separated by 12% SDS-PAGE and transferred to a polyvinylidene difluoride membrane (PVDF) (Millipore, Bedford, MA, USA). The membrane was blocked overnight with 3% skim milk in PBS with 0.05% Tween 20 (PBS-T) and then incubated with primary antibody using mouse-anti *H. longicornis* ferritin (HlFer1) sera (1:250)[23]. An antibody previously prepared for β–tubulin was used as a control [55]. It was

incubated at 37˚C for 1 h. After incubation with horseradish peroxidase (HRP)-conjugated goat anti-mouse IgG (1:50,000 dilution; Dako, Glostrup, Denmark) at 37˚C for 1 h, signals were detected using the ECL Prime detection reagent (GE Healthcare, Buckinghamshire, UK) and analyzed using FluorChem FC2 software (Alpha Innotech, Santa Clara, CA, USA). To be able to determine whether the detected signals using the HlFer1 or β–tubulin antibodies from *H. longicornis* would correspond to the Fer1 and β–tubulin of *I. scapularis*, the molecular weights of the bands detected were measured using FluorChem FC2 software (Alpha Innotech). The detected band for Fer1 at approximately 20 kDa corresponds to the predicted 19.7 kDa MW of Fer1 using the ExPASy software (https://web.expasy.org/cgi-bin/compute_pi/pi_tool). On the other hand, the approximately 49 kDa MW of β–tubulin corresponds to the predicted 49.9 kDa MW of *I. scapularis* β–tubulin (Accession no. XP_002406661.1) on which BLAST analysis shows that it has a 100% identity with the *H. longicornis* β–tubulin (Accession no. BAK41866.1). For further confirmation of the reactivity of the HlFer1 antibody with *I. scapularis* Fer, the knockdown of ISE6 cells with subsequent exposure to ferrous sulphate was performed, proceeded by the Western blotting of cell lysates. No band corresponding to Fer1 was observed in the knockdown group, indicating that the Fer1 band detected by the HlFer1 antibody is also the Fer1 of ISE6 cells.

4.2.7 Immunostaining of ISE6 cells

Ten microliters of cells was placed on chamber slides and allowed to air dry. The cells were then fixed with methanol for 10 min. Cells for immunostaining were washed with PBS. Cells were blocked for 1 h with 5% skim milk in PBS at room temperature; afterward, cells were incubated with a 1:50 dilution of mouse anti-HlFer1sera at room temperature for 1 h. Normal mouse serum was used as a negative control at the same dilution. Slides were then washed with PBS and incubated with Alexa Fluor 488-conjugated goat anti-mouse IgG (1: 1,000; Invitrogen, Carlsbad, CA, USA) at room temperature for 1 h. Following washes with PBS, the cells were mounted with VECTASHIELD with DAPI (Vector Laboratories, Burlingame, CA, USA). Images were taken using a confocal fluorescence microscope mounted with LSM 700 (Carl Zeiss, Jena, Germany).

4.2.8 Ferrozine assay of ISE6 cells

The ferrozine assay for measuring non-haem iron was adapted to determine the concentration of iron in ISE6 cells [142]. After knockdown and/or iron exposure, cells were collected, and cell lysates were collected using the method described above. Concentrated HCl (99.5%) was added and then heated to 95^{o}C. After cooling to room

temperature, the mixture was centrifuged, and the supernatant was obtained, to which was added 75 mM ascorbate or water. Afterward, 10 mM ferrozine (Sigma-Aldrich, St. Louis, MO, USA) was added. Saturated ammonium acetate was added to facilitate colour development. Absorbance was measured at 550 nm, and the iron concentration was calculated based on a molar extinction coefficient of the iron-ferrozine complex of 27,900 $M^{-1}cm^{-1}$ and based on the protein concentration. The protein concentration was measured using a Micro BCA Protein Assay Kit (Thermo Fisher Scientific, Rockdord, IL, USA). The total iron concentration is computed from samples with ascorbate. The ferrous iron concentration was computed from samples without ascorbate (reducing agent) [26,143,144], while the ferric iron concentration is computed from the difference between the total iron and ferrous iron concentration.

4.2.9 RNA interference (RNAi) using double-stranded RNA with lipofectin to ISE6 cells

RNA interference using double-stranded RNA (dsRNA) was performed to determine the effect of Fer and IRP on ISE6 survival and proliferation upon exposure to different doses of ferrous sulphate. The PCR primers used for the synthesis of dsRNA are listed in Table 4.1. The *Fer1* and *IRP* fragments were amplified by PCR from ISE6 cDNA

using oligonucleotides, including ISFer1 T7 forward with ISFer1 RNAi reverse and ISFer1 T7 reverse with ISFer1 RNAi forward primers, and ISIRP T7 forward with ISIRP RNAi reverse and ISIRP T7 reverse with ISIRP RNAi forward primers, to attach the T7 promoter recognition sites on both forward and reverse 5'ends. *Enhanced green fluorescent protein* (*EGFP*) gene fragment was amplified from *pEGFP* by PCR using oligonucleotides containing EGFP T7 forward and EGFP T7 reverse primers as well. PCR products were gel extracted and purified using a QIAquick Gel Extraction Kit (Qiagen, Hilden, Germany). The T7 RiboMAX Express RNAi System (Promega, Madison, WI, USA) was used to synthesised dsRNA by *in vitro* transcription. The successful construction of dsRNA was confirmed by running 1 μL of the dsRNA products in 1.5% agarose gel in a TAE buffer.

ISE6 cells were seeded in a 48-well plate of 250 μl of 0.5 $\times 10^6$ cells/ml and incubated at 34˚C overnight. The double-stranded RNA (400 ng/well), 15 μl of Opti medium, and 2.8 μl HilyMax (transfection reagent) were mixed and incubated at room temperature for 15 min. dsEGFP was used as a control. Cells in the plates were washed twice with PBS, and then 250 μl of culture media without FBS was added. The previously incubated dsRNA mixture was added to the medium in each well and incubated at 34˚C for 16 h. Two hundred and fifty microliters of the culture medium with FBS was added

and incubated further at 34˚C for 32 h. The transfected cells in some wells were harvested, and knockdown was confirmed using RT-PCR as previously described. Remaining knockdown wells were exposed to ferrous sulphate as previously described. Primers used in this study are shown in Table 4.1. Proliferation ability and survival were determined using MTT and Trypan blue assay as previously described.

4.2.10 Statistical analysis

Statistical analyses were performed using STATA15.0 software. The data were initially checked for normality and homogeneity assumptions using the Shapiro-Wilk W test for normality and Breusch-Pagan/ Cook-Weisberg test for heteroskedasticity. A one-way analysis of variance (ANOVA) or a Kruskall-Wallis test with Bonferonni multiple comparison tests was applied when appropriate. Statistical significance was set as $^{*}P<0.05$. Sample sizes were based on our previous results [25]. Sample sizes and reproducibility are indicated in the figure or table legends.

4.3 Result

4.3.1 Identification of Fer and IRP genes of ISE6

Identified *H. longicornis* and *I. ricinus* ferritins and IRPs were subjected to protein BLAST analysis to identify their homologues in *I. scapularis*. The BLAST

analysis revealed that *H. longicornis* Fer1 (Accession No. AAQ54713.1) has 86% identity, and *I. ricinus* Fer1 (Accession No. AAC19131.1) has 98% identity with *I. scapularis* Fer1 (Accession No. AAQ54714.1) (Fig. 4.1a). *H. longicornis* Fer2 (Accession No. BAN13552.1) has 63% identity, while *I. ricinus* Fer2 (Accession No. ACJ70653.1) has 98% identity with *I. scapularis* Fer2 (Accession No. XP_002415446.1) (Fig. 1a). Using the NCBI database, the gene sequences of the predicted *I. scapularis* ferritins were determined, and specific primers were designed to detect *I. scapularis* ferritin in ISE6 cells. The expected 474 base pairs (bp) band corresponding to *Fer1* mRNA was detected, while the expected 477 bp band corresponding to *Fer2* mRNA was not observed (Fig. 4.1b). For further confirmation of the absence of *Fer2* mRNA, another RT-PCR was performed using a different set of primers (ISFer2 RT forward B and ISFer2 RT reverse B), and no bands were observed (data not shown). The sequence of *IRP1* (EU885952) from *I. ricinus*, a tick closely related to *I. scapularis*, was used to design primers for *IRP* mRNA detection in which the expected 767 bp band corresponding to *IRP* was detected on ISE6 cell (Fig. 4.1b).

4.3.2 Induction of Fer expression by ferrous sulphate

To induce Fer1 expression via the removal of IRP from the *Fer1* mRNA, cells were exposed to high concentrations of Fe^{2+} through the addition of ferrous sulphate. In deciding an experimental concentration of ferrous sulphate for ISE6 cells, Trypan blue assay was performed to check for cellular mortality of cells treated with several concentrations of ferrous sulphate (0, 2, 10, and 20 mM) at different time points (0, 12, 24, and 48 h) (Fig. 4.2a). The Trypan blue assay showed that even immediately after the addition of ferrous sulphate, the survival of cells was affected. Concentrations of 10 and 20 mM of ferrous sulphate caused the mortality of almost all cells. This result could indicate that an increased level of ferrous sulphate in a cell could cause cellular toxicity. Western blotting of cell lysates after exposure to increasing concentrations of ferrous sulphate at different time points was also performed (Fig. 4.2b). An approximately 20 kDa band that corresponds to the Fer1 protein was faintly detected at 24 h but clearly seen after 48 h of exposure to 2 mM of ferrous sulphate. No bands at approximately 49 kDa corresponding to tubulin, as well as Fer1, were observed from 12 h to 48 h in 10 and 20 mM of ferrous sulphate–exposed cells because almost all the cells had already died. The maximum concentration of 2 mM of ferrous sulphate for 48 h was therefore used in the succeeding experiments.

To be able to determine the effect of lower doses of ferrous sulphate on ISE6 survival and the expression of Fer1, ISE6 cells were exposed to lower doses (0, 0.1, 1, and 2 mM) of ferrous sulphate for 48 h. A dose-dependent increase in mortality was observed (Fig. 4.3a).

To be able to determine whether Fer1 protein expression is transcriptionally regulated, RT-PCR was performed, which showed that the *Fer1* mRNA of ferrous sulphate–exposed cells did not show any difference in band intensity (Fig. 4.3b). On the other hand, dose-dependent Fer1 expression was also observed with Western blotting (Fig. 4.3c). Fer1 expression in cells exposed to ferrous sulphate for 48 h was further confirmed using an indirect immunofluorescent antibody test (IFAT) (Fig. 4.3d). Positive signals for Fer1 in the cytoplasm were more intense in ferrous sulphate–exposed cells as compared to non-exposed cells. These results show that the Fer1 protein of ISE6 cells could be expressed consistently when exposed to 2 mM ferrous sulphate for 48 h. The results could also indicate that the expressed Fer1 is post-transcriptionally regulated.

4.3.3 Effect of intracellular Fer silencing on intracellular ferrous iron concentration

To determine the effect on the ferrous and ferric ion concentrations in *Fer1* and *IRP* knockdown cells, ferrozine assay was performed on ferrous sulphate-enriched cells. *Fer1* and *IRP* knockdown ISE6 cells were exposed to different concentrations of ferrous sulphate (0, 0.1, 1, and 2 mM) and then subjected to the assay. In this assay, ferrous iron concentration was significantly greater in *Fer1* knockdown cells exposed to 1 and 2 mM than in EGFP and IRP knockdown cells (Fig. 4.4a). Conversely, ferric iron concentration was significantly lower in *Fer1* knockdown cells exposed to ferrous sulphate at 1 and 2 mM than in *EGFP* and *IRP* knockdown cells (Fig. 4.4b). These results are consistent with a role of Fer1 in the conversion of Fe^{2+} to Fe^{3+}. They also demonstrate that the induced Fer1 protein is functional in terms of storing iron.

4.3.4 Effect of intracellular Fer silencing on cellular mortality and proliferation

Ferritin proteins have already been demonstrated to be important in tick survival and reproduction [7,23]. Therefore, to investigate whether it would reflect on ISE6 cells, RNAi was conducted to determine whether *Fer1* and *IRP* gene silencing would affect the survival and proliferation of ISE6 cells. Gene silencing was confirmed by RT-PCR.

Knockdown of the *Fer1* gene with subsequent exposure to ferrous sulphate was investigated in Trypan blue and MTT assays. In the Trypan blue assays, with exposure to ferrous sulphate at 2 mM, *Fer1* knockdown cells showed apparently greater mortality than *EGFP* knockdown cells and significantly greater mortality than *IRP* knockdown cells (Fig. 4.5a). In the MTT assays, with exposure to ferrous sulphate from 0.1 to 2 mM, *Fer1* knockdown cells showed significantly lower cellular proliferation than *EGFP* and *IRP* knockdown cells (Fig. 4.5b). This could indicate the protective capability of Fer1 during periods of iron overload.

4.4 Discussion

Ticks are obligate blood-feeding ectoparasites known to be vectors of several diseases that are important to health and the economy [1]. Until now, the control of these ectoparasites has relied mainly on the use of chemical acaricides [36]. One of the methods being considered to control these arthropods is through the development of anti-tick vaccines [145]. Fer1 is one candidate molecule being considered for a tick vaccine [134]. Therefore, a thorough understanding of Fer1 is warranted; however, tick experiments regarding Fer1 always must consider the presence of Fer2 and the basal Fer1 protein level [7,23]. In this regard, the embryo-derived ISE6 cell line is an ideal candidate because of the absence of the Fer1 protein and *Fer2* mRNA on its natural state, as observed in the

present study. Although Oliver et al. showed that ISE6 cells differentiate towards a predominant neuron-like phenotype, their studies also demonstrated ISE6 cells can maintain certain proteomic characteristics due to their embryonic origin [139]. As cells possessing embryonic characteristics, this cell line could be used for elucidating both the function and regulation of Fer1.

Ferritin has been reported to be induced by several compounds, such as prostaglandins, oxalomalate, or hydrogen peroxide [146–148]. In the present study, I have tried to induce Fer1 expression in ISE6 cells by increasing the concentration of ferrous sulphate in the medium; in addition, the toxic effect of iron caused high mortality in ISE6 cells (Fig. 4.2a) when concentrations of iron were too high—10 to 20 mM. The immediate mortality with exposure to ferrous sulphate at high concentrations could represent accidental cell death (ACD). ACDs are usually caused by physical, mechanical, or chemical insults [149]. The cause of the ACDs in this study was suggested to be chemical insult because ferrous sulphate-enriched media tends to be acidic (pH 5.0), thus inducing change in intracellular pH.

High mortality was also observed in 2 mM ferrous sulphate–exposed tick cells (Fig. 4.2a). The addition of ferrous sulphate has resulted in increased ferrous iron concentration in the cellular environment [150]. Ferrous ions are more toxic than ferric

ions because when a ferrous ion reacts to H_2O_2 through the Fenton reaction, it could result in the generation of hydroxyl radicals. Highly reactive hydroxyl radicals could cause oxidative stress, such as lipid peroxidation, DNA strand breaks, and the degradation of other molecules [26,138]. In contrast with the ACD noted at high concentrations of ferrous sulphate, this cell mortality could be classified as iron-dependent regulated cell death (RCD), ferroptosis.[151] In ferroptosis, the iron-catalyzed lipid peroxidases accumulates to toxic levels due to the inactivation of the phospholipid peroxidase [149,151]. Although ferroptosis has not been established in ticks, ferroptopic death can be hypothesized as the cause of ISE6 cell mortality, and this hypothesis warrants further investigation in biochemical tests.

After 12 h of exposure, mortality did not appear to increase anymore (Fig. 4.2a). This could indicate that cells have developed a protective mechanism to cope with the increased oxidative stress, possibly by the sequestration of the ferrous iron molecule. This protective mechanism could be in the form of the increased transcription of anti-oxidative stress molecules, protein trafficking, or vacuolar function [19]. This is said to be an antioxidant response [152].

Western blotting and IFAT results have shown that at 48 h, the intracellular iron storage protein, Fer1, has been observed (Figs.4.3c and d). This phenomenon is consistent

with a previous theory on the role of IRP and Fer in the sequestration of free iron to protect tick cells from oxidative stress [7,138]. RT-PCR results have also shown that the mRNA level of ferritin did not greatly vary (Fig. 4.3b). However, a more accurate test such as quantitative real-time RT-PCR could directly measure the change in the mRNA transcription level. Nevertheless, the RT-PCR results could still indicate that the produced ferritin is post-transcriptionally regulated specifically by IRP-IRE interactions [153].

It takes time to express Fer1 after cells are exposed to inducers. In a previous experiment on mouse cell lines, Fer was induced by exposure to H_2O_2. The translational control of IRP peaked at 1 h and continually elevated until after 2 h, before the activity of the IRP decreased for the *Fer* mRNA to be available for translation. Synthesis of Fer starts at 4 h and continually increased for up to 24 h [154]. The time-dependent cytoprotective mechanism was also observed in porcine endothelium cells, wherein ferritin expression was not observed before 16 h and could protect cells [155]. Experiments in inducing Fer expression by oxalomalate indicated the induction of ferritin in human, rat, and mouse cell lines beginning 48 h after exposure [156]. It is also interesting to note that the slow feeding phase in ticks takes 6 to 9 days for *Ixodes* ticks [157]. This feeding phase may perhaps be a mechanism for protecting ticks from iron overload by the intake of iron just sufficient to trigger Fer1 translation. During the rapid

feeding phase and intracellular digestion, Fer1 protein would be readily available. However, further experiments are needed to prove this hypothesis.

Knockdown of *Fer1* and exposure to 1 or 2 mM of ferrous sulphate in ISE6 cells resulted in increased ferrous iron concentrations and decreased ferric iron concentrations in cells as observed in the ferrozine assay (Fig. 4.4). These results could indicate that the induced Fer1 is functionally capable of converting Fe^{2+} to a Fe^{3+} state [158]. Since Fer1 had not been induced during *Fer1* knockdown, the amount of Fe^{2+} increased; thus, the ability to induce oxidative stress also increased.

With exposure to 2 mM ferrous sulphate, *Fer1* knockdown yielded apparently greater mortality than EGFP knockdown and significantly greater mortality than *IRP* knockdown (Fig. 4.5a). This is a further indication of the time dependency for Fer1 translation due to the presence of IRP. Accordingly, Fer1 may already have been present in *IRP* knockdown cells when they were exposed to ferrous sulphate, thus protecting the cells and explaining the findings of lower mortality. In previous experiments using actual ticks, the knockdown of *Fer1* also resulted in decreased survival and reproduction when exposed to increased iron, such as during blood feeding [7,23]. On the other hand, the knockdown of *IRP* resulted in decreased mortality of ISE6 cells at lower doses of ferrous sulphate (Fig. 4.5a).

With exposure to 0.1 to 2 mM ferrous sulphate, *Fer1* knockdown also yielded lower cellular proliferation than *EGFP* and *IRP* knockdowns, providing a further indication of the cytoprotective capability of Fer1 (Fig. 4.5b). Since Fer1 is present in *EGFP* and *IRP* knockdown cells, they have greater protection from oxidative stress due to increased ferrous iron [26].

This evidence further strengthens the hypothesis that the cell death at 2 mM ferrous sulphate exposure is RCD, such as ferroptosis; ACD, which cannot be prevented or modulated and therefore cannot be targeted by interventions, RCD involves molecular mechanisms that can be targets for intervention [19,151]. In this case, the alteration could have occurred when lipid peroxidation was suppressed by the expression of Fer1, which in turn sequestered the iron molecules.

In summary, I induced the expression of the Fer1 protein in the *I. scapularis* embryo-derived cell line (ISE6) after exposure to 2 mM of ferrous sulphate for 48 h. I also showed that the Fer1 induced using this method has ferroxidase activity similar to the Fer1 in ticks. This study could be useful in understanding the iron metabolism in ticks, and the induction of intracellular ferritin, and represent a potentially major contribution to research on this molecule.

Tables and Figures in CHAPTER 4

Table 4.1 Gene-specific primers used in this study

Primers	Sequence [5' → 3']
ISFer1 RT forward	ACTGCGAAGCTCGCATCAACAA
ISFer1 RT reverse	ACAGGGTCTCCTTGTCGAACAT
ISFer2 RT forward	TTGCAAGCGCTGCGAGATGC
ISFer2 RT reverse	AGGCCCCTGCTCCCCAGAAT
ISFer2 RT forward B	ACAAAGTGGCACGCAAAGGT
ISFer2 RT reverse B	AAAACTCCTTCTTGTCCCCGAGCA
ISFer1 RNAi forward	TTGCAGCAGAAAACAGCCCTTG
ISFer1 RNAi reverse	TTGTCGAACATGTACTCTCCCAG
ISFer1 T7 forward	*TAATACGACTCACTATAGG*TTGCAGCAGAAAACAGCCCTTG
ISFer1 T7 reverse	*TAATACGACTCACTATAGG*TTGTCGAACATGTACTCTCCCAG
ISIRP RT forward	GCATGCATTGAAGATGCCGT
ISIRP RT reverse	GGAAGTAGGCCAACTCGACC
ISIRP RNAi forward	TCGACGTACATCAAGTGCCC
ISIRP RNAi reverse	GGAAGTAGGCCAACTCGACC
ISIRP T7 forward	*TAATACGACTCACTATAGG* TCGACGTACATCAAGTGCCC
ISIRP T7 reverse	*TAATACGACTCACTATAGG* GGAAGTAGGCCAACTCGACC
16s RT forward	CTGCTCAATGATTTTTTAAATTGCTGTGG
16s RT reverse	CCGGTCTGAACTCAGATCAAGTA
EGFP RNAi forward	GACGTAAACGGCCACAAGTT
EGFP RNAi reverse	TGCTCAGGTAGTGGTTGTCG
EGFP T7 forward	*TAATACGACTCACTATAGG*GACGTAAACGGCCACAAGTT
EGFP T7 reverse	*TAATACGACTCACTATAGG*TGCTCAGGTAGTGGTTGTCG

Italics denote T7 promoter sequences.

(a) Fer1

```
I. scapularis      1 MAATQPRQNYHVDCEARINKQINMEFYASYVYASMACYFDRDDVALPGFHKFFKKCSHEE
I. ricinus         1 MAATQPRQNYHVDCEARINKQINMEFYASYVYASMACYFDRDDVALPGFHKFFKKCSHEE
H. longicornis     1 MAATQPRQNYHIDCEARINKQINMELYASYVYTSMAYYFDRDDVALPGFHKFFKKSSEEE

I. scapularis     61 TEHAEKLMAYQNKRGGRVVLQPIAKPAQDEWGSGLEAMQAALELEKIVNQSLLELHKLAT
I. ricinus        61 TEHAEKLMAYQNKRGGRVVLQPIAKPAQDEWGSGLEAMQAALELEKIVNQSLLELHKLAT
H. longicornis    61 REHAAKLMKYQNMRGGRVVLQPIQKPAQDEWGSGLDAMQASLELEKSVNQSLLDLHKLAT

                                                                  Identity
I. scapularis    121 ERDDGQLCDFLEGNYLNEQVDAIKELSDYVTNLKRVGPGLGEYMFDKETLS     --
I. ricinus       121 EKDDGQLCDFLEGNYLNEQVEAIKELSEYVTNLKRVGPGLGEYMFDKETLS     98%
H. longicornis   121 DHNDAQLCDFLESEYLEEQVKAIKELSDYVTNLKRVGPGLGEYMFDKETLG     86%
```

Fer2

```
I. scapularis      1 QIPSVASRLLFICHSNNCTNSVLSGNNLFE--NLDKYPLQDECQAALQEHINVEMHASLV
I. ricinus         1 M------KQFVVILALLG--AATSGNNLFE--NLDKYPLQDECQAALQEHINVEMHASLV
H. longicornis     1 MIP-----ILIFAFALLC--VASAGNNLNEQVNQNKYFLHDRCRLGLQEQINAELHASLV

I. scapularis     59 YMQMAAHFDNNKVARKGFSTFFAENSKEEREHAQKIIDYINKRGSTVSLVNIDMPQITTW
I. ricinus        51 YMQMAAHFDNNKVARKGFSTFFAENSKEEREHAQKIIDYINKRGSTVSLVNIDMPLITTW
H. longicornis    54 YMQMAAYLGNNKVARAGFARFFSDQSSEEREHAQKLVDYVNLRGGTVSNVNVDMPATATW

I. scapularis    119 KSVLQALRDAISLENKVTNKLHAVHKTADEECKDPQLMDFLESEFLEEQVTSIDKLQRMI
I. ricinus       111 KSVLQALRDAISLENKVTNKLHAVHKIADEECKDPQLMDFLESEFLEEQVNSIDKLQRMI
H. longicornis   114 MSVLDTLQAALALEHQVTNRLHGLHALAADHCRDPQMTDFLEQEFLAEQMHSIDKLQRII

                                                          Identity
I. scapularis    179 TVLSNMDSGTGEYLLDRELLGDKKEF     --
I. ricinus       171 TVLSNMDSGTGEYLLDRELLGDKKEF     98%
H. longicornis   174 TQLQNMDTGLGEFLLDRELRREDSDK     63%
```

(b)

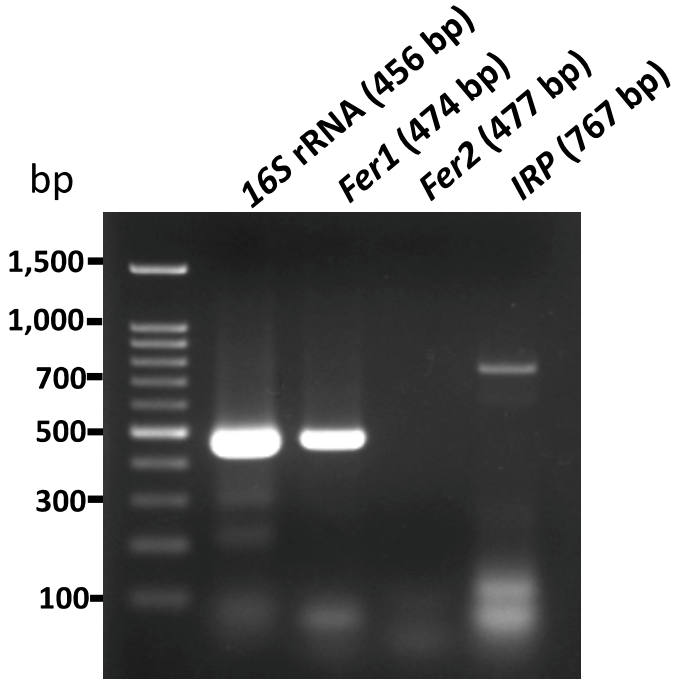

Fig. 4.1 Identification of the ferritin protein and genes of ISE6 cells. (a) Multiple sequence alignment of the amino acid sequences of Fer1 and Fer2 of *Ixodes scapularis* with *Ixodes ricinus* and *Haemaphysalis longicornis* ferritins. Identical residues are shaded black, while similar residues are shaded gray. The percent identities with Fer1 and Fer2 are placed at the end of the sequences. The GenBank accession numbers of ferritin sequences are as follows: *I. scapularis* Fer1 (AAQ54714.1), *I. scapularis* Fer2 (XP_002415446.1), *I. ricinus* Fer1 (AAC19131.1), *I. ricinus* Fer2 (ACJ70653.1), *H. longicornis* Fer1 (AAQ54713.1), and *H. longicornis* Fer2 (BAN13552.1). (b) RT-PCR of ISE6 cells for *Fer1*, *Fer2,* and *IRP*. Total RNA was extracted from ISE6 cells. cDNA was synthesised and subjected to RT-PCR. PCR products were run on 1.5% agarose gel and stained with ethidium bromide. 16S rRNA was used as a loading control. The PCR result are representatives of three separate experiments.

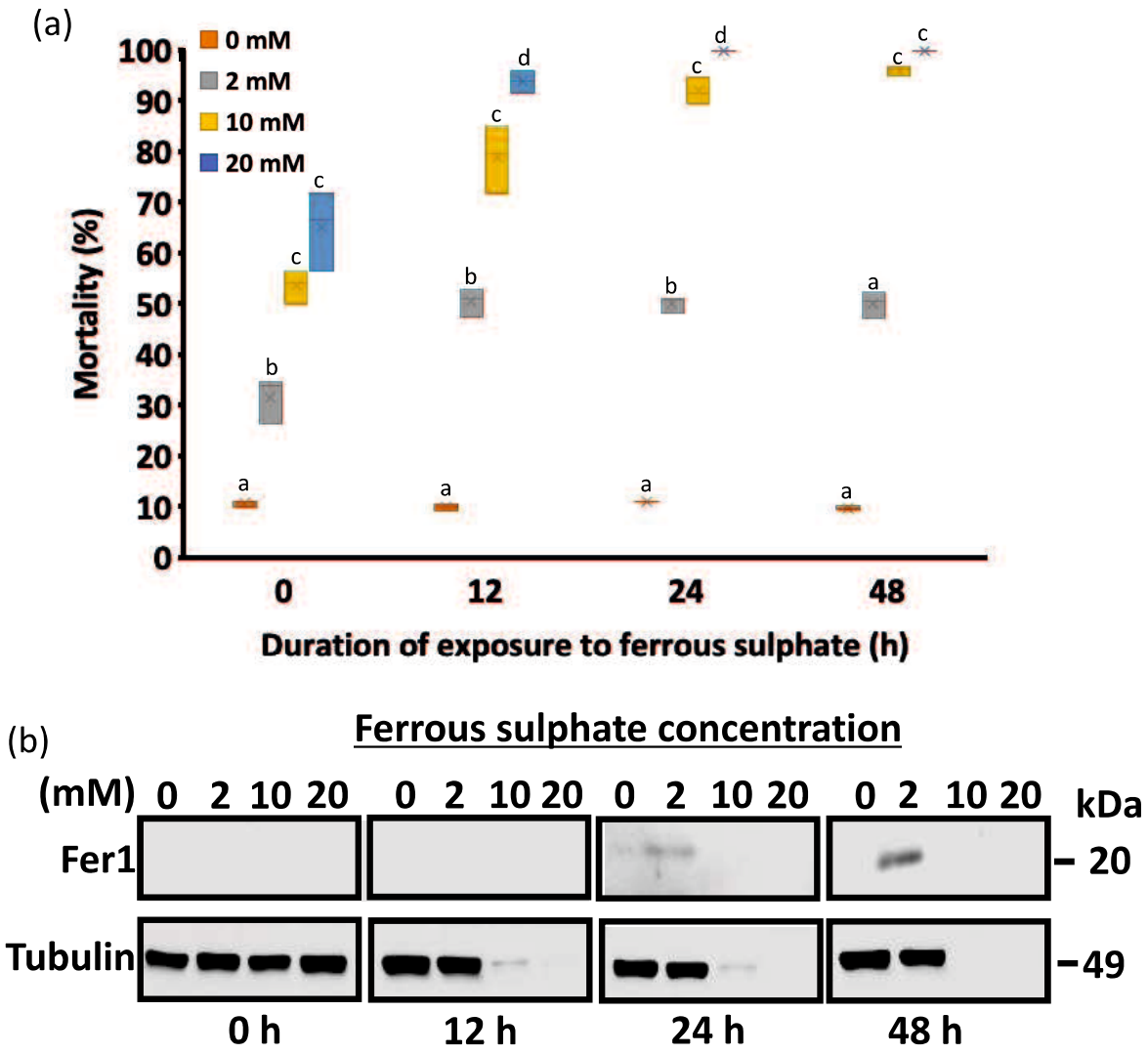

Fig. 4.2 (a) Box and whisker plot showing the distribution of mortality in percentage of ISE6 cells exposed to different concentrations of ferrous sulphate at different time points using Trypan blue stain. A one-way ANOVA with Bonferonni multiple comparison tests was performed. Time points with the same letter are not significantly different at $P<0.05$. (b) Western blotting of ISE6 cells exposed to different concentrations of ferrous sulphate at different time points. Protein analysis of Fer1 was observed using Western blotting. Anti-mouse tubulin was used as a loading control. The Western blotting results are representatives of three separate experiments. The data presented are results of three independent experiments with the Trypan blue staining performed in two technical replicates for each experiment.

(a)

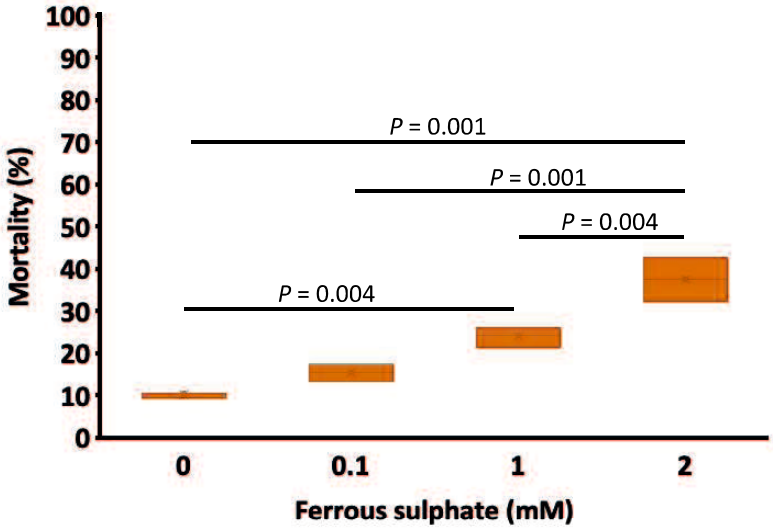
100
90
80
70
60
50
40
30
20
10
0
Mortality (%)
P = 0.001
P = 0.001
P = 0.004
P = 0.004
0
0.1
1
2
Ferrous sulphate (mM)

(b)

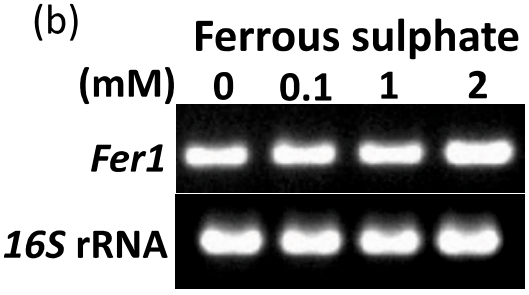
Ferrous sulphate
(mM) 0 0.1 1 2
Fer1
16S rRNA

(c)

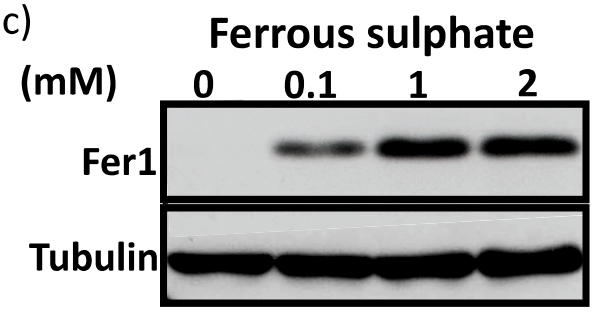
Ferrous sulphate
(mM) 0 0.1 1 2
Fer1
Tubulin

(d)

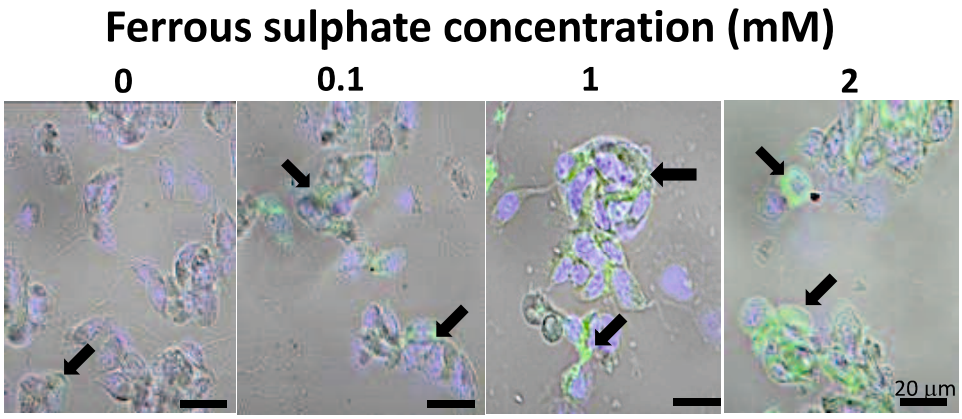
Ferrous sulphate concentration (mM)
0
0.1
1
2
20 µm

Fig. 4.3 (a) Box and whisker plot showing the distribution of mortality in percentage of ISE6 cells exposed to different concentrations of ferrous sulphate for 48 h. Mortality was checked after 48 h using Trypan blue stain. A one-way ANOVA with Bonferonni multiple comparison tests was performed. (b) *Fer1* mRNA expression of ferrous sulphate (0, 0.1, 1, and 2 mM)–exposed cells for *Fer1* was observed using RT-PCR. 16S rRNA was used as a loading control. The RT-PCR result is representative of three separate experiments. (c) Fer1 protein expression of ferrous sulphate (0, 0.1, 1, and 2 mM)–exposed cells for Fer1 was observed using Western blotting. Anti-mouse tubulin was used as a loading control. The Western blotting result is representative of three separate experiments. (d) Localization of Fer1 protein was observed using IFAT. Arrowheads indicate positive fluorescence. The IFAT result is representative of three separate experiments. Bar = 10 μm. The data presented are results of three independent experiments with the Trypan blue staining performed in two technical replicates for each experiment.

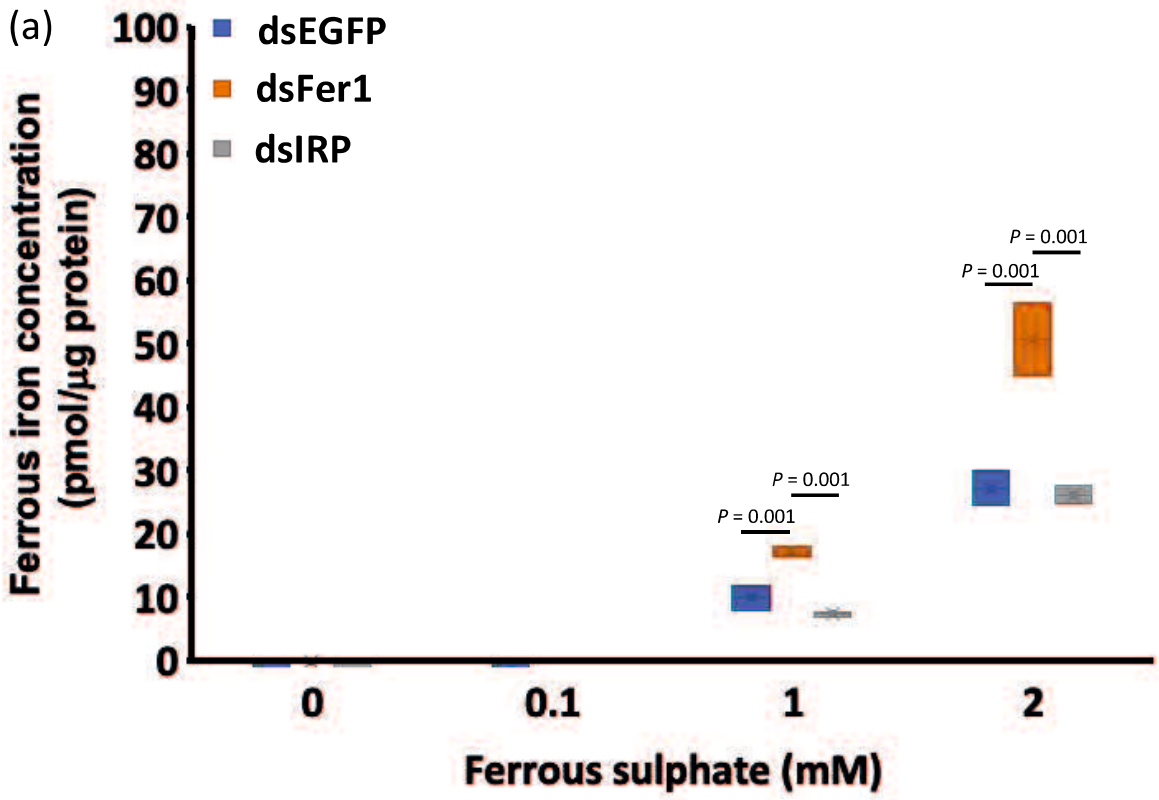
(a)
dsEGFP
dsFer1
dsIRP
Ferrous iron concentration (pmol/µg protein)
100
90
80
70
60
50
40
30
20
10
0
P = 0.001
P = 0.001
P = 0.001
P = 0.001
0
0.1
1
2
Ferrous sulphate (mM)

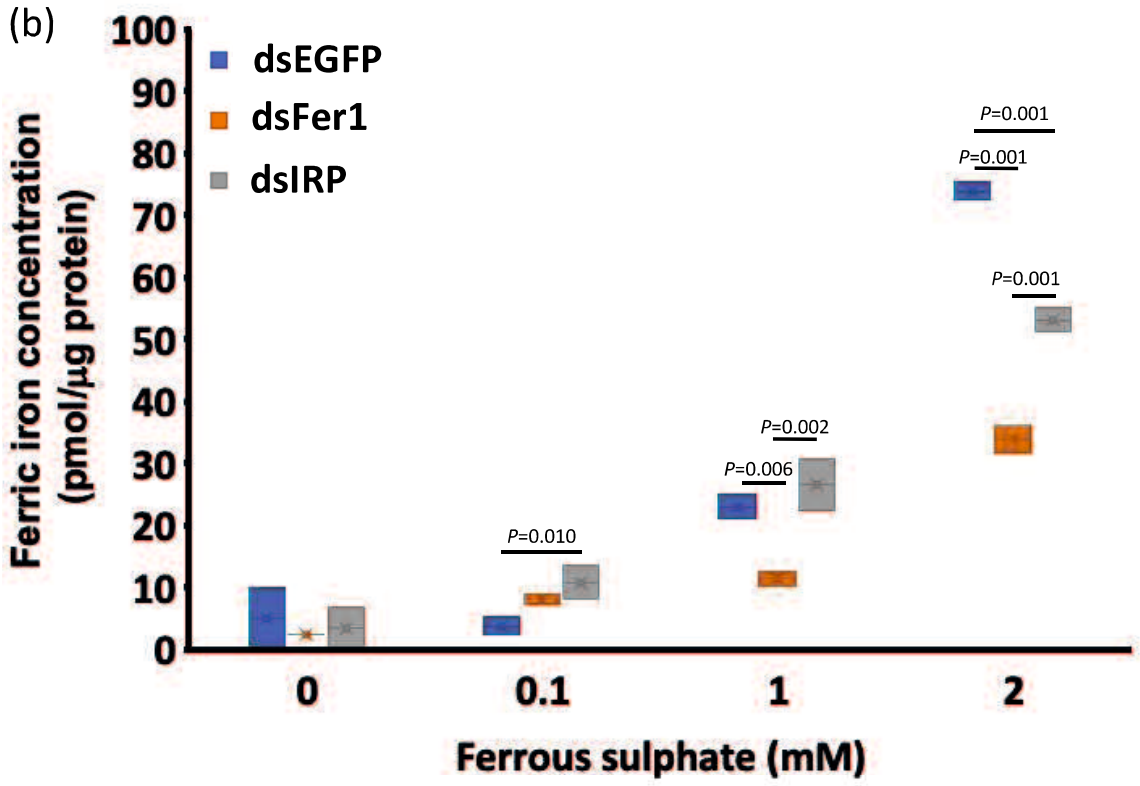
(b)
dsEGFP
dsFer1
dsIRP
Ferric iron concentration (pmol/µg protein)
100
90
80
70
60
50
40
30
20
10
0
P=0.001
P=0.001
P=0.001
P=0.002
P=0.006
P=0.010
0
0.1
1
2
Ferrous sulphate (mM)

Fig. 4.4 (a) Box and whisker plot showing the distribution of ferrous iron concentration of knocked down ISE6 cells exposed to different concentrations of ferrous sulphate as determined by ferrozine assay. Ferrous iron was determined using a ferrozine assay in the absence of a reducing agent. A one-way ANOVA with Bonferonni multiple comparison tests was performed (b) Box and whisker plot showing the distribution of ferric iron concentration of knocked down ISE6 cells exposed to different concentrations of ferrous sulphate as determined by ferrozine assay. Ferric iron was determined using the ferrozine assay by determining the difference between the total and ferrous iron concentrations. A one-way ANOVA with Bonferonni multiple comparison tests was performed. The data presented are results of three independent experiments with the ferrozine assay performed in two technical replicates for each experiment.

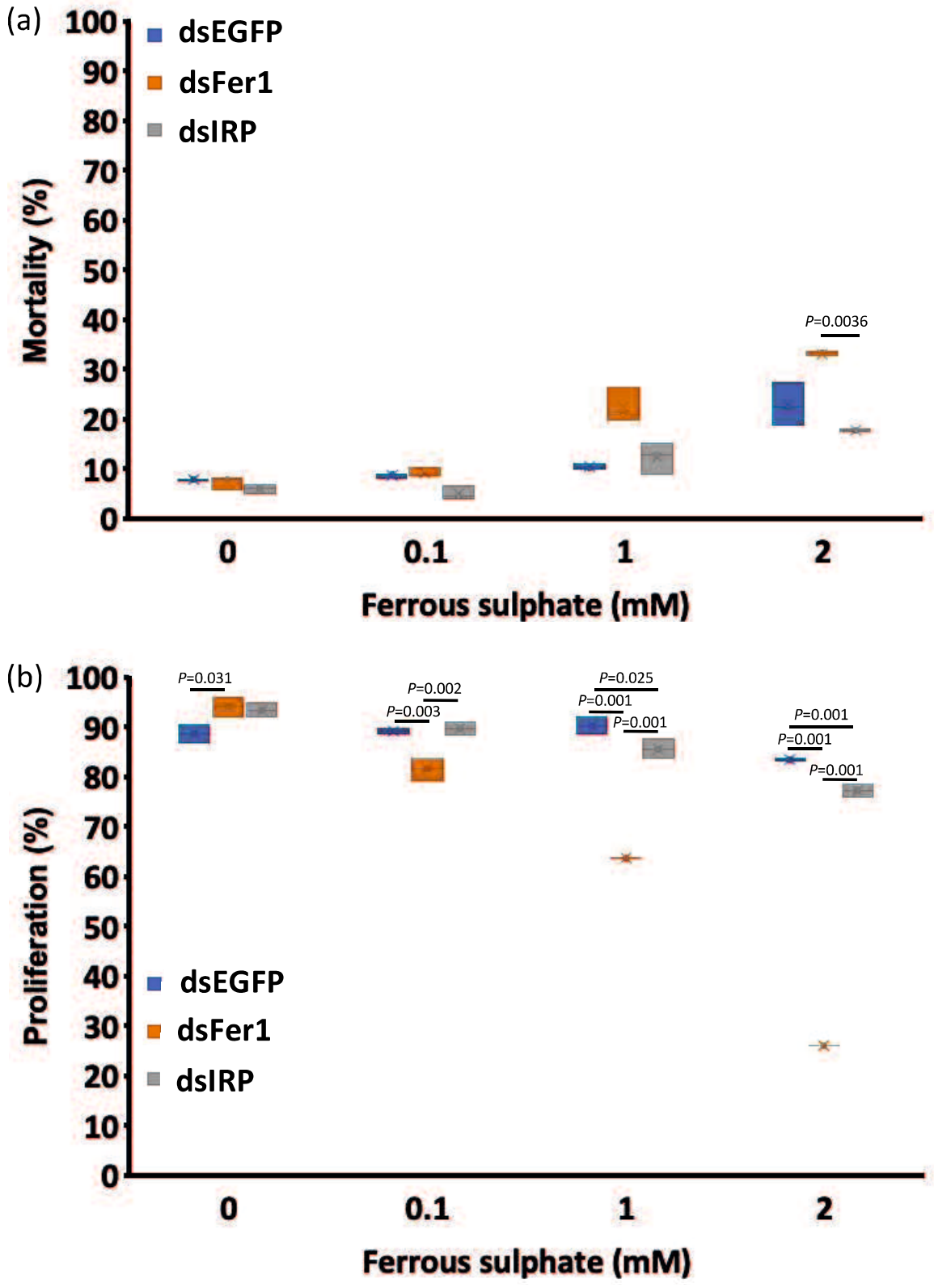
(a)
dsEGFP
dsFer1
dsIRP
Mortality (%)
100
90
80
70
60
50
40
30
20
10
0
P=0.0036
0
0.1
1
2
Ferrous sulphate (mM)
(b)
P=0.031
P=0.002
P=0.003
P=0.025
P=0.001
P=0.001
P=0.001
P=0.001
P=0.001
Proliferation (%)
dsEGFP
dsFer1
dsIRP
0
0.1
1
2
Ferrous sulphate (mM)

Fig. 4.5 (a) Box and whisker plot showing the distribution of the mortality of the knockdown ISE6 cells exposed to ferrous sulphate in percentage using Trypan blue stain at different time points. A Kruskall –Wallis test with Bonferonni multiple comparison tests was performed to analyse the mortality data. (b) Box and whisker plot showing the distribution of the proliferation rate in percentage of knockdown and ferrous sulphate exposed ISE6 cells using MTT assay at different time points. A one-way ANOVA with Bonferonni multiple comparison tests was performed to analyse the proliferation rate data. The data presented are results of three independent experiments with the Trypan blue and MTT assays performed in two technical replicates for each experiment.

CHAPTER 5

Characterization of a *Haemaphysalis longicornis* ferritin-derived promoter in an *Ixodes scapularis*-derived tick cell line (ISE6)

This work was published as:

Hernandez EP, Kusakisako K, Hatta T, Tanaka T. (2019). Characterization of an iron-inducible *Haemaphysalis longicornis* tick-derived promoter in an *Ixodes scapularis*-derived tick cell line (ISE6). *Parasit Vectors*, **12**, 321.

.

5.1 Introduction

Due to numerous reports of acaricide resistance in ticks, alternative approaches are warranted for tick and tick-borne pathogen control [159]. Gene-manipulation techniques have been used in mosquitoes and have resulted in a decrease in mosquito populations and in the transmission of mosquito-borne pathogens [160]. However, gene-manipulation techniques in ticks mainly involved RNA interference (RNAi). RNAi techniques for specific tick molecules have been used mostly in the analysis of tick biological function and the interaction of ticks and tick-borne pathogens but not as the main method to control them [161]. This may be because RNAi is low throughput, labor-intensive, and relatively slow to yield results [162]. Therefore, an alternative gene-manipulation technique such as introduction of foreign genes in the ticks, could be explored to control ticks and tick-borne pathogens.

Haemaphysalis longicornis is a hard tick that can be found in East Asia and Australia and that has recently attracted much attention because of reports of infestation with this species in several states in the USA. It is also considered a vector of the severe fever with thrombocytopenia syndrome virus (SFTSV) affecting humans [1,163]. Numerous studies on *H. longicornis*, from its survival against acaricides to its vector competence against several viruses, have already been conducted [34,164]. It is necessary

to control this tick species due to its effects on human and animal health and the economy. One possible method of tick and tick-borne disease control is the development of transgenic ticks.

The development of transgenic ticks requires an effective promoter derived from the organisms themselves. In mosquitoes, it is believed that the best candidate promoters for the expression of foreign genes are those that are inducible during blood-feeding due to their strength, tissue specificity, and synchrony of expression with the pathogen infection [165]. This could also be the case in ticks. Our previous study has identified two promoters from *H. longicornis*: the *actin* and *ferritin1* promoters. The *actin* promoter could effectively express the foreign gene in an *Ixodes scapularis* embryo-derived cell line (ISE6), but the ability of the *ferritin1* promoter to express a foreign gene was not demonstrated. It was hypothesized that this is due to the presence of iron-regulatory proteins (IRPs) in the untranslated region that prevents effective translation of the foreign gene [166] . On the other hand, our recent study showed a dose-dependent ferritin expression on a tick cell line after the addition of iron [24].

During blood-feeding, the actin gene and protein of ticks are constitutively expressed [23,167]. In the same manner, the *ferritin1* mRNA is constitutively expressed, however, its protein is inducible by blood-feeding due to the presence of iron in the blood

diet [23]. Therefore, the ferritin promoter could be a good candidate in the development of an inducible promoter system for the tick cell line that could be similar to the blood-feeding in ticks. Here, the promoter region of the *ferritin1* gene of *H. longicornis* (*HlFer1*) was analyzed and its activity demonstrated using the ISE6 cell line.

5.2 Materials and methods

5.2.1 In silico analysis of HlFer1 promoter sequence

Analysis of the *HlFer1* promoter region was conducted to determine the functional region of the previously identified *HlFer1* promoter. Transcription starting site (TSS) analysis was done by first aligning the ESTs for *HlFer1* using MAFFT software (https://mafft.cbrc.jp/alignment/software/). Then a WebLogo image of the TSS was made (https://weblogo.berkeley.edu/logo.cgi). Using the neural network promoter program (http://www.fruitfly.org/seq_tools/promoter.html), the possible promoter regions were identified. Further characterization of the promoter regions was done using gene promoter-mining software (http://gpminer.mbc.nctu.edu.tw/).

5.2.2 Renilla luciferase reporter construct

To establish a purely tick promoter reporter plasmid, the *H. longicornis actin*

(*HlActin*) promoter was used to replace the SV40 promoter of the *Renilla luciferase* (hrLuc) of the pmirGLO plasmid vector (Promega, Madison, WI, USA). First, the previously identified *HlActin* promoter region was amplified from the previously constructed pmirGLO-*HlActin* pro [166] using a primer pair of HlActin-Renilla F and HlActin-Renilla R (Table 5.1) by PCR with KOD-Plus-Neo (Toyobo, Osaka, Japan). After amplification, the PCR products were electrophorosed in 1.0% agarose gel. The PCR product was purified using a QIAquick Gel Extraction Kit (Qiagen, Hilden, Germany). The pmirGLO vector was then double-digested using *Kpn*I and *Pfm*I to remove the SV40 promoter. After double digestion, the plasmid vector was electrophorosed in 1.0% agarose gel and purified using a QIAquick Gel Extraction Kit (Qiagen). The digested vector and purified product were mixed with an In-Fusion HD cloning kit (Takara, Shiga, Japan). After the ligation of pmirGLO/*HlActin*-hrLuc, the plasmid was transformed into the *Escherichia coli* Stellar strain and purified using a Plasmid Midi Kit (Qiagen).

5.2.3 Firefly luciferase construct

The previously constructed pmirGLO/*HlActin*-hrLuc was digested using *Bgl*II and *Hind*III at 37 °C for 2 h to remove the PGK promoter. After double digestion, the

plasmid vector was electrophoresed in 1.0% agarose gel and purified using a QIAquick Gel Extraction Kit (Qiagen). The *HlFer1* promoter sequence was amplified from the previously constructed pmirGLO-*HlFer1* plasmid using KOD-Plus-Neo (Toyobo) with the indicated primer sets (Table 5.1). The *HlFer1* promoter sequences were purified using a QIAquick Gel Extraction Kit (Qiagen). The purified vector was mixed with and ligated using an In-Fusion HD cloning kit (Takara). After ligation, the plasmids were transformed into the *E. coli* Stellar strain and purified using a Plasmid Midi Kit (Qiagen). For the pmirGLO-no promoter-Luc2/*HlActin*-hrLuc, the purified vector was allowed to self-ligate using DNA Ligation Kit Ver 2.1 (Takara) and incubated at 16 °C overnight. It was then transformed into the *E. coli* DH5α strain and purified using a Plasmid Midi Kit (Qiagen). Finally, the pmirGLO/*HlFer1*(F0-F4 and no promoter)-Luc2/HlAct-hrLuc plasmids were obtained. Plasmid inserts from the clones were sequenced from the beginning to the end of the target promoter sequence using a BigDye Terminator v. 3.1 Cycle Sequencing Kit (Applied Biosystems, Foster City, CA, USA) with sequencing primers derived from the pmirGLO vector. A diagram for the constructed plasmid was created using SnapGene Viewer software (www.snapgene.com) (Fig. 5.1).

5.2.4 Tick cell culture and transient transfection of plasmid vectors

The ISE6 cell line from the embryo of *I. scapularis* was grown and maintained as previously described in Chapter 4.

ISE6 cells were seeded in a 24-well plate at 0.5 ml/well of 1.0×10^6 cells/ml and incubated at 34 °C overnight. The plasmid vector (1.5 μg/well), 50 μl of Opti-MEM (Gibco, Grand Island, NY, USA), and 1.5 μl of Lipofectamine 2000 (Invitrogen, Carlsbad, CA, USA) were mixed and incubated at room temperature for 5 min. Then the incubated mixture was added to the medium in each well, and the cells were incubated for 2 days at 34 °C and replaced with different concentrations (0, 0.1, 1 and 2 mM) ferrous sulfate–enriched iron media, then further incubated for 4 days according to Chapter 4 [24]. The transfected cells were harvested and assayed for firefly and *Renilla* luciferase activities as described below.

5.2.5 Dual luciferase assays

The firefly and *Renilla* luciferase activities were assayed using a Dual-Glo Luciferase Assay System with Passive Lysis Buffer (Promega) and the microplate reader (SH-9000Lab, Corona Electric, Ibaraki, Japan), following the manufacturer's protocol. The firefly luciferase activity corresponding to the *Renilla* luciferase activity was

calculated (relative luciferase activity).

5.2.6 Construction of yellow fluorescent protein (Venus) expression plasmid vector using HlFer1 promoter regions

Yellow fluorescent protein (Venus) expression vectors with an *HlFer1*(F2) promoter region were constructed. To produce a pmirGLO/*Fer1* (F2)-Venus plasmid, the *Fer1* (F2) promoter was amplified by PCR using KOD-Plus-Neo (Toyobo) with pmirGLO-HlFer2-Venus F and pmirGLO-HlFer2-Venus R primers, while the *Venus* gene was also amplified using pmirGLO-Venus F and pmirGLO Venus-*Xho*I R. These PCR products were purified using a QIAquick Gel Extraction Kit (Qiagen). The pmirGLO plasmid was double digested with *Bgl*II and *Xho*I to remove the PGK promoter and *luciferase* gene from the vector. The obtained vector and two purified products were mixed with an In-Fusion HD Cloning Kit (Takara) and incubated. After ligation, the plasmid was transformed into the *E. coli* Stellar cells and purified using a Plasmid Midi Kit (Qiagen). The pmirGLO/no promoter-Venus was constructed by blunt ligation of the purified *Venus* gene with the digested vector using DNA Ligation Kit Vector 2.1 (Takara).

5.2.7 Transfection of Venus expression plasmid into ISE6 cells and comparison of promoter activities using fluorescence microscopy and western blotting

Transfection was performed as mentioned above. As a negative control, Lipofectamine 2000 (Invitrogen) was used without the plasmid. The previously synthesized pmirGLO-*HlActin*-Venus was used as a positive control. The incubated mixture was added to each well, and after 2 days, the media were replaced with 1 mM ferrous sulfate-enriched media and incubated at 34 °C for 4 days according to previous studies for promoter activity [162]. The transfected cells were observed under fluorescence microscopy (IX71, Olympus, Tokyo, Japan).

Another set of transfected cells was collected and subjected to western blotting as described by Kusakisako et al. [134]. Briefly, transfected cells were collected and suspended in phosphate-buffered saline (PBS) and sonicated for 6 min at 45 kHz using a VS-100III ultrasonic cleaner (AS ONE, Osaka, Japan), then centrifuged at 20,100 × *g*. The supernatant was resolved in a 12% SDS-polyacrylamide gel electrophoresis (SDS-PAGE) under a reducing condition. The proteins were then transferred onto a polyvinylidene difluoride membrane (Immobilon-P; Millipore, Danvers, MA, USA). The membranes were then blocked for 1 h at room temperature with 0.3% skimmed milk in PBS containing 0.05% Tween 20 (PBS-T, blocking solution). After blocking, the

membranes were incubated in a 1:1000 dilution anti-green fluorescent protein (GFP) pAb (MBL, Nagano, Japan) in a blocking solution at 4 °C overnight. The antiserum against recombinant *H. longicornis* β-tubulin was used as a loading control. After incubation, the membranes were washed three times with PBS-T and then incubated with a 1:50,000 dilution of horseradish peroxidase (HRP)-conjugated goat anti-mouse or anti-rabbit IgG (Dako, Glostrup, Denmark) in a blocking solution for 1 h at room temperature. The membranes were then washed five times using PBS-T. After washing, the bands were detected using Amersham™ ECL™ Prime Western Blotting Detection Reagent (GE Healthcare, Buckinghamshire, UK) and viewed using FluorChem®FC2 software (Alpha Innotech, San Leandro, CA, USA).

5.2.8 Statistical analysis

Statistical analyses were performed using STATA15.0 software. The data were initially checked for normality and homogeneity assumptions using the Shapiro-Wilk W-test for normality and Breusch-Pagan/Cook-Weisberg test for heteroskedasticity. A one-way analysis of variance (ANOVA) with Bonferroni multiple comparison *post-hoc* tests was applied. Statistical significance was set as $P<0.05$. Data presented are the results of at least two independent experiments.

5.3 Results

5.3.1 Analysis of the HlFer1 promoter region sequence

To determine the core promoter region of the previously identified *HlFer1* promoter sequence [166], analysis of the promoter sequence was performed. Initially, the transcription starting site (TSS) was identified. Alignment of *HlFer1* candidate sequences from the expressed sequence tag (EST) library was performed using MAFFT alignment software (Fig. 5.2a). Based on the alignment, a WebLogo image of the TSS region was made (Fig. 5.2b). To further investigate the core promoter sequence containing the TSS region of the *HlFer1* gene, the sequence of the *HlFer1* promoter region was subjected to a neural network for promoter prediction (NNPP) program in the Berkeley Drosophila Genome Project. Based on the alignment and the prediction software, the [T] nucleotide was the estimated TSS among the sequences (Figs. 5.2 and 5.3a).

The NNPP program also predicted several promoter sequences from the *HlFer1* promoter region (Fig. 5.3a). This promoter region was also evaluated using promoter-mining software to determine the important components of the promoter regions, such as the TATA and GC box, and match them with the predicted promoter sequence. Based on the findings, five promoter sequences were identified as candidates for an optimal promoter region of *HlFer1* and tentatively labeled as *HlFer1* (F0) for the 2848 nucleotide

(nt) whole promoter, *HlFer1* (F1) for the 821 nt promoter, *HlFer1* (F2) for the 638 nt promoter, *HlFer1* (F3) for the 450 nt promoter, and *HlFer1* (F4) for the 185 nt promoter (Fig. 3b). These results indicate that the identified promoter region has a high possibility of being the true promoter region of *HlFer1*.

5.3.2 Evaluation of the HlFer1 promoter sequences activity in ISE6 cells using a dual luciferase assay

Promoter-replacing expression vectors were constructed based on a pmirGLO plasmid vector with the phosphoglycerate kinase (PGK) promoter as the original promoter. The PGK promoter was replaced by truncated *HlFer1* promoters to evaluate the promoter activity of the candidate *HlFer1* promoter sequences in ISE6 cells. The previously identified *HlActin* promoter was used instead of the SV40 promoter to maintain consistency in using a tick-derived promoter. It has been previously demonstrated that the interaction between the iron-responsive element (IRE) and IRP may have resulted in the depressed activity of the *HlFer1* promoter. Therefore, different concentrations of ferrous sulfate were used in the media to liberate the IRP from the IRE for translation induction. A dose-dependent luciferase activity for the different truncated promoters up to 1 mM ferrous sulfate was observed. With 2 mM ferrous sulfate, decreased

activity was observed at the *HlFer1* (F1), *HlFer1* (F2), and *HlFer1* (F3) truncates (Fig. 5.4). Among the promoters, the *HlFer1* (F2) possessed the highest luciferase activity in all of the ferrous iron-enriched media, followed by the *HlFer1* (F1) and *HlFer1* (F3) truncates, except at a 2 mM ferrous sulfate concentration, wherein *HlFer1* (F3) has a slightly higher activity than *HlFer1* (F1). The *HlFer1* (F0) and *HlFer1* (F4) sequences exhibited the lowest relative luciferase activity, and their relative luciferase activity did not differ significantly (Fig. 5.4). These results demonstrate that the *HlFer1* (F4) being the smallest truncated promoter and still exhibited activity could be the core promoter region, while the *HlFer1* (F2) showed optimal promoter activity in the presence of 1 mM ferrous sulfate.

5.3.3 Demonstration of the promoter activity of the HlFer1 promoter regions in ISE6 cells under fluorescence microscopy and Western blotting

Expression vectors of a yellow fluorescent protein, Venus, were constructed to evaluate the *HlFer1* (F2) promoter activity under fluorescence microscopy to show the activity of this truncated promoter. The previously constructed pmirGLO-*HlAct* pro-Venus and pmirGLO-*HlFer1*(F2)-Venus, wherein the PGK promoter and *luciferase* gene were replaced by the *HlFer1*(F2) promoter and the *Venus* gene, respectively, in the pmirGLO

plasmid were evaluated. The mentioned vectors were transfected to ISE6 cells, and then the cells were enriched with 1 mM ferrous sulfate. The fluorescence of Venus was observed under fluorescence microscopy at day 4 after ferrous sulfate enrichment. The fluorescence microscopy test showed that the addition of 1 mM ferrous sulfate resulted in the increased fluorescence intensity of pmirGLO-*HlFer1*(F2)-Venus transfected cells; however, the addition of 1 mM ferrous sulfate did not affect the intensity of pmirGLO-*HlAct* pro-Venus transfected cells. No apparent difference in intensity was observed between pmirGLO-*HlAc*t pro-Venus and pmirGLO-*HlFer1*(F2)-Venus transfected ISE6 cells (Fig. 5.5a). Venus proteins were also investigated using western blotting. Western blot analysis showed that the addition of 1 mM ferrous sulfate to the ISE6 cells transfected with pmirGLO-*HlFer1*(F2)-Venus resulted in expression of the Venus protein in ISE6 cells (Fig. 5.5b). These results demonstrate that the promoter activity for a foreign gene is not limited to the *luciferase* gene but also occurs in other genes, such as the *Venus* gene.

5.4 Discussion

Genetic manipulation of mosquitoes, particularly the introduction of foreign gene, has been shown to impair the transmission of malaria parasites [165,168]. The development of ticks that possess genes that could affect the infection and transmission

of tick-borne pathogens, then, could be explored as a promising strategy to control tick-borne diseases. Since gene regulation is a critical, well-coordinated, and complex process, an effective promoter is essential for the expression of a foreign gene into the target organism [166].

Promoters are considered to be gene-regulatory sequences found immediately upstream of the TSS [169]. In this study, the promoter region of *HlFer1* was characterized for its possible use in the development of transgenic ticks and recombinant protein expression system in tick cell lines.

The core promoter is the minimal DNA sequence that is sufficient to initiate gene transcription [170]. It is where the transcription machinery is assembled [171]. The core promoter is generally 50 to 100 nt within the TSS [169]. Using the EST database promoter analysis software, the TSS [T] is predicted to be 138-bp upstream of the open reading frame sequence in the *HlFer1* gene. The TSS is included in the initiator element, which is, in turn, a key feature of the core promoter sequence [170]. Aside from the initiator element, another common core promoter element is the TATA box [171]. In metazoans, the TATA box is usually located around 30 nt upstream of the TSS, wherein the optimal spacing between the +1 TSS and the first T is around 30–31 nt upstream [170,171]. The TATA sequence serves as the binding site for the transcription factor II D (TFIID). In this

study, the TATA box was predicted to be 32 nt upstream of the TSS (Fig. 5.3b). Based on these results, the F4 sequence promoter was hypothesized as part of the core promoter region of the *HlFer1* promoter.

In vitro studies have shown that the core promoter is sufficient to initiate promoter activity, but an upstream promoter sequence may be necessary to generate activity *in vivo* [172]. The upstream sequence is also known as the extended promoter sequence. The extended promoter sequence is considered to contain regulatory elements that can modulate the downstream gene sequences [169,171]. Therefore, several *HlFer1* sequences upstream of the core promoter region were evaluated using a reporter assay to determine the promoter sequence with the optimal activity (Fig. 5.3b).

A dual reporter assay, such as the dual luciferase reporter assay, has been commonly used in cell lines to evaluate promoter activity [166,173,174]. The use of a dual reporter system has been very advantageous in measuring gene expression. It is sensitive, allows experimental variations due to the presence of a control reporter gene, and has a high-throughput platform [175]. The dual luciferase assay has also been shown to be of value in tick cell lines [162] and has been used in evaluation of tick promoter. In this experiment, I used the previously identified *HlAct* promoter sequence from the *H. longicornis* tick [166] as the promoter of the control reporter gene and the *HlFer1*

promoter sequences for the experimental reporter gene. Since there are no available cell lines for the *H. longicornis* tick, the embryo-derived *I. scapularis* cell line (ISE6) was utilized to evaluate the core promoter sequence of the different candidates in the *HlFer1* promoter sequences since the activity of *HlAct* and *HlFer1* promoter has already been established in this tick cell line [166].

Although the *HlFer1* promoter was tested for activity in our previous study, it showed depressed or no transcriptional activity [166]. This could be attributed not to the absence of transcriptional activity but rather to the presence of an IRE in the *HlFer1* mRNA, which interacts with the IRP that hinders the protein translation. On a previous study, an increasing HlFer1 protein expression was observed during blood-feeding despite no difference in the expression of *HlFer1* mRNA expression. It was then hypothesized that the increasing expression was due to the liberation of IRP from IRE due to the increased iron in the tick blood meal [23]. The same mechanism of intracellular ferritin protein expression was also proposed in *Ixodes* ticks [7]. In our recent study on the ISE6 cell line, Fer1 protein expression was induced by the addition of 0.1 to 2 mM ferrous sulfate to the media and incubation for at least 2 days [24]. It could be safe to assume therefore that the mechanism of intracellular ferritin translation in *Haemaphysalis* and *Ixodes* ticks, as well as *Ixodes* cells are all regulated by iron concentration. Therefore,

ferrous sulfate enrichment on *HlFer1* promoter transfected ISE6 cells was utilized to determine whether it would result in luciferase activity due to liberation of the IRP and eventually, protein translation. A dose-dependent increase in activity was observed to peak in 1 mM ferrous sulfate–enriched media. The lower luciferase activity with 2 mM ferrous sulfate could be attributed to the possible increased cell mortality at the increased ferrous concentration, as was observed in our previous study [24]. With 1 mM ferrous sulfate, the *HlFer1* (F2) promoter showed the highest activity, followed by *HlFer1* (F1), *HlFer1* (F3), *HlFer1* (F4), and *HlFer1* (F0), with *HlFer1* (F4) and *HlFer1* (F0) not differing significantly, thus strengthening our hypothesis that the *HlFer1* (F4) promoter is the core promoter region. SinceIconsider this region to be the core promoter region, its activity could also be considered the basal activity of the promoter region [169]. The increased promoter activity of the *HlFer1* (F3) and *HlFer1* (F2) promoter regions could indicate that these extended regions contain the enhancers or positive regulatory elements. The decrease in the activity of the *HlFer1* (F1) and especially the *HlFer1* (F0) region could indicate that these regions contain the silencers or negative regulatory elements. This is consistent with human cell lines, in which the -350 to -40 nt region showed enhanced transcriptional activity, while the region further upstream, especially -500 to -1000 nt, showed a decline in transcriptional activity [169]. This is also consistent with

tick promoters, wherein the promoter region -649 nt from the TSS of the ribosomal protein L4 (rpL4) promoter of *Rhipicephalus microplus* showed a 17-fold higher promoter activity when compared with the 1191 nt originally cloned promoter. Meanwhile, a three-fold increase was observed when the -1005 to -495 sequences were deleted from the *EF1-α* promoter of the same tick species, indicating the presence of repressive elements in the upstream sequences of the promoters [162].

To further confirm the activity of the gene-expression vectors in ISE6 cells, *Venus* gene-expression vectors (pmirGLO/*HlAct*-Venus and pmirGLO/*HlFer1*(F2)-Venus) were constructed. More intense Venus fluorescence within transfected cells of the ferrous sulfate-enriched ISE6 cells was detected in pmirGLO-*HlFer1* (F2)-Venus transfected groups as compared to those without ferrous sulfate enrichment. Meanwhile, no difference in the ferrous sulfate-enrichment and non-enrichment was observed on pmirGLO-*HlAct* pro-Venus transfected cells. It would then be of interest to know if this Fer1 promoter sequence could also be found in *I. scapularis* and would exhibit same or higher activity. Nonetheless, I believed that the *HlFer1* promoter sequence maintained its promoter activity. These results also demonstrate the iron inducibility of the activity of the ferritin derived promoter.

In this chapter, I took advantage of presence of an IRE in the intracellular *Fer* mRNA to identify and develop an iron-inducible promoter that could be used in tick cell line. Since many tick-borne pathogens are acquired during blood-feeding, a blood-feeding inducible tick promoter is necessary to the development of transgenic ticks for tick-borne pathogen control. Since blood-feeding would be difficult to simulate in tick cells, an increased iron environment would be a good alternative, since there is also an increased iron intake during blood-feeding. In this case, an iron-inducible promoter could be a valuable tool in such studies. The promoter could then be used in cell lines for the study of antimicrobial peptides against tick-borne pathogens that could be expressed during blood-feeding in the development of transgenic ticks.

Table and Figures in CHAPTER 5

Table 5.1 Oligonucletiode primer sequences used for construction of the plasmid

Primer	**Sequence (5'→3')**
pmirGLO-HlActin-Renilla F	AACTTGGTTAGGTACGGCTTCGGACGAAGGCCA
pmirGLO-HlActin-Renilla R	CCATGGTGGCTCCAGGTTGACTGTTTAGCTGCAC
pmirGLO-HlFer0-Luc2 F	GGCGTAGAGGATCGATCCCGGTTCGACACCCTG
pmirGLO-HlFer0-Luc2 R	CCGGATTGCCAAGCTTTTCGTCGGTTATTTCCGG
pmirGLO-HlFer1-Luc2 F	GGCGTAGAGGATCGATTTAGGCGCCAAAAATTGAG
pmirGLO-HlFer1-Luc2 R	The same reverse primer sequence of pmirGLO-HlFer0-Luc2R
pmirGLO-HlFer2-Luc2 F	GGCGTAGAGGATCGAGTTTTAAAGCTATAAACAGCG
pmirGLO-HlFer2-Luc2 R	The same reverse primer sequence of pmirGLO-HlFer0-Luc2R
pmirGLO-HlFer3-Luc2 F	GGCGTAGAGGATCGAAAGGAAAAGTATAAAAACGGC
pmirGLO-HlFer3-Luc2 R	The same reverse primer sequence of pmirGLO-HlFer0-Luc2R
pmirGLO-HlFer4-Luc2 F	GGCGTAGAGGATCGAGCGGCGGAATCGTATATAA
pmirGLO-HlFer4-Luc2 R	The same reverse primer sequence of pmirGLO-HlFer0-Luc2R
pmirGLO-HlFer0-Venus F	The same forward primer sequence of pmirGLO-HlFer0-Luc2F
pmirGLO-HlFer0-Venus R	GCCCTTGCTCACCATTTTCGTCGGTTATTTCCGG
pmirGLO-HlFer2-Venus F	The same forward primer sequence of pmirGLO-HlFer2-Luc2F
pmirGLO-HlFer2-Venus R	The same reverse primer sequence of pmirGLO-HlFer0-VenusR
pmirGLO-Venus F	ATGGTGAGCAAGGGCGAGGAG
pmirGLO-Venus-*Xho*I R	GACTCTAGACTCGAGTTACTTGTACAGCTCGTCC
pmirGLO-sequence F	GTACCCTCTGGTTGCATAGGT
pmirGLO-sequence R	AGCCCATAGCGCTTCATAGC

Hl, *Haemaphysalis longicornis*; Fer, ferritin1; Luc2, firefly luciferase.

Underline denotes the restriction enzyme recognition site mentioned in the primer name.

Fig. 5.1 Schematic diagram of the constructed pmirGLO/HlFer Luc2/HlActin-hrLuc plasmid, created using a SnapGene Viewer. Luciferase (Luc2) indicates the firefly luciferase gene, while hrLuc is the *Renilla* luciferase gene. Ori indicates the origin of replication. The cer region is the stability region of the plasmid [176]. The Kozak sequences are consensus sequences that play a role in the translation process [177]. The poly (A) signal is for the termination of the transcription [178]

a

```
Contigs   Sequence 5′→3′
S03044-01_O17-( --ggccatgtttggtcga
S02086B-09_E02  ------------gtcga
S03044-15_A11-( -----gatgtttggtcga
S03044-20_M20-( -----gatgtttggtcga
S03044-25_B20-( -----gatgtttggtcga
S03044-26_D01-( -----gatgtttggtcga
S03044-27_F06-( -----gatgtttggtcga
S03152B-03_O20  -----gatgtttggtcga
S03152B-09_F17  -----gatgtttggtcga
S03152B-12_H17  ----tgatgtttggtcga
S03152B-13_K23  -----gatgtttggtcga
S03152B-15_F17  -----gatgtttggtcga
S03152A-03_L10  -----gatgtttggtcga
S03152A-04_E01  -----gatgtttggtcga
S03152A-24_K20  -----gatgtttggtcga
S03152A-27_I22  ---gtgatgtttggtcga
S03152A-35_C19  -----gatgtttggtcga
S03152A-36_E14  -----gatgtttggtcga
S02086B-06_C21  -----gatgtttggtcga
S02086B-09_I19  -----gatgtttggtcga
S02086B-26_J21  -----gatgtttggtcga
S02142-15_K02   -----gatgtttggtcga
S02142-22_C12   -----gatgtttggtcga
S02142-26_D22   --tgtgatgtttggtcga
S02142-29_I10   ---gtgatgtttggtcga
S03152A-31_E02  ---atgatgtttggtcga
S02142-21_H08   ---ttgatgtttggtcga
S03044-07_I12-( -------ggtttggtcga
S02086B-02_M23  -------ggtttggtcga
S02086B-10_B04  -------ggtttggtcga
S02142-09_J16   -------ggtttggtcga
S02142-31_F06   -----ggggtttggtcga
S02086A-33_I04  -attagatgtttggtcga
S03152B-25_K14  -----ggttttggtcga
S02142-15_D13   -----ggttttggtcga
S03044-14_E03-( ------ggttttggtcga
S03044-01_C08-( ------ggttttggtcga
S03152B-17_L19  ------ggttttggtcga
S02142-05_I05   ------ggttttggtcga
S02086B-31_E02  ----ggttttttggtcga
S02086A-32_D16  ggttttttttttggtcca
S02086B-01_G14  -----gatgtttttttcga
```

b

Fig. 5.2 Prediction of the TSS of *HlFer1*. **a** Multiple-sequence alignment of the EST sequence of *HlFer1*. For easier alignment, sequences from the iron-responsive element (IRE) and downstream sequence were not included. Highlighted in blue is the predicted TSS. **b** WebLogo image of the TSS. The initial [G] of the 5' termini were assumed to be the cap of the mRNA

a

Start	End	Score	Promoter Sequence
16	66	0.91	CTGATATATATATATATATATATATATACAGGAACAAAGTTTTCCTGGAC
25	75	1.00	ATATATATATATATATATACAGGAACAAAGTTTTCCTGGACGCCGGTAGA
438	488	0.94	GCCCATCAACTAAAAAACAACGCAGCAGCGGATAGCCCCCAAGCATTTGC
573	623	0.85	CTGTATATATATATATATATATATATATACGATAATGAACCATTTTGC
583	633	1.00	ATATATATATATATATATATACGATAATGAACCATTTTGCAGCAGTTTCC
831	881	0.84	AACAAGGCTAAATAAAAAAGAAGTAGTACGTAGCGAAACAAGGACGCCGG
1486	1536	0.94	AAAAAAAAAAAAAAAAAGGATGGCAATGGTCAGCCGGTGTAACGACCAAA
2028	2078	0.91	TTTAGGCGCCAAAAATTGAGGCGGCCGGCCCACTCTCCTTCCTGCAAAGG
2210	2260	0.86	GTTTTAAAGCTATAAACAGCGTGTGATTACGCTAAACACTGCCCAGCACG
2444	2494	1.00	AAGGAAAAGTATAAAAACGGCCTCGCAGCCCTTGGTGGCCAACTGAAAGT
2671	2721	0.99	CGGAATCGTATATAAACGGTTTCCGATCGTCTCCGCCATGTTTGGTCGA

b

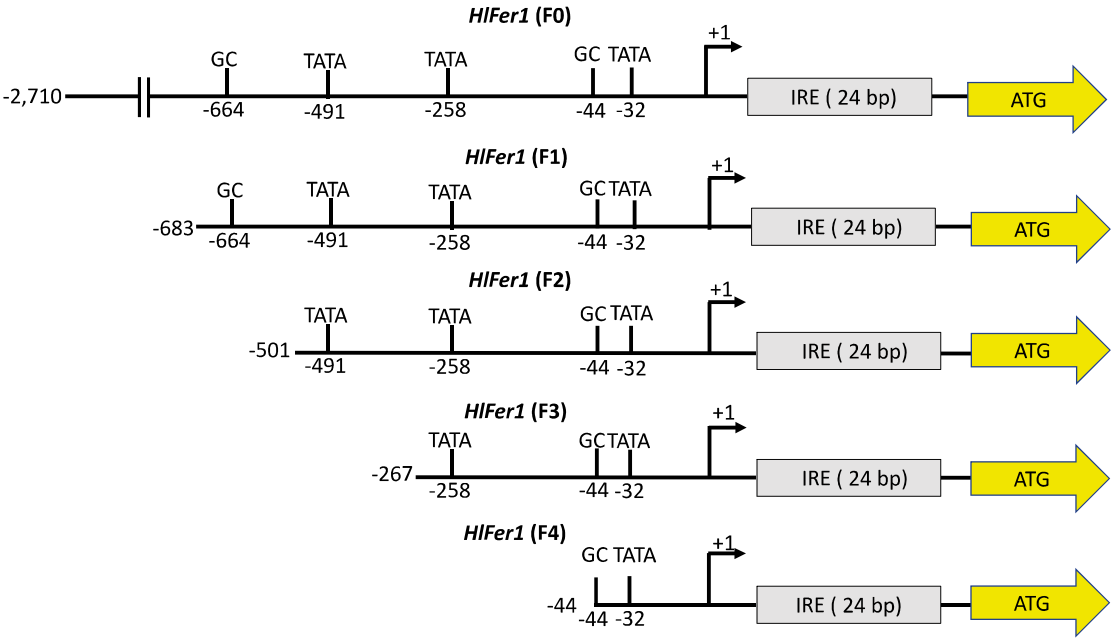

Fig. 5.3 a Analysis of the predicted *HlFer1* promoter sequences using the neural network promoter program. Beginning and ending nucleotide sequence of the predicted promoter are indicated from the whole promoter sequence. The score indicates the likelihood of the sequence to be the promoter: values closer to 1 indicate higher likelihood. The predicted TSSs in each predicted promoter sequences are shown in a larger font. **b** Graphical representation of the truncated *HlFer1* promoter sequences. Predicted TATA and GC boxes are indicated. Positions are relative to the transcription starting site (TSS)

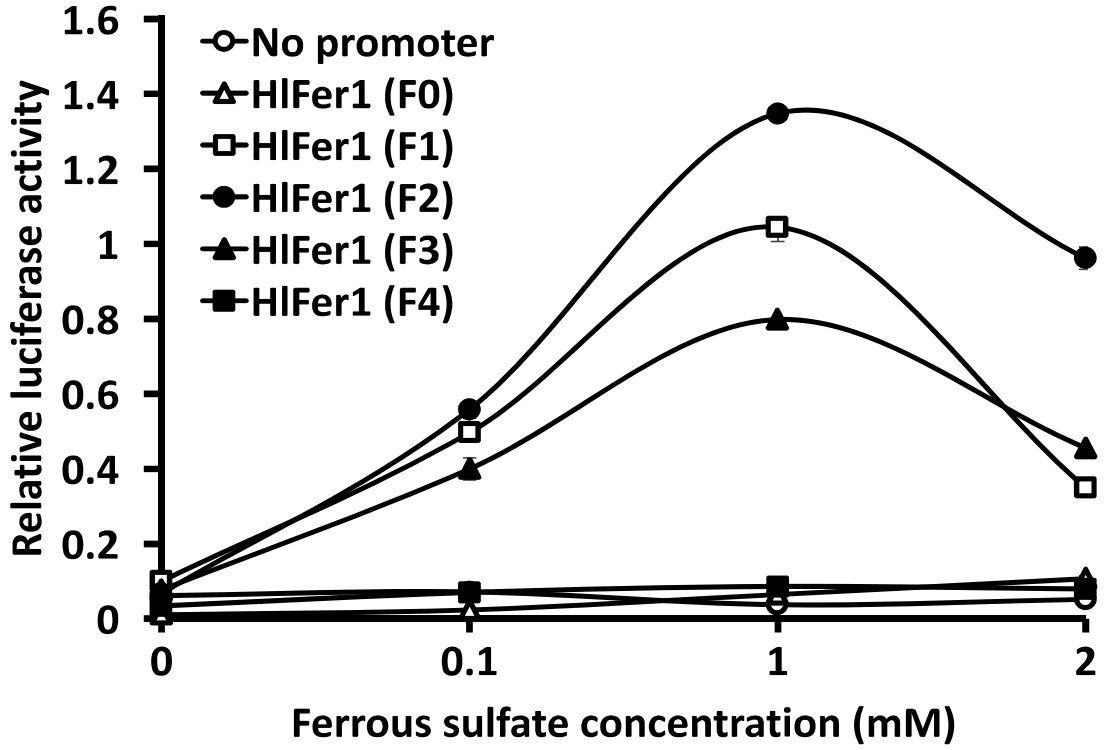

Fig. 5.4 Evaluation of the *HlFer1* promoter truncates using relative luciferase activity in ISE6 cells enriched with different concentrations of ferrous sulfate. The pmirGLO plasmids containing *HlFer1* promoter truncates were transfected to ISE6 cells using a 1:1 Lipofectamine 2000 transfection reagent. The cells were incubated for 2 days, replaced with different concentrations of ferrous sulfate (0, 0.1, 1 and 2 mM) enriched media, incubated for another 4 days, and then tested for luciferase activity using a Dual-Glo Luciferase Assay System following the manufacturer's protocol

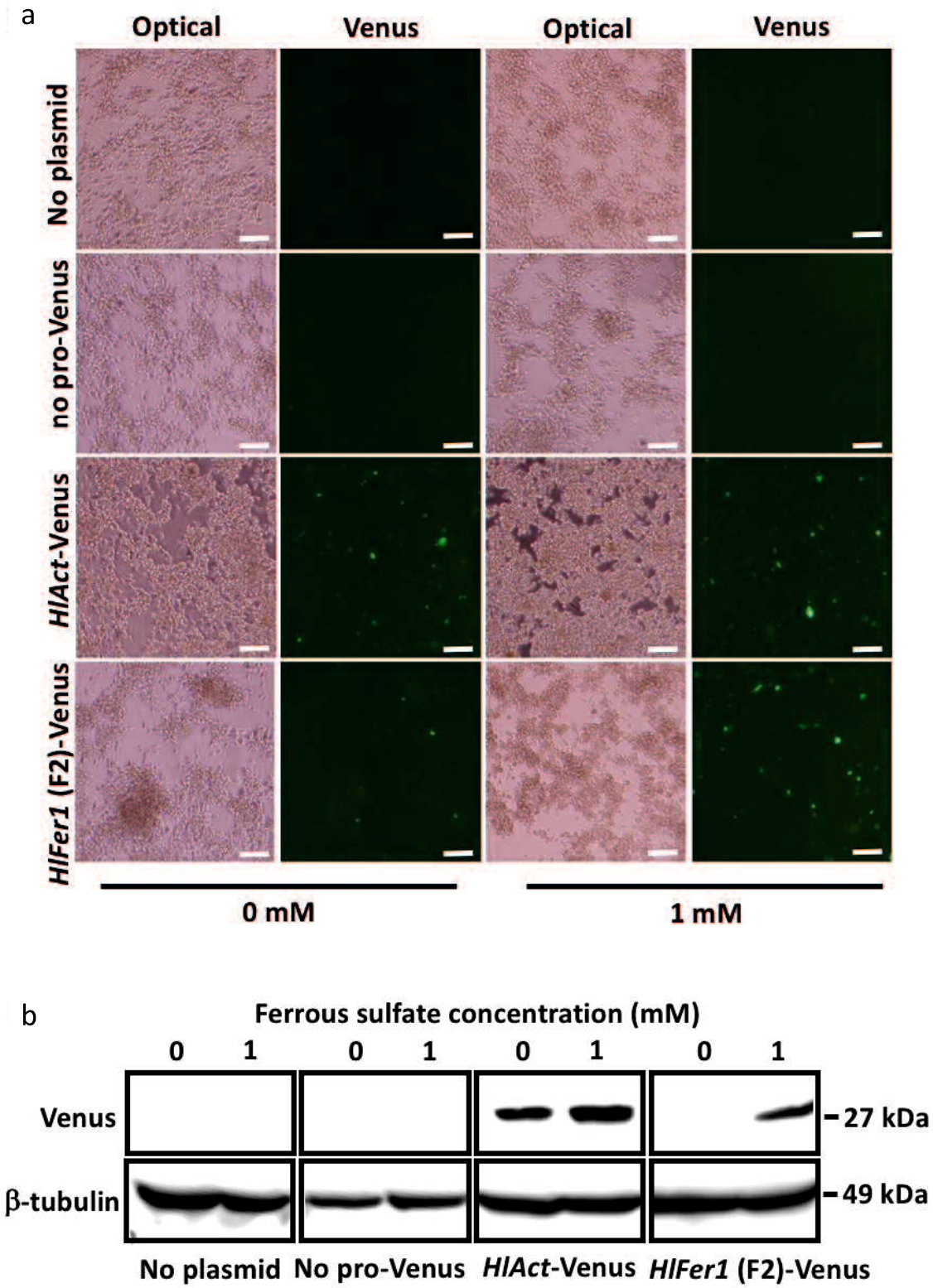
a
Optical
Venus
Optical
Venus
No plasmid
no pro-Venus
HlAct-Venus
HlFer1 (F2)-Venus
0 mM
1 mM
b
Ferrous sulfate concentration (mM)
0
1
0
1
0
1
0
1
Venus
β-tubulin
27 kDa
49 kDa
No plasmid
No pro-Venus
HlAct-Venus
HlFer1 (F2)-Venus

Fig. 5.5 Observation of *HlFer1* (F2) promoter activity using Venus in ISE6 cells *via* fluorescence microscopy (**a**) and western blotting (**b**). The pmirGLO-no promoter-Venus, pmirGLO-*HlAct* pro-Venus, and pmirGLO-*HlFer1*(F2)-Venus plasmids (1.5 μg) with 1.5 μl Lipofectamine 2000 were transfected into 1×10^6 ISE6 cells in a 24-well plate. Media enriched with 1 mM ferrous sulfate were used 2 days after transfection. Cells were observed under a fluorescence microscope after 4 days of medium enrichment. Western blotting results are representative data of three separate experiments. *Scale-bars*: 100 μm

SUMMARY AND CONCLUSION

Ticks are obligate blood-feeding arthropods. The same blood-feeding behavior has made ticks the most important vectors of diseases in domestic and wild animals, and the second-most important in humans. Ticks' blood-feeding behavior exposes them to a multitude of pathogens that they will later transmit. At present, the main method to control ticks and tick-borne pathogens is through chemical acaricides. With the advent of resistance to these acaricides, new methods such as tick vaccination and transgenic arthopods are currently being explored for tick and tick-borne pathogen control.

Due to their blood-feeding behavior, ticks are also exposed to increased ROS. These ROS are generated not only from the Fenton reaction due to the ferrous iron and heme in the blood meal but also from the neutrophils and macrophages contained in the blood. ROS are also generated by the natural microflora of the tick. Therefore, redox management is very important not only for the survival of the tick, but also for their development and reproduction. Therefore, ticks have developed a complex anti-oxidant mechanism to cope with oxidative stress that mostly involved specialized molecules.

Now, these oxidative stress-related molecules have become targets in the development of anti-tick vaccines [133,134,145,179–183]. Therefore, it is important to look not only at the vaccine's ability to prevent tick infestation and its effect on the blood-

feeding, development and reproductive parameters in ticks, but also at the vaccine's effect on the ticks' susceptibility to acaricides.

It is also of importance to understand the properties of these abundant molecules of ticks and harness these properties in the development of ingenious way to control these ticks.

In Chapter 1, I identified a new GST (HlGST2) in the hard tick *H. longicornis.* Both the previously identified HlGST and newly identified HlGST2 were characterized *in silico*, using various available software applications; *in vitro*, through studying the enzymatic activity and kinetics; and *in vivo*, through its gene and protein expression in whole ticks and different organs during blood-feeding and organ localization. The results have shown a positive correlation between the degree and localization of the GSTs with the degree and localization of oxidative stress occurring within the tick during blood-feeding. This close relationship indicate that GSTs play a possible role in coping with oxidative stress brought about by blood-feeding.

In Chapter 2, the identified GSTs of *H. longicornis* were further explored in their role to detoxify acaricides. The HlGST is shown to play an important role in the detoxification of pyrethroids such as flumethrin, wherein the inhibition of enzymatic activity was observed. *HlGST* gene expression was also induced by sublethal doses of

flumethrin, and the knockdown of *HlGST* resulted in the increased susceptibility of larvae and male ticks to flumethrin. On the other hand, HlGST2 plays an important function in the metabolism of organophosphates, such as chlorpyrifos. Chlorpyrifos inhibited the GST activity of recombinant HlGST2. *HlGST2* gene induction upon exposure to sublethal doses of chlorpyrifos was also observed. More importantly, larval susceptibility to chlorpyrifos significantly increased upon *HlGST2* knockdown. The data also showed that GSTs have a more important role in larval survival as compared to ticks at other stages upon exposure to sublethal doses of acaricides. In this chapter I have also shown that environmental factors as well as GST pool composition could play a role in the ability of acaricides to induce GST gene expression as observed in male and female ticks. These results have shown the importance of specific GSTs in the acaricide detoxification mechanism.

In Chapter 3, the role of GSTs and ferritins was investigated during embryogenesis, the only developmental stage that does not require blood meal. Even without blood-meal, embryogenesis still involves energy production and iron metabolism and therefore would also result in the formation of ROS leading to oxidative stress. The study showed that ticks could be utilizing oxidative stress–related molecules that were previously indicated during blood feeding, such as GSTs and Fer2 to cope with oxidative

stress. This is manifested by the increasing or constant expression of these molecules during the course of embryogenesis. This is further supported by the effect on egg fertility in previous knockdown and vaccination studies involving these molecules.

In Chapter 4, the property of Fer1 was explored furtherly. Since in chapter 3, the Fer1 expression was not observed on developing embryos, I utilized the *I. scapularis* embryo-derived cell line to understand such phenomenon. As it was previously hypothesized that this phenomenon is a result of the interaction of the IRE in the *Fer1* mRNA and the IRP, the addition of ferrous sulphate was used to liberate the IRP. I have induced the expression of the FER1 protein in the *I. scapularis* embryo-derived cell line (ISE6) after exposure to 2 mM of ferrous sulphate for 48 h. I have also shown that the Fer1 induced using this method has ferroxidase activity similar to the Fer1 in ticks. This study could be useful in understanding the iron metabolism in ticks and the induction of intracellular ferritin.

In Chapter 5, the findings in chapter 4 was used to develop an iron-inducible promoter that could be used in tick cell line. Since many tick-borne pathogens are acquired during blood-feeding, a blood-feeding inducible tick promoter is necessary to the development of transgenic ticks for tick-borne pathogen control. Since blood-feeding would be difficult to simulate in tick cells, an increased iron environment would be a good

alternative, since there is also an increased iron intake during blood-feeding. In this case, an iron-inducible promoter could be a valuable tool in such studies. The promoter could then be used in cell lines for the study of antimicrobial peptides against tick-borne pathogens that could be expressed during blood-feeding in the development of transgenic ticks.

Taken altogether, the results in this dissertation showed that the oxidative stress related molecules specifically GSTs are important for the survival of the ticks during blood-feeding, acaricide metabolism, and embryonic development. Targeting it, as currently being done in some vaccination experiments could be a good strategy for tick control and for the arrestment of acaricide resistance. Aside from being target for tick control, the oxidative stress molecule such as ferritin possesses unique characteristics such as the presence of IRE that makes it inducible by blood-feeding. Utilizing this property could be a good approach in the development of creative solution such as transgenic ticks, for its spatial and temporal characteristics in the quest to fight tick and tick-borne diseases.

ACKNOWLEDGEMENT

First and foremost, I give thanks and return all the glory to the Almighty God who made all of these possible. I would also like to express my gratitude to the Japanese Government Ministry of Education, Culture, Sports, Science and Technology (MEXT) for financially supporting my studies.

I am greatly indebted to my adviser, Dr. Tetsuya Tanaka (Laboratory of Infectious Diseases, Kagoshima University) for his guidance, support, and patience in me during the course of my study. All of these achievements are fruits of his invaluable mentorship.

I also would like to thank my co-supervisors, Dr. Tomohide Matsuo (Laboratory of Parasitology, Kagoshima University), Dr. Mitsuya Shiraishi (Laboratory of Veterinary Physiology, Kagoshima University), Dr. Tsuyoshi Yamaguchi (Laboratory of Veterinary Hygiene, Tottori University) and Dr. Kyoko Tsukiyama-Kohara (Transboundary Animal Disease Center, Kagoshima University). Their invaluable comments and constructive criticisms greatly contributed to the outputs of my research and dissertation.

I also would like to extend my sincerest gratitude to Dr. Takeshi Hatta (Laboratory of Parasitology, Kitasato University School of Medicine) and Dr. Kentaro Yoshii (Laboratory of Public Health, Hokkaido University) for their insightful inputs on

my studies, and their patience towards me, despite that I do not belong to their laboratory or university.

I am also thankful to all my co-authors in all my publication: Dr. Kozo Fujisaki (National Agricultural and Food Research Organization), Dr Naotoshi Tsuji (Laboratory of Parasitology, Kitasato University School of Medicine), and Dr. Rika Umemiya-Shirafuji (Research Center for Protozoan Diseases, Obihiro University of Agriculture and Veterinary Medicine) for their invaluable contributions. I would also like to thank the funders of my research: National Research Center for Protozoan Diseases, Obihiro University of Agriculture and Veterinary Medicine, Morinaga Foundation, and Japan Society for the Promotion of Science.

I also would like to express my heartfelt gratitude to the former and present members of the Laboratory of Infectious Diseases especially to Dr. Remil Linggatong Galay (University of the Philippines), Dr. Hiroko Maeda (Charles River Laboratories, Japan Inc.), Dr. Kodai Kusakisako (Hokkaido University), Dr. Melbourne Talactac (Cavite State University), Dr. Kei Shimazaki, and Ms. Hiroko Niihara for their assistance, support, and friendship. I would also like to extend my gratitude to the former professor of my laboratory, Dr. Masami Mochizuki for accepting me as a research student.

I also would like to extend my sincerest gratitude to all the former and present Filipino students especially to my batchmate Dr. Iris Ann Borlongan (University of the Philippines), and the Filipino community in Kagoshima. I also would like to thank the members of Ronson Volleyball Circle and all my Japanese and foreign friends who have made me feel at home here in Japan and for all the memories that we have shared.

I would always be indebted to Dr. Helen Molina who opened my eyes in research, Dr. Ignacia Tanaka who encouraged me to pursue my studies here in Japan, Mr. Irwin Melo who served as my mentor and believed that I can be whatever I want to be, and my aunt Mrs. Cristita Pacia Navarro who served as my inspiration to pursue graduate studies.

I would like to acknowledge my family, especially my siblings and their family, Philip Anthony, Leah, and Maria Cecilia, as well as my friends back in the Philippines, for their prayers, encouragement, and love. Finally, I would like to dedicate this to my father, Cecilio, and my mother, Adoracion, I hope I keep making you proud,

REFERENCES

1. Sonenshine DE, Roe RM, editors. (2014). Biology of Ticks. 2nd ed. New York: Oxford University Press.
2. Hoogstraal H. (1985). Argasid and nuttalliellid ticks as parasites and vectors. *Adv Parasitol*, **24**,135–238.
3. Olmeda-García AS, Rodríguez-Rodríguez JA, Rojo-Vázquez FA. (1993). Experimental transmission of *Dipetalonema dracunculoides* (Cobbold 1870) by *Rhipicephalus sanguineus* (Latreille 1806). *Vet Parasitol*, **47**, 339–342.
4. de la Fuente J, Estrada-Pena A, Venzal JM, Kocan KM, Sonenshine DE. (2008). Overview: Ticks as vectors of pathogens that cause disease in humans and animals. *Front Biosci*, **13**, 6938–6946.
5. Jongejan F, Uilenberg G. (2004). The global importance of ticks. *Parasitology*,**129**, S3-14.
6. Perner J, Sobotka R, Sima R, Konvickova J, Sojka D, de Oliveira PL, et al. (2016). Acquisition of exogenous haem is essential for tick reproduction. *Elife*, **7**, 5.
7. Hajdusek O, Sojka D, Kopacek P, Buresova V, Franta Z, Sauman I, et al. (2009) Knockdown of proteins involved in iron metabolism limits tick reproduction and development. *Proc Natl Acad Sci USA*, **106**, 1033–1038.
8. Galay RL, Umemiya-Shirafuji R, Mochizuki M, Fujisaki K, Tanaka T. (2015). Iron metabolism in hard ticks (Acari: Ixodidae): the antidote to their toxic diet. *Parasitol Int*, **64**,182–189.
9. Mori H, Galay RL, Maeda H, Matsuo T, Umemiya-Shirafuji R, Mochizuki M, et al. (2014). Host-derived transferrin is maintained and transferred from midgut to ovary in *Haemaphysalis longicornis* ticks. *Ticks Tick Borne Dis*. **5**,121–126.
10. Graça-Souza AV, Maya-Monteiro C, Paiva-Silva GO, Braz GRC, Paes MC, Sorgine MHF, et al. (2006). Adaptations against heme toxicity in blood-feeding arthropods. *Insect Biochem Mol Biol*, **36**, 322–335.
11. Narasimhan S, Sukumaran B, Bozdogan U, Thomas V, Liang X, DePonte K, et al. (2007). A tick antioxidant facilitates the Lyme disease agent's successful migration from the mammalian host to the arthropod vector. *Cell Host Microbe,* **2**, 7–18.
12. Narasimhan S, Fikrig E. (2015). Tick microbiome: the force within. *Trends Parasitol*, **31,** 315–323.
13. Ray PD, Huang B-W, Tsuji Y. (2012). Reactive oxygen species (ROS) homeostasis and redox regulation in cellular signaling. *Cell Signal,* **24**, 981–990.
14. Freitas DRJ, Rosa RM, Moraes J, Campos E, Logullo C, Da Silva Vaz I, et al.

(2007). Relationship between glutathione S-transferase, catalase, oxygen consumption, lipid peroxidation and oxidative stress in eggs and larvae of *Boophilus microplus* (Acarina: Ixodidae). *Comp Biochem Physiol, Part A Mol Integr Physiol*, **146**, 688–694.

15. Crispell G, Budachetri K, Karim S. (2016). *Rickettsia parkeri* colonization in *Amblyomma maculatum*: the role of superoxide dismutases. *Parasit Vectors,* **9**, 291.
16. Fomenko DE, Koc A, Agisheva N, Jacobsen M, Kaya A, Malinouski M, et al. (2011). Thiol peroxidases mediate specific genome-wide regulation of gene expression in response to hydrogen peroxide. *Proc Natl Acad Sci USA*, **108**, 2729–2734.
17. Sundaresan M, Yu ZX, Ferrans VJ, Irani K, Finkel T. (1995). Requirement for generation of H_2O_2 for platelet-derived growth factor signal transduction. *Science*, **270**, 296–299.
18. Holmström KM, Finkel T. (2014). Cellular mechanisms and physiological consequences of redox-dependent signalling. *Nat Rev Mol Cell Biol*, **15**, 411–421.
19. Thorpe GW, Fong CS, Alic N, Higgins VJ, Dawes IW. (2004). Cells have distinct mechanisms to maintain protection against different reactive oxygen species: oxidative-stress-response genes. *Proc Natl Acad Sci USA*, **101**, 6564–6569.
20. Kumar D, Budachetri K, Meyers VC, Karim S. (2016). Assessment of tick antioxidant responses to exogenous oxidative stressors and insight into the role of catalase in the reproductive fitness of the gulf coast tick, *Amblyomma maculatum*. *Insect Mol Biol*, **25,** 283–294.
21. Pohanka M. Role of oxidative stress in infectious diseases. A review. *Folia Microbiol (Praha)*, **58**, 503–13.
22. Kusakisako K, Galay RL, Umemiya-Shirafuji R, Hernandez EP, Maeda H, Talactac MR, et al. (2016). 2-Cys peroxiredoxin is required in successful blood-feeding, reproduction, and antioxidant response in the hard tick *Haemaphysalis longicornis*. Parasit Vectors, **9**, 457.
23. Galay RL, Aung KM, Umemiya-Shirafuji R, Maeda H, Matsuo T, Kawaguchi H, et al. (2013). Multiple ferritins are vital to successful blood feeding and reproduction of the hard tick *Haemaphysalis longicornis*. *J Exp Biol*, **216**, 1905–1915.
24. Hernandez EP, Kusakisako K, Talactac MR, Galay RL, Yoshii K, Tanaka T. (2018). Induction of intracellular ferritin expression in embryo-derived *Ixodes scapularis* cell line (ISE6). *Sci Rep*, **8**, 16566.

25. Kusakisako K, Hernandez EP, Talactac MR, Yoshii K, Umemiya-Shirafuji R, Fujisaki K, et al. (2018). Peroxiredoxins are important for the regulation of hydrogen peroxide concentrations in ticks and tick cell line. *Ticks Tick Borne Dis*. **9**, 872–881.
26. Galay RL, Umemiya-Shirafuji R, Bacolod ET, Maeda H, Kusakisako K, Koyama J, et al. (2014). Two kinds of ferritin protect ixodid ticks from iron overload and consequent oxidative stress. *PLoS One*, **9**, e90661.
27. Budachetri K, Crispell G, Karim S. (2017). *Amblyomma maculatum* SECIS binding protein 2 and putative selenoprotein P are indispensable for pathogen replication and tick fecundity. *Insect Biochem Mol Biol,* 88, 37–47.
28. Budachetri K, Kumar D, Karim S. (2017). Catalase is a determinant of the colonization and transovarial transmission of *Rickettsia parkeri* in the gulf coast tick *Amblyomma maculatum*. *Insect Mol Biol*, 26, 414–419.
29. Reeves MA, Hoffmann PR. (2009). The human selenoproteome: recent insights into functions and regulation. *Cell Mol Life Sci*, **66**, 2457–2478.
30. Pereira LS, Oliveira PL, Barja-Fidalgo C, Daffre S. (2001). Production of reactive oxygen species by hemocytes from the cattle tick *Boophilus microplus*. *Exp Parasitol*, **99**, 66–72.
31. Villar M, Ayllón N, Alberdi P, Moreno A, Moreno M, Tobes R, et al. (2015). Integrated metabolomics, transcriptomics and proteomics identifies metabolic pathways affected by *Anaplasma phagocytophilum* infection in tick cells. *Mol Cell Proteomics,* **14**, 3154–3172.
32. Sherratt PJ, Hayes JD. (2001) Glutathione S-transferases. In: Enzyme Systems that Metabolise Drugs and Other Xenobiotics. Ioannides C, editor. Chichester, UK: John Wiley & Sons, Ltd, 319–352.
33. Hayes JD, Pulford DJ. (1995).The glutathione S-transferase supergene family: regulation of GST and the contribution of the isoenzymes to cancer chemoprotection and drug resistance. *Crit Rev Biochem Mol Biol*, **30**, 445–600.
34. Hernandez EP, Kusakisako K, Talactac MR, Galay RL, Hatta T, Fujisaki K, et al. (2018), Glutathione S-transferases play a role in the detoxification of flumethrin and chlorpyrifos in *Haemaphysalis longicornis*. *Parasit Vectors*, **11**, 460.
35. Duscher GG, Galindo RC, Tichy A, Hummel K, Kocan KM, de la Fuente J. (2014). Glutathione S-transferase affects permethrin detoxification in the brown dog tick, *Rhipicephalus sanguineus*. *Ticks Tick Borne Dis,* **5**, 225–233.
36. Ghosh S, Kumar R, Nagar G, Kumar S, Sharma AK, Srivastava A, et al. (2015). Survey of acaricides resistance status of *Rhipicephalus* (*Boophilus*) *microplus*

collected from selected places of Bihar, an eastern state of India. *Ticks Tick Borne Dis*, **6**, 668–675.

37. Rosa de Lima MF, Sanchez Ferreira CA, Joaquim de Freitas DR, Valenzuela JG, Masuda A. (2002). Cloning and partial characterization of a *Boophilus microplus* (Acari: Ixodidae) glutathione S-transferase. *Insect Biochem Mol Biol*, **32**, 747–754.
38. Perner J, Kotál J, Hatalová T, Urbanová V, Bartošová-Sojková P, Brophy PM, et al. (2018). Inducible glutathione S-transferase (IrGST1) from the tick *Ixodes ricinus* is a haem-binding protein. *Insect Biochem Mol Biol*, **95**, 44–54.
39. Hernandez EP, Kusakisako K, Talactac MR, Galay RL, Hatta T, Matsuo T, et al. (2018). Characterization and expression analysis of a newly identified glutathione S-transferase of the hard tick *Haemaphysalis longicornis* during blood-feeding. *Parasit Vectors*, **11**, 91.
40. Dreher-Lesnick SM, Mulenga A, Simser JA, Azad AF. (2006). Differential expression of two glutathione S-transferases identified from the American dog tick, *Dermacentor variabilis*. *Insect Mol Biol*, **15**, 445–453.
41. Perner J, Provazník J, Schrenková J, Urbanová V, Ribeiro JMC, Kopáček P. (2016). RNA-seq analyses of the midgut from blood- and serum-fed *Ixodes ricinus* ticks. *Sci Rep*, **6**, 36695.
42. Mulenga A, Simser JA, Macaluso KR, Azad AF. (2004). Stress and transcriptional regulation of tick ferritin HC. *Insect Mol Biol*, **13**, 423–433.
43. Guneidy RA, Shahein YE, Abouelella AMK, Zaki ER, Hamed RR. (2014). Inhibition of the recombinant cattle tick *Rhipicephalus* (*Boophilus*) *annulatus* glutathione S-transferase. *Ticks Tick Borne Dis*, **5**, 528–536.
44. da Silva Vaz Jnr I, Imamura S, Ohashi K, Onuma M. (2004). Cloning, expression and partial characterization of a *Haemaphysalis longicornis* and a R*hipicephalus appendiculatus* glutathione S-transferase. *Insect Mol Biol*, **13**, 329–335.
45. Zheng H, Li AY, Teel PD, Pérez de León AA, Seshu J, Liu J. (2015). Biological and physiological characterization of in vitro blood feeding in nymph and adult stages of *Ornithodoros turicata* (Acari: Argasidae). *J Insect Physiol*, **75**, 73–79.
46. Tripathy A, Kar SK. (2015). Feeding stage, species, body part and sex-specific activity of glutathione S-transferase in mosquito. *Trop Biomed*, **32**, 65–75.
47. Hayes PC, Bouchier IA, Beckett GJ. (1991). Glutathione S-transferase in humans in health and disease. *Gut*, **32**, 813–818.
48. Maheo K, Antras-Ferry J, Morel F, Langouët S, Guillouzo A. (1997). Modulation of glutathione S-transferase subunits A2, M1, and P1 expression by interleukin-1beta in rat hepatocytes in primary culture. *J Biol Chem,* **272**, 16125–16132.

49. Coecke S, Vanhaecke T, Foriers A, Phillips IR, Vercruysse A, Shephard EA, et al. (2000). Hormonal regulation of glutathione S-transferase expression in co-cultured adult rat hepatocytes. *J Endocrinol*, **166**, 363–371.
50. He H, Chen AC, Davey RB, Ivie GW, George JE. (1999). Characterization and molecular cloning of a glutathione S-transferase gene from the tick, *Boophilus microplus* (Acari: Ixodidae). *Insect Biochem Mol Biol,* **29**, 737–743.
51. Shahein YE, El Sayed El-Hakim A, Abouelella AMK, Hamed RR, Allam SA-M, Farid NM. (2008). Molecular cloning, expression and characterization of a functional GSTmu class from the cattle tick *Boophilus annulatus*. *Vet Parasitol*, **152**, 116–126.
52. Fujisaki K. (1978). Development of acquired resistance precipitating antibody in rabbits experimentally infested with females of *Haemaphysalis longicornis* (Ixodoidea: Ixodidae). *Natl Inst Anim Health Q Tokyo*, **18**, 27–38.
53. Habig WH, Pabst MJ, Jakoby WB. (1974). Glutathione S-transferases. The first enzymatic step in mercapturic acid formation. *J Biol Chem*, **249**,7130–7139.
54. Aung KM, Boldbaatar D, Liao M, Umemiya-Shirafuji R, Nakao S, Matsuoka T, et al. (2011). Identification and characterization of class B scavenger receptor CD36 from the hard tick, *Haemaphysalis longicornis*. *Parasitol Res*, **108**, 273–285.
55. Umemiya-Shirafuji R, Tanaka T, Boldbaatar D, Tanaka T, Fujisaki K. (2012). Akt is an essential player in regulating cell/organ growth at the adult stage in the hard tick *Haemaphysalis longicornis*. *Insect Biochem Mol Biol*, **42**, 164–173.
56. Bathige SDNK, Umasuthan N, Saranya Revathy K, Lee Y, Kim S, Cho MY, et al. (2014). A mu class glutathione S-transferase from Manila clam *Ruditapes philippinarum* (RpGSTμ): cloning, mRNA expression, and conjugation assays. *Comp Biochem Physiol C Toxicol Pharmacol,***162,** 85–95.
57. Reddy BPN, Prasad GBKS, Raghavendra K. (2011). *In silico* analysis of glutathione S-transferase supergene family revealed hitherto unreported insect specific δ- and ε-GSTs and mammalian specific μ-GSTs in *Ixodes scapularis* (Acari: Ixodidae). *Comput Biol Chem*, **35**, 114–120.
58. da Silva Vaz I, Torino Lermen T, Michelon A, Sanchez Ferreira CA, Joaquim de Freitas DR, Termignoni C, et al. (2004). Effect of acaricides on the activity of a *Boophilus microplus* glutathione S-transferase. *Vet Parasitol*, **119**, 237–245.
59. Kingsley LJ, Lill MA. (2015). Substrate tunnels in enzymes: structure-function relationships and computational methodology. *Proteins,* **83**, 599–611.
60. Clark AG. (1989). The comparative enzymology of the glutathione S-transferases

from non-vertebrate organisms. *Comp Biochem Physiol B*, **92**, 419–446.

61. Daniel V. (1993). Glutathione S-transferases: gene structure and regulation of expression. *Crit Rev Biochem Mol Biol,* **28**, 173–207.
62. Rudenko N, Golovchenko M, Edwards MJ, Grubhoffer L. (2005). Differential expression of *Ixodes ricinus* tick genes induced by blood feeding or *Borrelia burgdorferi* infection. *J Med Entomol*, **42**, 36–41.
63. Toh SQ, Glanfield A, Gobert GN, Jones MK. (2010). Heme and blood-feeding parasites: friends or foes? *Parasit Vectors*, **3**, 108.
64. Tirloni L, Islam MS, Kim TK, Diedrich JK, Yates JR, Pinto AFM, et al. (2015). Saliva from nymph and adult females of *Haemaphysalis longicornis*: a proteomic study. *Parasit Vectors*, **8**, 338.
65. Kim TK, Tirloni L, Pinto AFM, Moresco J, Yates JR, da Silva Vaz I, et al. (2016). *Ixodes scapularis* tick saliva proteins sequentially secreted every 24 h during blood feeding. *PLoS Negl Trop Dis*, **10**, e0004323.
66. Radulović ŽM, Kim TK, Porter LM, Sze S-H, Lewis L, Mulenga A. (2014). A 24-48 h fed *Amblyomma americanum* tick saliva immuno-proteome. B*MC Genomics*, **15**, 518.
67. Mukherjee SB, Aravinda S, Gopalakrishnan B, Nagpal S, Salunke DM, Shaha C. (1999). Secretion of glutathione S-transferase isoforms in the seminiferous tubular fluid, tissue distribution and sex steroid binding by rat GSTM1. *Biochem J*, **340**, 309–320.
68. Howie AF, Hayes PC, Bouchier IA, Hayes JD, Beckett GJ. (1989). Glutathione S-transferase in human bile. *Clin Chim Acta*, **184**, 269–278.
69. Kura T, Takahashi Y, Takayama T, Ban N, Saito T, Kuga T, et al. (1996). Glutathione S-transferase-pi is secreted as a monomer into human plasma by platelets and tumor cells. *Biochim Biophys Acta*, **1292**, 317–323.
70. Tate LG, Herf DA. (1978). Characterization of glutathione S-transferase activity in tissues of the blue crab, *Callinectes sapidus*. *Comp Biochem and Physiol C,* **61**, 165–169.
71. James MO, Bowen ER, Dansette PM, Bend JR. (1979). Epoxide hydrase and glutathione S-transferase activities with selected alkene and arene oxides in several marine species. *Chem Biol Interact*, **25**, 321–344.
72. Oesch F, Schmassmann H, Ohnhaus E, Althaus U, Lorenz J. (1980). Monooxygenase, epoxide hydrolase, and glutathione-S-transferase activities in human lung. Variation between groups of bronchogenic carcinoma and non-cancer patients and interindividual differences. *Carcinogenesis,* **1**, 827–835.

73. Gopalakrishnan B, Aravinda S, Pawshe CH, Totey SM, Nagpal S, Salunke DM, et al. (1998). Studies on glutathione S-transferases important for sperm function: evidence of catalytic activity-independent functions. *Biochem J,* **329**, 231–241.
74. Matsuo T, Okura N, Kakuda H, Yano Y. (2013). Reproduction in a metastriata tick, *Haemaphysalis longicornis* (Acari: Ixodidae). *J Acarol Soc Jpn*, **22**, 1–23.
75. de Oliveira PR, Mathias MIC, Bechara GH. (2007). Vitellogenesis in the tick *Amblyomma triste* (Koch, 1844) (Acari: Ixodidae) role for pedicel cells. *Vet Parasitol*, **143**, 134–139.
76. Parizi LF, Utiumi KU, Imamura S, Onuma M, Ohashi K, Masuda A, et al. (2011) Cross immunity with *Haemaphysalis longicornis* glutathione S-transferase reduces an experimental *Rhipicephalus* (*Boophilus*) *microplus* infestation. *Exp Parasitol*, **127**, 113–118.
77. Almazán C, Lagunes R, Villar M, Canales M, Rosario-Cruz R, Jongejan F, et al. (2010). Identification and characterization of *Rhipicephalus* (*Boophilus*) *microplus* candidate protective antigens for the control of cattle tick infestations. *Parasitol Res*, **106**, 471–479.
78. Bhattacharjee P, Paul S, Banerjee M, Patra D, Banerjee P, Ghoshal N, et al. (2013). Functional compensation of glutathione S-transferase M1 (GSTM1) null by another GST superfamily member, GSTM2. *Sci Rep*, **3**, 2704.
79. Tang L, Guo B, van Wijnen AJ, Lian JB, Stein JL, Stein GS, et al. (1998). Preliminary crystallographic study of glutathione S-transferase fused with the nuclear matrix targeting signal of the transcription factor AML-1/CBF-alpha2. *J Struct Biol*, **123**, 83–85.
80. Kelley LA, Sternberg MJE. (2009). Protein structure prediction on the Web: a case study using the Phyre server. *Nat Protoc*, **4**, 363–371.
81. Sivakumar T, Igarashi I, Yokoyama N. (2016). *Babesia ovata*: Taxonomy, phylogeny and epidemiology. *Vet Parasitol*, **229**, 99–106.
82. Lu H, Ren Q, Li Y, Liu J, Niu Q, Yin H, et al. (2015). The efficacies of 5 insecticides against hard ticks *Hyalomma asiaticum*, *Haemaphysalis longicornis* and *Rhipicephalus sanguineus*. *Exp Parasitol*, **157**, 44–47.
83. Beugnet F, Franc M. (2012). Insecticide and acaricide molecules and/or combinations to prevent pet infestation by ectoparasites. *Trends Parasitol*, **28**, 267–279.
84. Wilce MCJ, Parker MW. (1994). Structure and function of glutathione S-transferases. *Biochim Biophys Acta.* **1205**, 1–18.
85. Qin G, Jia M, Liu T, Zhang X, Guo Y, Zhu KY, et al. (2013). Characterization and

functional analysis of four glutathione S-transferases from the migratory locust, *Locusta migratoria*. *PLoS One,* **8**, e58410.

86. Prapanthadara L, Promtet N, Koottathep S, Somboon P, Ketterman AJ. (2000). Isoenzymes of glutathione S-transferase from the mosquito *Anopheles dirus* species B: the purification, partial characterization and interaction with various insecticides. *Insect Biochem Mol Biol*, **30**, 395–403.
87. Bartley K, Wright HW, Bull RS, Huntley JF, Nisbet AJ. (2015). Characterisation of *Dermanyssus gallinae* glutathione S-transferases and their potential as acaricide detoxification proteins. *Parasit Vectors*, **8**, 350.
88. Kusakisako K, Masatani T, Miyata T, Galay RL, Maeda H, Talactac MR, et al. Functional analysis of recombinant 2-Cys peroxiredoxin from the hard tick *Haemaphysalis longicornis*. *Insect Mol Biol*, **25**, 16–23.
89. Hatta T, Matsubayashi M, Tsuji N. (2014). Microarray analysis of acaricide-inducible gene expression in the hard tick, *Haemaphysalis longicornis*. *Bull Natl Inst Anim Health*, **120**, 69–72.
90. Galay RL, Hernandez EP, Talactac MR, Maeda H, Kusakisako K, Umemiya-Shirafuji R, et al. (2016). Induction of gene silencing in *Haemaphysalis longicornis* ticks through immersion in double-stranded RNA. *Ticks Tick Borne Dis,* **7**, 813–816.
91. Matthews CK, van Holde KE. (1990). Biochemistry. California: The Benjamin/Cummings Publishing Company.
92. Qin G, Jia M, Liu T, Xuan T, Yan Zhu K, Guo Y, et al. (2011). Identification and characterisation of ten glutathione S-transferase genes from oriental migratory locust, *Locusta migratoria manilensis* (Meyen). *Pest Manag Sci*. **67**, 697–704.
93. Avinash B, Venu R, Alpha Raj M, Srinivasa Rao K, Srilatha C, Prasad TNVKV. (2017). *In vitro* evaluation of acaricidal activity of novel green silver nanoparticles against deltamethrin resistance *Rhipicephalus* (*Boophilus*) *microplus*. *Vet Parasitol*, **237**, 130–136.
94. Hemingway J. (2000). The molecular basis of two contrasting metabolic mechanisms of insecticide resistance. *Insect Biochem Mol Biol*, **30**, 1009–1015.
95. Grant DF, Matsumura F. (1989). Glutathione S-transferase 1 and 2 in susceptible and insecticide resistant *Aedes aegypti*. *Pestic Biochem Physiol*, **33**, 132–143.
96. Kostaropoulos I, Papadopoulos AI, Metaxakis A, Boukouvala E, Papadopoulou-Mourkidou E. (2001). Glutathione S–transferase in the defence against pyrethroids in insects. *Insect Biochem Mol Biol*, **31**, 313–319.
97. Shi L, Wei P, Wang X, Shen G, Zhang J, Xiao W, et al. (2016). Functional analysis

of esterase TCE2 gene from *Tetranychus cinnabarinus* (Boisduval) involved in acaricide resistance. *Sci Rep,* **6**, 18646.

98. Liao C-Y, Zhang K, Niu J-Z, Ding T-B, Zhong R, Xia W-K, et al. (2013). Identification and characterization of seven glutathione S-transferase genes from citrus red mite, *Panonychus citri* (McGregor). *Int J Mol Sci*, **14**, 24255–24270.
99. Enayati AA, Ranson H, Hemingway J. (2005). Insect glutathione transferases and insecticide resistance. *Insect Mol Biol*, **14**, 3–8.
100. Mounsey KE, Pasay CJ, Arlian LG, Morgan MS, Holt DC, Currie BJ, et al. (2010). Increased transcription of glutathione S-transferases in acaricide exposed scabies mites. *Parasit Vectors*, **3**, 43.
101. Hadaway AB. (1971). Some factors affecting the distribution and rate of action of insecticides. *Bull World Health Organ*, **44**, 221–224.
102. Prapanthadara LA, Hemingway J, Ketterman AJ. (1993). Partial purification and characterization of glutathione S-transferases involved in DDT resistance from the mosquito *Anopheles gambiae*. *Pestic Biochem Physiol*, **47**, 119–133.
103. Gong Y, Li T, Zhang L, Gao X, Liu N. (2013). Permethrin induction of multiple cytochrome P450 genes in insecticide resistant mosquitoes, *Culex quinquefasciatus*. *Int J Biol Sci*, **9**, 863–871.
104. Li C, Guo X, Zhang Y, Dong Y, Xing D, Yan T, et al. (2016). Identification of genes involved in pyrethroid-, propoxur-, and dichlorvos- insecticides resistance in the mosquitoes, *Culex pipiens* complex (Diptera: Culicidae). *Acta Trop*, **157**, 84–95.
105. Saldivar L, Guerrero FD, Miller RJ, Bendele KG, Gondro C, Brayton KA. (2008). Microarray analysis of acaricide-inducible gene expression in the southern cattle tick, *Rhipicephalus* (*Boophilus*) *microplus*. *Insect Mol Biol*, **17**, 597–606.
106. Qin G, Liu T, Guo Y, Zhang X, Ma E, Zhang J. (2014). Effects of chlorpyrifos on glutathione S-transferase in migratory locust, *Locusta migratoria. Pestic Biochem Physiol*, **109**, 1–5.
107. Zhou W-W, Liang Q-M, Xu Y, Gurr GM, Bao Y-Y, Zhou X-P, et al. (2013). Genomic insights into the glutathione S-transferase gene family of two rice planthoppers, *Nilaparvata lugens* (Stål) and *Sogatella furcifera* (Horváth) (Hemiptera: Delphacidae). *PLoS One*, **8**, e56604.
108. Zhang N, Liu J, Chen S-N, Huang L-H, Feng Q-L, Zheng S-C. (2016). Expression profiles of glutathione S-transferase superfamily in *Spodoptera litura* tolerated to sublethal doses of chlorpyrifos. *Insect Sci*, **23**, 675–687.
109. Vandenberghe Y, Tee L, Rogiers V, Yeoh G. (1992). Transcriptional- and post-

transcriptional-dependent regulation of glutathione S-transferase expression in rat hepatocytes as a function of culture conditions. *FEBS Lett,* **313**, 155–159.

110. Jakoby WB, Keen JH. (1977). A triple-threat in detoxification: the glutathione S-transferases. *Trends Biochem Sci*, **2**, 229–231.
111. Kostrapoulos I, Mantzari A, Papodapoulos AI. (1996). Alteration of some glutathione charactersistics during the development of *Tenebrio molitor* (Insecta: Coleoptera). *Insect Biochem Mol Biol*, **26***,* 962–969.
112. Strode C, Steen K, Ortelli F, Ranson H. (2006). Differential expression of the detoxification genes in the different life stages of the malaria vector *Anopheles gambiae*. *Insect Mol Biol,* **15**, 523–530.
113. Raghavan RK, Barker SC, Cobos ME, Barker D, Teo EJM, Foley DH, et al. (2019). Potential spatial distribution of the newly introduced long-horned tick, *Haemaphysalis longicornis* in North America. *Sci Rep*, **9**, 498.
114. Zhang T-T, Qiu Z-X, Li Y, Wang W-Y, Li M-M, Guo P, et al. (2019). The mRNA expression and enzymatic activity of three enzymes during embryonic development of the hard tick *Haemaphysalis longicornis*. *Parasit Vectors*, **12**, 96.
115. Martins R, Ruiz N, Fonseca RN da, Vaz Junior I da S, Logullo C. (2018). The dynamics of energy metabolism in the tick embryo. *Rev Bras Parasitol Vet*, **27**, 259–266.
116. Hentze MW, Muckenthaler MU, Andrews NC. (2004). Balancing acts: molecular control of mammalian iron metabolism. *Cell*, **117**, 285–297.
117. Whiten SR, Eggleston H, Adelman ZN. (2017). Ironing out the details: exploring the role of iron and heme in blood-sucking arthropods. *Front Physiol*, **8**, 1134.
118. Hu M-L, Frankel EN, Leibovitz BE, Tappel AL. (1989). Effect of dietary lipids and vitamin E on in vitro lipid peroxidation in rat liver and kidney homogenates. *J Nutr*, **119**, 1574–1582.
119. Santos VT, Ribeiro L, Fraga A, de Barros CM, Campos E, Moraes J, et al. (2013). The embryogenesis of the tick *Rhipicephalus* (*Boophilus*) *microplus*: the establishment of a new chelicerate model system. *Genesis*, **51**, 803–18.
120. Ufer C, Wang CC. (2011). The roles of glutathione peroxidases during embryo development. *Front Mol Neurosci*, **4**, 12.
121. Campos E, Façanha AR, Costa EP, Fraga A, Moraes J, da Silva Vaz I, et al. (2011). A mitochondrial membrane exopolyphosphatase is modulated by, and plays a role in, the energy metabolism of hard tick *Rhipicephalus* (*Boophilus*) *microplus* embryos. *Int J Mol Sci,* **12**, 3525–3535.
122. Campos E, Façanha A, Moraes J, da Silva Vaz I, Masuda A, Logullo C. (2007). A

mitochondrial exopolyphosphatase activity modulated by phosphate demand in *Rhipicephalus* (*Boophilus*) *microplus* embryo. *Insect Biochem Mol Biol*, **37**, 1103–1107.

123. Shiraishi S, Yano Y, Uchida TA. (1990). Embryogenesis in the cattle tick, *Haemaphysalis longicornis*. *J Fac Agr, Kyushu Univ*, **34**, 265–272.
124. Raikhel AS, Dhadialla TS. (1992). Accumulation of yolk proteins in insect oocytes. *Annu Rev Entomol*, **37**, 217–251.
125. Budachetri K, Karim S. (2015). An insight into the functional role of thioredoxin reductase, a selenoprotein, in maintaining normal native microbiota in the gulf coast tick (*Amblyomma maculatum*). *Insect Mol Biol*, **24**, 570–581.
126. Kusakisako K, Fujisaki K, Tanaka T. (2018). The multiple roles of peroxiredoxins in tick blood feeding. *Exp Appl Acarol*, **75**, 269–280.
127. Winata CL, Korzh V. (2018). The translational regulation of maternal mRNAs in time and space. *FEBS Lett*, **592**, 3007–3023.
128. Dworkin MB, Dworkin-Rastl E. (1990). Functions of maternal mRNA in early development. *Mol Reprod Dev*, **26**, 261–297.
129. Ibrahim MA. (1998). Traffic of the tick embryo basic protein during embryogenesis of the camel tick *Hyalomma dromedarii* (Acari: Ixodidae). *Exp Appl Acarol*, **22**, 481–495.
130. Tierbach A, Groh KJ, Schönenberger R, Schirmer K, Suter MJ-F. (2018). Glutathione S-transferase protein expression in different life stages of zebrafish (*Danio rerio*). *Toxicol Sci*, **162**, 702–712.
131. González-Morales N, Mendoza-Ortíz MÁ, Blowes LM, Missirlis F, Riesgo-Escovar JR. (2015). Ferritin is required in multiple tissues during *Drosophila melanogaster* development. *PLoS One*, **10**, e0133499.
132. Oldiges DP, Laughery JM, Tagliari NJ, Leite Filho RV, Davis WC, da Silva Vaz I, et al. (2016). Transfected *Babesia bovis* expressing a tick GST as a live vector vaccine. *PLoS Negl Trop Dis*, **10**, e0005152.
133. Sabadin GA, Parizi LF, Kiio I, Xavier MA, da Silva Matos R, Camargo-Mathias MI, et al. (2017). Effect of recombinant glutathione S-transferase as vaccine antigen against *Rhipicephalus appendiculatus* and *Rhipicephalus sanguineus* infestation. *Vaccine*, **35**, 6649–6656.
134. Galay RL, Miyata T, Umemiya-Shirafuji R, Maeda H, Kusakisako K, Tsuji N, et al. (2014). Evaluation and comparison of the potential of two ferritins as anti-tick vaccines against *Haemaphysalis longicornis. Parasit Vectors*, **7**, 482.
135. Hajdusek O, Almazán C, Loosova G, Villar M, Canales M, Grubhoffer L, et al.

(2010). Characterization of ferritin 2 for the control of tick infestations. *Vaccine*, **28**, 2993–2998.

136. Abbaspour N, Hurrell R, Kelishadi R. (2014). Review on iron and its importance for human health. *J Res Med Sci*, **19**, 164–174.
137. Dunn LL, Suryo Rahmanto Y, Richardson DR. (2007). Iron uptake and metabolism in the new millennium. *Trends Cell Biol*, **17**, 93–100.
138. Harrison PM, Arosio P. (1996). The ferritins: molecular properties, iron storage function and cellular regulation. *Biochim Biophys Acta*, **1275**, 161–203.
139. Oliver JD, Chávez ASO, Felsheim RF, Kurtti TJ, Munderloh UG. (2015). An *Ixodes scapularis* cell line with a predominantly neuron-like phenotype. *Exp Appl Acarol*, **66**, 427–442.
140. Munderloh UG, Liu Y, Wang M, Chen C, Kurtti TJ. (1994). Establishment, maintenance and description of cell lines from the tick *Ixodes scapularis*. *J Parasitol*, **80**, 533–543.
141. Yoshii K, Goto A, Kawakami K, Kariwa H, Takashima I. (2008). Construction and application of chimeric virus-like particles of tick-borne encephalitis virus and mosquito-borne Japanese encephalitis virus. *J Gen Virol*, **89**, 200–211.
142. Missirlis F, Holmberg S, Georgieva T, Dunkov BC, Rouault TA, Law JH. (2006). Characterization of mitochondrial ferritin in *Drosophila*. *Proc Natl Acad Sci USA*, **103**, 5893–5898.
143. Hunter RC, Asfour F, Dingemans J, Osuna BL, Samad T, Malfroot A, et al. (2013). Ferrous iron is a significant component of bioavailable iron in cystic fibrosis airways. *MBio*, **4**, e00557.
144. Robinson KM, McHugh KJ, Mandalapu S, Clay ME, Lee B, Scheller EV, et al. (2014). Influenza A virus exacerbates *Staphylococcus aureus* pneumonia in mice by attenuating antimicrobial peptide production. *J Infect Dis*, **209**, 865–875.
145. de la Fuente J, Kocan KM, Blouin EF. (2007). Tick vaccines and the transmission of tick-borne pathogens. *Vet Res Commun*, **31**, S85–90.
146. Santamaria R, Bevilacqua MA, Maffettone C, Irace C, Iovine B, Colonna A. (2006). Induction of H-ferritin synthesis by oxalomalate is regulated at both the transcriptional and post-transcriptional levels. *Biochim Biophys Acta*, **1763**, 815–822.
147. Elia G, Polla B, Rossi A, Santoro MG. (1999). Induction of ferritin and heat shock proteins by prostaglandin A1 in human monocytes. Evidence for transcriptional and post-transcriptional regulation. *Eur J Biochem*, **264**, 736–745.
148. Cairo G, Tacchini L, Pogliaghi G, Anzon E, Tomasi A, Bernelli-Zazzera A.

Induction of ferritin synthesis by oxidative stress. (1995). Transcriptional and post-transcriptional regulation by expansion of the “free” iron pool. *J Biol Chem*, **270**, 700–703.

149. Galluzzi L, Bravo-San Pedro JM, Vitale I, Aaronson SA, Abrams JM, Adam D, et al. (2015). Essential versus accessory aspects of cell death: recommendations of the NCCD 2015. *Cell Death Differ*, **22**, 58–73.
150. He W, Feng Y, Li X, Wei Y, Yang X. (2008). Availability and toxicity of Fe(II) and Fe(III) in Caco-2 cells. *J Zhejiang Univ Sci B*, **9**, 707–712.
151. Stockwell BR, Friedmann Angeli JP, Bayir H, Bush AI, Conrad M, Dixon SJ, et al. (2017). Ferroptosis: A regulated cell death nexus linking metabolism, redox biology, and disease. *Cell*, **171**, 273–285.
152. Espinosa-Diez C, Miguel V, Mennerich D, Kietzmann T, Sánchez-Pérez P, Cadenas S, et al. (2015). Antioxidant responses and cellular adjustments to oxidative stress. *Redox Biol*, **6**,183–197.
153. Anderson CP, Shen M, Eisenstein RS, Leibold EA. (2012). Mammalian iron metabolism and its control by iron regulatory proteins. *Biochim Biophys Acta*. **1823**, 1468–1483.
154. Tsuji Y, Ayaki H, Whitman SP, Morrow CS, Torti SV, Torti FM. (2000). Coordinate transcriptional and translational regulation of ferritin in response to oxidative stress. *Mol Cell Biol*, **20**, 5818–5827.
155. Balla G, Jacob HS, Balla J, Rosenberg M, Nath K, Apple F, et al. (1992). Ferritin: a cytoprotective antioxidant strategem of endothelium. *J Biol Chem*, **267**, 18148–18153.
156. Santamaria R, Irace C, Festa M, Maffettone C, Colonna A. (2004). Induction of ferritin expression by oxalomalate. *Biochim Biophys Acta*, **1691**, 151–159.
157. Sojka D, Franta Z, Horn M, Caffrey CR, Mareš M, Kopáček P. (2013). New insights into the machinery of blood digestion by ticks. *Trends Parasitol*, **29**, 276–285.
158. Harrison PM. (1986). The structure and function of ferritin. *Biochem Educ*, **14**, 154–162.
159. Jongejan F, Uilenberg G. (1994). Ticks and control methods. *Rev Sci Tech*, **13**, 1201–1226.
160. Paes de Andrade P, Aragão FJL, Colli W, Dellagostin OA, Finardi-Filho F, Hirata MH, et al. (2016). Use of transgenic *Aedes aegypti* in Brazil: risk perception and assessment. *Bull World Health Organ*, **94**, 766–771.
161. de la Fuente J, Kocan KM, Almazán C, Blouin EF. (2007). RNA interference for

the study and genetic manipulation of ticks. *Trends Parasitol*, **23**, 427–433.

162. Tuckow AP, Temeyer KB. (2015). Discovery, adaptation and transcriptional activity of two tick promoters: Construction of a dual luciferase reporter system for optimization of RNA interference in *Rhipicephalus* (*Boophilus*) *microplus* cell lines. *Insect Mol Biol*, **24**, 454–466.
163. Luo L-M, Zhao L, Wen H-L, Zhang Z-T, Liu J-W, Fang L-Z, et al. (2015). *Haemaphysalis longicornis* ticks as reservoir and vector of severe fever with thrombocytopenia syndrome virus in China. *Emerging Infect* Dis, **21**, 1770–1776.
164. Talactac MR, Yoshii K, Hernandez EP, Kusakisako K, Galay RL, Fujisaki K, et al. (2018). Vector competence of *Haemaphysalis longicornis* ticks for a Japanese isolate of the Thogoto virus. *Sci Rep*, **8**, 9300.
165. Moreira LA, Ito J, Ghosh A, Devenport M, Zieler H, Abraham EG, et al. (2002). Bee venom phospholipase inhibits malaria parasite development in transgenic mosquitoes. *J Biol Chem,* **277**, 40839–40843.
166. Kusakisako K, Ido A, Masatani T, Morokuma H, Hernandez EP, Talactac MR, et al. (2018). Transcriptional activities of two newly identified *Haemaphysalis longicornis* tick-derived promoter regions in the *Ixodes scapularis* tick cell line (ISE6). *Insect Mol Biol*, **27**, 590–602.
167. da Silva Vaz I, Imamura S, Nakajima C, de Cardoso FC, Ferreira CAS, Renard G, et al. (2005). Molecular cloning and sequence analysis of cDNAs encoding for *Boophilus microplus*, *Haemaphysalis longicornis* and *Rhipicephalus appendiculatus* actins. *Vet Parasitol*, **127**, 147–155.
168. Ito J, Ghosh A, Moreira LA, Wimmer EA, Jacobs-Lorena M. (2002). Transgenic anopheline mosquitoes impaired in transmission of a malaria parasite. *Nature*, **417**, 452–455.
169. Cooper SJ, Trinklein ND, Anton ED, Nguyen L, Myers RM. (2006). Comprehensive analysis of transcriptional promoter structure and function in 1% of the human genome. *Genome Res*, **16**, 1–10.
170. Butler JEF, Kadonaga JT. (2002). The RNA polymerase II core promoter: a key component in the regulation of gene expression. *Genes Dev*, **16**, 2583–2592.
171. Roy AL, Singer DS. (2015). Core promoters in transcription: old problem, new insights. *Trends Biochem Sci*, **40**, 165–171.
172. Zhang MQ. (1998). Identification of human gene core promoters *in silico*. *Genome Res*, **8**, 319–326.
173. Solberg N, Krauss S. (2013). Luciferase assay to study the activity of a cloned promoter DNA fragment. *Methods Mol Biol*, **977**, 65–78.

174. Alcaraz-Pérez F, Mulero V, Cayuela ML. (2008). Application of the dual-luciferase reporter assay to the analysis of promoter activity in Zebrafish embryos. *BMC Biotechnol*, **8**:81.
175. McNabb DS, Reed R, Marciniak RA. (2005). Dual luciferase assay system for rapid assessment of gene expression in *Saccharomyces cerevisiae*. *Eukaryotic Cell*, **4**, 1539–1549.
176. Colloms SD, Sykora P, Szatmari G, Sherratt DJ. (1990). Recombination at ColE1 cer requires the *Escherichia coli* xerC gene product, a member of the lambda integrase family of site-specific recombinases. *J Bacteriol*, **172**, 6973–6980.
177. De Angioletti M, Lacerra G, Sabato V, Carestia C. (2004). Beta+45 G --> C: a novel silent beta-thalassaemia mutation, the first in the Kozak sequence. *Br J Haematol,* **124**, 224–31.
178. Proudfoot NJ, Furger A, Dye MJ. (2002). Integrating mRNA processing with transcription. *Cell*, **108**, 501–512.
179. Valle MR, Guerrero FD. (2018). Anti-tick vaccines in the omics era. *Front Biosci (Elite Ed)*, **10**, 122–136.
180. Parizi LF, Reck J, Oldiges DP, Guizzo MG, Seixas A, Logullo C, et al. (2012). Multi-antigenic vaccine against the cattle tick *Rhipicephalus* (*Boophilus*) *microplus*: a field evaluation. *Vaccine*, **30**, 6912–6917.
181. Merino O, Alberdi P, Pérez de la Lastra JM, de la Fuente J. (2013). Tick vaccines and the control of tick-borne pathogens. *Front Cell Infect Microbiol*, **3**, 30.
182. Seixas A, Oliveira P, Termignoni C, Logullo C, Masuda A, da Silva Vaz I. (2012). *Rhipicephalus* (*Boophilus*) *microplus* embryo proteins as target for tick vaccine. *Vet Immunol Immunopathol*, **148**, 149–156.
183. Ndawula C, Sabadin GA, Parizi LF, da Silva Vaz I. (2019). Constituting a glutathione S-transferase-cocktail vaccine against tick infestation. *Vaccine*, **37**, 1918–1927.